HELSINKI UNIVERSITY OF TECHNOLOGY
Department of Electrical and Communications Engineering
Radio Laboratory

Juho Poutanen

Interaction between mobile terminal antenna and user

Thesis submitted in partial fulfillment of the requirements for the degree of Master of Science in Espoo ___.___.2007

Supervisor

Professor Pertti Vainikainen

Instructor

M.Sc. Juha Villanen

HELSINKI UNIVERSITY OF TECHNOLOGY **ABSTRACT OF THE MASTER'S THESIS**

Author:	Juho Poutanen
Name of the thesis:	Interaction between mobile terminal antenna and user
Date:	10.9.2007 **Number of pages**: 100
Department:	Department of Electrical and Communications Engineering
Professorship:	Radio Engineering
Supervisor:	Professor Pertti Vainikainen
Instructor:	M.Sc. Juha Villanen

In this master's thesis, interaction between mobile terminal antenna and user is studied. The increased amount of electromagnetic radiation in the environment has increased the common concern over the possible health risks of wireless devices. However, to minimize the amount of energy absorbed to the user is advantageous from the technical point of view, as well. The reduction of power absorbed by the user not only reduces any possible health hazards but also makes the antenna more efficient. This master's thesis aims at improving understanding on how mobile terminal antennas behave in the vicinity of the user. The results give valuable information for antenna designers in order to be able to design antennas with as low interaction with the user as possible in the future.

At first, general theory behind mobile terminal antennas is studied. This is followed by introducing some of the recently suggested solutions for internal handset antennas. The theory of how radiowaves propagate inside dielectric materials is presented next and also dielectric properties of human body tissues are discussed. After introducing the necessary theory behind the studied problem, the simulation studies are started. In the simulations, the field distributions inside and nearby dielectric material are studied. It is shown that the permittivity of the material strongly affects the field distributions. Also the frequency dependence of antenna parameters such as the bandwidth, *SAR* and radiation efficiency is investigated. Clear connections between these parameters are found. A technique to increase the efficiency of a mobile terminal antenna by reducing the *SAR* is also presented and analyzed. It is shown that when the antenna is placed beside the head, the radiation efficiency can be increased by 16 %-units and that the *SAR* values can be simultaneously reduced up to 46 % with the introduced method. All simulations are carried out by using the so called coupling element based antenna structure.

The results of this thesis show that even if fully understanding and predicting all the processes of the interaction between the mobile terminal antenna and the user may be a difficult task, trends in the behavior can be found by using simple simulation models. Many of the presented conclusions can be utilized when designing handset antennas that operate optimally in all possible environments.

Keywords: Handset antenna, coupling element structure, specific absorption rate (*SAR*), radiation efficiency, bandwidth

TEKNILLINEN KORKEAKOULU **DIPLOMITYÖN TIIVISTELMÄ**

Tekijä:	Juho Poutanen
Työn nimi:	Matkapuhelinantennin ja käyttäjän välinen vuorovaikutus
Päivämäärä:	10.9.2007 **Sivumäärä**: 100
Osasto:	Sähkö- ja tietoliikennetekniikan osasto
Professuuri:	Radiotekniikka
Työn valvoja:	Professori Pertti Vainikainen
Työn ohjaaja:	DI Juha Villanen

Tässä diplomityössä tutkitaan matkapuhelinantennin ja käyttäjän välistä vuorovaikutusta. Ympärillämme oleva ja jatkuvasti lisääntynyt sähkömagneettinen säteily on lisännyt huolta langattomien laitteiden turvallisuudesta. Kun matkapuhelinatennni suunnitellaan siten, että käyttäjään absorboituva teho on mahdollisimman vähäistä, samalla sekä minimoidaan kaikki mahdolliset terveysriskit että saadaan antennin hyötysuhde mahdollisimman korkeaksi. Tämän diplomityön tavoitteena on parantaa ymmärrystä siitä, miten matkapuhelimen antenni ja sen käyttäjä vaikuttavat toisiinsa. Tuloksia, jotka työssä saavutettiin, voidaan tulevaisuudessa käyttää hyväksi suunniteltaessa antenneja, joiden käyttäjävuorovaikutus on mahdollisimman pieni.

Aluksi työssä käydään läpi matkapuhelimen antenneihin liittyvää teoriaa. Tämän jälkeen esitellään muutamien tyypillisten sisäisten matkapuhelinantennien rakennetta. Teoriaa siitä, miten radioaallot etenevät dielektrisessä aineessa käydään läpi seuraavaksi. Myös ihmisen kehossa olevien kudosten sähköisiä ominaisuuksia esitellään. Kun aiheeseen liittyvä tarpeellinen teoria on esitetty, aloitetaan simulointitulosten esittely. Aluksi tutkitaan antennin lähelle asetetun dielektrisen aineen vaikutusta antennin kenttäjakaumiin. Kenttäjakaumia tutkitaan sekä aineen sisällä, että sen läheisyydessä. Osoitetaan, että aineen permittiivisyys vaikuttaa antennin synnyttämiin kenttiin merkittävästi. Seuraavaksi tutkitaan antennin eri parametrien, kuten kaistanleveyden, ominaisabsorptionopeuden (*SAR*) ja hyötysuhteen käyttäytymistä taajuuden funktiona. Näiden parametrien väliltä löydetään selkeitä yhteyksiä. Lopuksi esitellään ja analysoidaan tekniikkaa, jolla antennin hyötysuhdetta saadaan parannettua pienentämällä *SAR*-arvoja. Näytetään, että pään vieressä sijaitsevan antennin säteilyhyötysuhdetta voidaan parantaa 16 %-yksikköä, ja että *SAR*-arvoa saadaan samanaikaisesti pienennettyä 46 %. Kaikissa simuloinneissa antennina käytetään kytkentäelementtiin perustuvaa antennirakennetta.

Työn tulokset osoittavat, että vaikka matkapuhelinantennin ja sen käyttäjän väliseen vuorovaikutukseen liittyvät prosessit saattavat olla vaikeita täysin ymmärtää, niin käytettäessä yksinkertaisia simulointimalleja käyttäymisessä esiintyvät trendit voidaan kuitenkin saada selville. Monia työssä esitettyjä johtopäätöksiä voidaan käyttää hyväksi suunniteltaessa mahdollisimman pienen käyttäjävuorovaikutuksen omaavia matkapuhelinantenneja.

Avainsanat: Matkapuhelimen antenni, kytkentäelementtirakenne, ominaisabsorptionopeus (*SAR*), säteilyhyötysuhde, kaistanleveys

Preface

The work for this master's thesis has been done at the Radio Laboratory of Helsinki University of Technology (TKK) under the supervision of Professor Pertti Vainikainen.

Professor Vainikainen deserves my deepest gratitude for giving me the opportunity to work in his highly recognized research group at the Radio Laboratory among this interesting and challenging subject. Somewhere in the middle of all his busyness, he has always found time to give invaluable guidance and suggestions for this thesis.

I have been extremely lucky to have Mr. Juha Villanen as my instructor during the thesis. For many reasons, I have no doubt that he has been absolutely the best possible instructor for me. Even though he has been very busy with his dissertation, he has been able to share his expertise with me. Without his contribution, I would never have finished this thesis.

The working atmosphere in the Lab has been throughout my time here very good. For this I want to express my gratitude to the whole personnel. Especially I would like to thank Mr. Clemens Icheln for his patient help with the computers. Also the guys who started in the Lab at the same time as I in 2005, Mikko Kyrö, Jukka Koivunen and Risto Valkonen, deserve special acknowledgements for their help and support in various situations along the way.

Throughout my entire studies, my family has given me their full support. Both mental and financial support that they have given me during the years has been invaluable.

Otaniemi, September 6, 2007

Juho Poutanen

TABLE OF CONTENTS

Abbreviations

ANSI	American National Standards Institute
CENELEC	European Committee for Electrical Standardization
DECT	Digital Enhanced Cordless Telecommunications
DRA	Dielectric Resonator Antenna
DVB-H	Digital Video Broadcasting Handheld
EMC	Electromagnetic Compatibility
FDTD	Finite Difference Time Domain
GSM	Global System for Mobile Communications
ICNIRP	International Commission on Non-Ionizing Radiation Protection
IEEE	Institute of Electrical and Electronics Engineers
PCB	Printed Circuit Board
PEC	Perfect Electric Conductor
PIFA	Planar Inverted-F Antenna
RF	Radio Frequency
STUK	Radiation and Nuclear Safety Authority
UMTS	Universal Mobile Telecommunications System
UPML	Uniaxial Perfectly Matched Layer
WIMAX	Worldwide Interoperability for Microwave Access
WLAN	Wireless Local Area Network

List of symbols

B_r	relative bandwidth
BW_{abs}	absolute bandwidth
c	speed of light
C	capacitance
C_{user}	capacitance caused by user
CF	center frequency
d	distance from an antenna
D	directivity
D_a	largest extent of antenna
E	electric field strength
E_n	normal component of electric field
E_t	tangential component of electric field
f_r	resonant frequency
f_{rc}	resonant frequency of chassis
G	conductance
G_{pw}	power gain
G_{user}	conductance caused by user
H	magnetic field strength
I	current integral
J	current
J_s	surface current density
l	length of a parasitic radiator
l_{ch}	length of a mobile handset chassis
L	inductance
L_{refl}	reflection loss
L_{retn}	return loss
P_{in}	accepted power
P_l	loss power
P_{rad}	radiated power
Q	quality factor of a resonator
Q_0	unloaded quality factor
Q_c	conductor quality factor
Q_d	dielectric quality factor
Q_e	external quality factor

Q_l	loaded quality factor
Q_{rad}	radiation quality factor
Q_{user}	user quality factor
r_1	near-field distance
r_2	far-field distance
R_a	resistive part of antenna impedance
R_r	radiation resistance
R_σ	ohmic resistance
S	standing wave criterion
S_{11}	reflection coefficient
S_{max}	maximum power density
SAR	specific absorption rate
T	coupling coefficient
$VSWR$	voltage standing wave ratio
x	variable
X_a	reactive part of antenna impedance
y	variable
Y_0	input admittance
z	variable
Z_0	characteristic impedance
Z_L	impedance of a load

δ	penetration depth
ε	complex permittivity
ε_0	free space permittivity
ε_r	relative permittivity
ε_r'	real part of relative permittivity
ε_r''	imaginary part of relative permittivity
ε_{rd}''	dielectric part of imaginary part of relative permittivity
η_m	matching efficiency
η_{rad}	radiation efficiency
η_{tot}	total efficiency
λ	wavelength
μ	complex permeability

ρ	reflection coefficient
ρ_d	density of tissue
ω	angular frequency
ω_r	resonant angular frequency
σ	ionic conductivity of tissue
σ_{eff}	effective conductivity

1 INTRODUCTION

The development of wireless communication systems has been shockingly rapid during the recent decades. The growing enthusiasm for adding more and more systems into portable devices has set many challenges to antenna designers. In addition to e.g. the large bandwidth requirements of antennas operating in today's multisystem mobile terminals, the hugely increased amount of electromagnetic radiation everywhere in the environment has increased the concern with the possible health risks of wireless devices. Although the most common fear in people's minds is the concern with the potential risk of having a brain cancer or other serious disease, investigations on mobile terminals in the vicinity of a user are important also from the technical point of view; the reduction of power absorbed by the user not only reduces any potential health hazards but also makes the antennas more efficient. Rising from these aspects, antenna designers have been forced to pay a growing amount of interest in reducing the radiation absorbed into user. Fully understanding the process of how and why the fields generated by a mobile terminal antenna are absorbed to the user would enable the antennas to be designed from the very beginning so that the energy absorbed to the user could be minimized. As a strong interrelation between antenna size, bandwidth, radiation efficiency and *SAR* (Specific Absorption Rate) is well known to exist, to design a mobile terminal antenna that operates as desired in all possible environments, is a great challenge.

Generally speaking, the desire to be able to design the mobile terminal antennas to perform optimally both in free space and beside the user in any possible talk-positions has from the beginning provided the motivation for the studies of this master's thesis. In order to minimize the complexity of the problem, the studies of this thesis have been carried out at a very fundamental and simple level. Many of the used models and techniques may thus even seem to be quite far from

a real mobile phone environment. However, the achieved results can be straightforwardly applied to more complex scenarios, as well.

This thesis includes altogether seven chapters. The general theory behind mobile terminal antennas is introduced in Chapter 2. This includes discussion about the interrelation between the most important performance parameters of a mobile terminal antenna such as the impedance bandwidth, radiation efficiency and quality factor. Also the fundamentals of the issue of interaction between the user and the antenna are explained in Chapter 2. In Chapter 2, also some of the recently suggested solutions for internal antenna structures are introduced. The effect of the mobile phone "chassis" to the antenna performance is also discussed. In Chapter 3, the energy absorption mechanisms in biological bodies are studied. This includes discussion about the dielectric properties of different human body tissues. A review on the earlier studies related to the general energy absorption mechanism in human tissue is also given in Chapter 3. The three first chapters provide the necessary background for the reader to be able to understand the concepts discussed in the later parts of the work. In Chapter 4, the simulation studies of the thesis are started by analyzing the near fields of a coupling element based antenna inside and nearby dielectric material. In Chapter 5, the frequency dependence of important parameters of the antenna beside dielectric material is studied. In Chapter 6, a method to increase the radiation efficiency of a mobile terminal antenna by reducing the energy absorbed to the user's head is introduced and analyzed. Finally, in Chapter 7, the overall conclusions of the thesis are given.

2 MOBILE TERMINAL ANTENNAS

2.1 Introduction

Antennas for today's mobile terminals are by their nature often small. The size reduction, however, sets limits to other important parameters of an antenna; designing a small antenna is always a trade-off between size, bandwidth and efficiency. In this chapter, the interrelations between the most important performance parameters of a mobile terminal antenna are discussed by introducing the concepts of impedance bandwidth, radiation efficiency and quality factor. Also the fundamentals of the issue of interaction between the user and the antenna are explained. In the last part of this chapter, some of the recently suggested solutions for internal mobile terminal antennas are introduced.

2.2 Reflection coefficient

In a situation where the impedance Z_L of a load (e.g. an antenna) differs from the characteristic impedance Z_0 of a transmission line, a part of the voltage reflects back from the load. The reflection coefficient caused by the load can be calculated from

$$\rho = \frac{Z_L - Z_0}{Z_L + Z_0}, \tag{2.1}$$

and is often depicted by the scattering parameter S_{11}. If impedances Z_L and Z_0 are equal, no voltage is reflected and the load is said to be perfectly matched to the transmission line at the studied frequency [1].

The impedance of an antenna consists of resistive R_a and reactive X_a components according to Equation (2.2):

$$Z_a = R_a + jX_a . \tag{2.2}$$

A series equivalent circuit model for the impedance parameters of an antenna is presented in Figure 2.1.

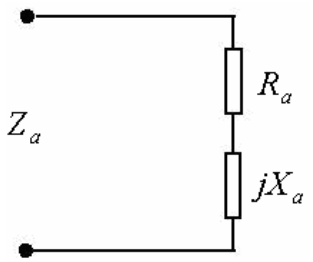

Figure 2.1 Impedance parameters of an antenna.

The resistive part of the impedance further consists of radiation and ohmic losses, $R_a = R_r + R_\sigma$, whereas the reactive part is caused by the energy stored in the antenna's reactive near fields. At antenna's resonant frequency, the reactive part of the impedance disappears, i.e. $X_a = 0$ [2].

Perfect matching is impossible to achieve in a wide frequency range. However, in many cases a slight mismatching is accepted. E.g. for small handset antennas $|\rho| = |S_{11}| \leq$ -6 dB is often considered adequate for the operating frequency range [2].

2.3 Bandwidth

When dealing with small mobile terminal antennas, bandwidth most often refers to impedance bandwidth. A widely used criterion for the bandwidth of internal mobile phone antennas is the frequency range where the condition $|\rho| = |S_{11}| \leq$ -6 dB is satisfied. The corresponding values for voltage standing wave ratio $VSWR \leq 3$, reflection loss $L_{refl} \leq 1.26$ dB and return loss $L_{retn} \geq 6$ dB can be calculated from Equations (2.3), (2.4) and (2.5) [1]:

$$VSWR = \frac{1+|\rho|}{1-|\rho|} \tag{2.3}$$

$$L_{refl} = 10\log\frac{1}{1-|\rho|^2} \tag{2.4}$$

$$L_{retn} = 10\log\frac{1}{|\rho|^2} \tag{2.5}$$

Bandwidth can also be expressed relative to center frequency. Relative bandwidth is defined in terms of absolute impedance bandwidth BW_{abs} and center frequency CF of the impedance band according to Equation (2.6):

$$B_r = \frac{BW_{abs}}{CF}. \tag{2.6}$$

Table 2.1 presents bandwidth requirements for different wireless systems that can be applied in portable devices [4]. It should be noted that in Table 2.1, the presented frequency bands especially for WLAN and WIMAX standards are only examples and that those standards are in use at other frequency bands, as well.

Table 2.1 Frequency bands of different systems [4].

System	CF [MHz]	BW_{abs} [MHz]	B_r [%]
GSM 850	859	70	8.1
E-GSM 900	920	80	8.7
GSM 1800	1795	170	9.5
UMTS	2035	270	13.3
WLAN (802.11g)	2450	100	4.1
WLAN (802.11a)	5250	200	3.8
WIMAX	3500	500	14.3

2.4 Quality factors

Microstrip-type antennas in mobile devices are always based on the resonance phenomenon [8]. Thus, the common resonator theory can be extended to the analysis of the antennas treated in this thesis. The quality factor Q of a resonator can be considered as its ability to store electromagnetic energy. It is defined as

$$Q = 2\pi f_r \frac{Total\ stored\ energy}{Energy\ dissipated\ in\ one\ cycle} = \frac{\omega_r W}{P_l}, \tag{2.7}$$

where f_r is the resonant frequency, $\omega_r=2\pi f_r$, W the stored energy and P_l the loss power. The concept of Q can be applied in antenna theory and understanding of it leads to an understanding of fundamental limitations in miniature antenna design [1],[7].

Nearby the resonant frequency, an antenna element can be modeled also by a parallel resonant equivalent circuit (compare with Figure 2.1) presented in Figure 2.2.

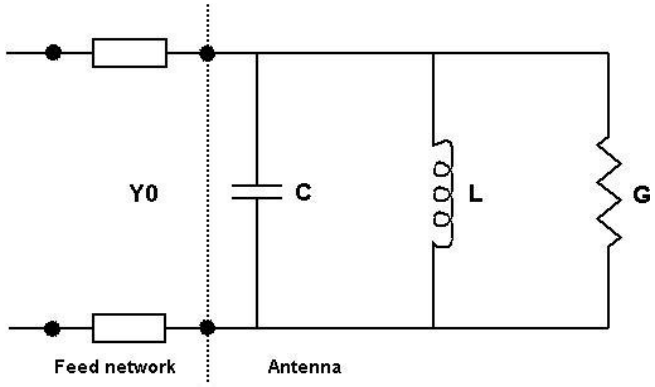

Figure 2.2 Equivalent circuit of a resonant antenna.

For a resonant circuit, different quality factors can be defined. When the resonator is not connected to an external circuit, the quality factor of the resonator is called the unloaded quality factor Q_0 which describes resonator's internal losses. The external quality factor Q_e in turn characterizes the power lost through the connection to the external circuit. Q_0 and Q_e can be defined in terms of the capacitance C, the inductance L and the conductance G seen from the input of the antenna:

$$Q_0 = \frac{\omega_r C}{G} = \frac{1}{G\omega_r L} \tag{2.8}$$

$$Q_e = \frac{\omega_r C}{Y_0} = \frac{1}{Y_0 \omega_r L}. \tag{2.9}$$

The unloaded quality factor Q_0 can be further divided into radiation quality factor Q_{rad}, dielectric quality factor Q_d and conductor quality factor Q_c. In an ideal case, Q_0 and Q_{rad} are equal but in practice also conductors and dielectrics cause losses. The connection between these four quality factors can be presented as [8]

$$\frac{1}{Q_0} = \frac{1}{Q_{rad}} + \frac{1}{Q_d} + \frac{1}{Q_c}. \tag{2.10}$$

The loaded quality factor Q_l takes into account both the unloaded and the external quality factors and can be calculated from [1]

$$\frac{1}{Q_l} = \frac{1}{Q_0} + \frac{1}{Q_e}. \tag{2.11}$$

Quality factor, on the other hand, describes the frequency selectivity of a resonator. The greater the *Q*-factor is, the narrower the bandwidth of the resonator becomes. Unloaded quality factor Q_0 is inversely proportional to the relative bandwidth B_r of the antenna [5]:

$$B_r = \frac{1}{Q_0}\sqrt{\frac{(TS-1)(S-T)}{S}}, \tag{2.12}$$

where S is the criterion for maximum *VSWR* and $T = Y_0 / G$ the coupling coefficient. When the antenna is critically coupled ($|\rho| = 0$ at f_r) T equals unity and Equation (2.12) reduces to [5]

$$B_r = \frac{1}{Q_0}\frac{S-1}{\sqrt{S}}. \tag{2.13}$$

However, the maximum available bandwidth is not reached when the antenna is critically coupled. In order to optimize the relative bandwidth of an antenna the coupling coefficient T should be taken as [5]

$$T_{opt} = \frac{1}{2}\left(S + \frac{1}{S}\right), \tag{2.14}$$

which is called optimal overcoupling. The corresponding maximum relative bandwidth becomes

$$B_r = \frac{1}{Q_0}\frac{S^2-1}{2S}. \tag{2.15}$$

From the above equations it is easily seen that reducing the unloaded quality factor Q_0 increases the available bandwidth. If the decrease in Q_0 is realized by adding resistive parts into the antenna structure, the dielectric losses of the antenna increase and thus the antenna efficiency decreases, which in most cases is not acceptable. Therefore, to increase the bandwidth, other techniques must be used instead. The bandwidth of an antenna can be increased, for instance, by adding more resonators into the antenna structure, which leads to multiresonant antenna structures; multiple resonances, realized by using parasitic elements or resonant matching circuits, are tuned close to each other to obtain a wider bandwidth [2]. Also advantage of the fact, that at specific frequencies the phone chassis works as the main radiator can be taken to improve the available bandwidth

without the unacceptable decrease in efficiency [6]. Antennas using the chassis as the primary radiator are discussed more in detail in Section 2.7.

2.5 Radiation efficiency

The radiation efficiency η_{rad} of an antenna is defined as the ratio of the power P_{rad} radiated by an antenna to the power P_{in} accepted by the antenna [9]:

$$\eta_{rad} = \frac{P_{rad}}{P_{in}}. \tag{2.16}$$

By using the impedance parameters (see Fig. 2.1) of an antenna, the radiation efficiency can be written as [3]

$$\eta_{rad} = \frac{R_r}{R_r + R_\sigma}, \tag{2.17}$$

where R_r represents the radiation resistance and R_σ the ohmic losses in the antenna structure.

Radiation efficiency can be presented also in terms of quality factors [8]

$$\eta_{rad} = \frac{Q_0}{Q_{rad}} = \frac{{Q_{rad}}^{-1}}{{Q_{rad}}^{-1} + {Q_c}^{-1} + {Q_d}^{-1}}, \tag{2.18}$$

where Q_0 is the unloaded quality factor, Q_{rad}, the radiation quality factor, Q_d the dielectric quality factor and Q_c the conductor quality factor.

From the different definitions described above, it is evident that radiation efficiency as such does not take impedance matching into account. The total efficiency of an antenna considers also mismatching and can be calculated from [10]

$$\eta_{tot} = \eta_{rad}\eta_m, \tag{2.19}$$

where $\eta_m = 1 - |\rho|^2$ is the matching efficiency.

2.6 User interaction

2.6.1 Absorption of radiation into user

During the recent years, the issue of electromagnetic interaction between human tissue and a portable device has been intensively studied to improve the understanding of radiation safety of mobile communication systems. In the case of a mobile phone, a substantial part of the power radiated from the antenna is indeed absorbed into user's head, hand and the rest of the body. According to current knowledge, however, the only influence that the radiation has on human is the rise in tissue temperature. The temperature rise on the surface of brain is known to be not more than 0.3 degrees, which is not known to have any physiological significance, whatsoever. As a comparison, the normal fluctuation is around ±1°C, and in exhausting physical exercise even a temperature rise of two degrees is quite common [11].

Although the increase in tissue temperature is too small to cause any biological damage, it is possible in theory that electric fields may, by some unknown non-thermal mechanism, disturb normal cell function. Hence, in addition to tissue heating, also other possible health hazards of mobile phone radiation have been furiously studied. Apparently, the most popular subject of research has been to study the possible connection between mobile phone radiation and brain cancer. On the basis of research results obtained from these studies, however, it hasn't been possible to conclude that radiation from mobile phones would be detrimental to health [11].

The primary dosimetric parameter for evaluating the absorption of electromagnetic radiation to human is Specific Absorption Rate, *SAR*. *SAR* is a measure to quantify the microwave energy absorbed by unit mass of tissue and defined as

$$SAR = \sigma_{eff} \frac{E^2}{\rho}, \tag{2.20}$$

where σ_{eff} is the effective conductivity of the tissue, E the root-mean-square value of the induced electric field strength, and ρ the tissue density. The unit of *SAR* is watts per kilogram (W/kg) or milliwatts per gram (mW/g) and it denotes the time rate of RF (Radio Frequency) energy absorption at a given location inside the tissue. In practice, *SAR* is always determined as an average value over a finite, most often 1 or 10 g, tissue mass [2], [11].

Table 2.2 presents the recommended limits for local maximum *SAR* values in an uncontrolled environment set by IEEE (Institute of Electrical and Electronics Engineers) and ICNIRP (International Commission on Non-Ionizing Radiation Protection). In Europe the ICNIRP recommendations are the most widely followed, while the slightly stricter standards set by IEEE are applied in the United States [11],[12], [13].

Table 2.2. Recommended maximum local SAR values set by IEEE and ICNIRP [12], [13]

	IEEE	**ICNIRP**
Whole body averaged SAR (W/kg)	0.08	0.08
Spatial peak SAR (W/kg) in body except hands, wrists, feet, ankles (includes e.g. the head)	1.6	2
Averaging mass (g)	1	10
Spatial peak SAR (W/kg) in hands, wrists, feet, ankles	4	4
Averaging mass (g)	10	10
Averaging time in all cases (min)	30	6

The recommendations presented in Table 2.2 give valuable information for antenna designers. That is, the radiation safety of mobile communication devices can be designed and tested by using these levels as references.

The fundamentals of the interaction mechanisms between electromagnetic fields and dielectric material, such as human tissue, are further discussed in the subsequent chapters of this thesis.

2.6.2 Reduction of radiation efficiency

Besides the health issues, it is essential from antenna efficiency point of view to minimize the energy absorbed to the user's head and the rest of the body; the smaller is the portion of power that human tissues absorb, the larger is the share that radiates into the surrounding free space. In fact, the portion of power absorbed into the user pretty far determines the total radiation efficiency of the system including the phone and the user. Especially at GSM900 band the contribution of power that is absorbed into the user is commonly very big; with internal mobile phone antennas, commonly even more than 90 % of the total radiated power can be lost due to the presence of the user.

There is no doubt that the radiated power is partly lost also in mobile phone parts, such as battery, display and all the plastic components. However, free space radiation efficiency of a commercial mobile phone can be still in the order of 80 % (corresponding to approximately 1 dB losses in the

structure) or more, as long as the phone is nicely designed [2]. In the simulation studies of this thesis the antenna structures are modeled as PEC (perfect electric conductor), which means zero losses - and thus 100 % radiation efficiency - in free space. The effect of the user can be easily separated from the results, since all the losses that occur are caused by the user.

2.7 Internal mobile terminal antennas

When designing a modern mobile phone, a great deal of imagination is required from the antenna designer. It is not only the steady reduction in the mobile phone size, but also the need for the enormous variety of different frequency bands, that has recently caused headache to antenna designers. In order to realize compact antenna elements with adequate bandwidth, high efficiency and feasible size, several types of antenna structures have been proposed. Especially planar antennas, including microstrip and printed antennas, and other types of flat and low-profile antennas have been widely applied in mobile communication devices during the recent years. In addition to reduction in mobile phone size, the trend has been to place the antenna fully inside the device, which has - among many other reasons - lead to a decreasing use of traditional external antennas, like whips or helices.

In this section, some of the recently suggested solutions for internal antenna structures are introduced. The treatment, though, starts by taking a look at the effect of the mobile phone "chassis" to the antenna performance, which regardless of the antenna structure in question is a crucial one. The concepts of PIFA (planar inverted-F antenna), DRA (dielectric resonator antenna), chip antenna and coupling element based antenna are then explained. Although the studies in the later parts of the thesis are all carried out by using coupling element based antennas, it is very likely that the results in many respects would follow similar trends with other internal antenna structures, as well.

2.7.1 The effect of phone chassis on antenna performance

The phone chassis - formed by the PCB (Printed Circuit Board) and the metallic shielding of the device - is known to have a crucial role in the performance of a small handset antenna. Parameters such as impedance bandwidth, *SAR* and radiation efficiency are strongly dependent on whether the chassis is at resonance or not. According to related studies [14], [15], the basic behavior is that the maximum bandwidth is reached at the chassis resonant frequencies and at the same time an increase is *SAR*s and a decrease in radiation efficiency occur. The trend was confirmed in [16]; however, it was concluded that the effect of the chassis is significant at first and second order

resonances and that at higher frequencies the wavemodes of the antenna element grow into the main contributor.

Furthermore, the radiation properties of an antenna-chassis combination are clearly dependent on the chassis resonant frequencies. The contribution of the power radiated by the chassis wavemodes is most significant around the low-order resonances of the chassis. The first and the second order resonances of a chassis can be approximated using Equations (2.21) and (2.22) [15]:

$$f_{rc,1st} = (0.73...0.78) \cdot \frac{c}{2l_{ch}} \tag{2.21}$$

$$f_{rc,2nd} = (0.83...0.85) \cdot \frac{c}{l_{ch}}, \tag{2.22}$$

where c is the speed of light and l_{ch} the length of the chassis. As an example, in [15] it was noticed that at 900 MHz the radiation by the antenna element wavemodes typically represent less than 10 % of the total radiated power. The rest of the radiated power is dissipated by the half-wave dipole-type current distribution of the chassis. This implies that the antenna element mainly works as a matching element coupling signals to the chassis wavemode. At higher frequencies the role of antenna element wavemodes becomes more and more significant. At 1800 MHz, according to [15], the share of the antenna element originated radiation is typically around 50 %. Figure 2.3 shows an example of the current distributions on the chassis backside of a coupling element based antenna (explained later in Section 2.7.5) at 900 MHz and 1800 MHz. The length of the chassis of the antenna in question is 100 mm, which is effectively fairly close to half of a wavelength at 900 MHz.

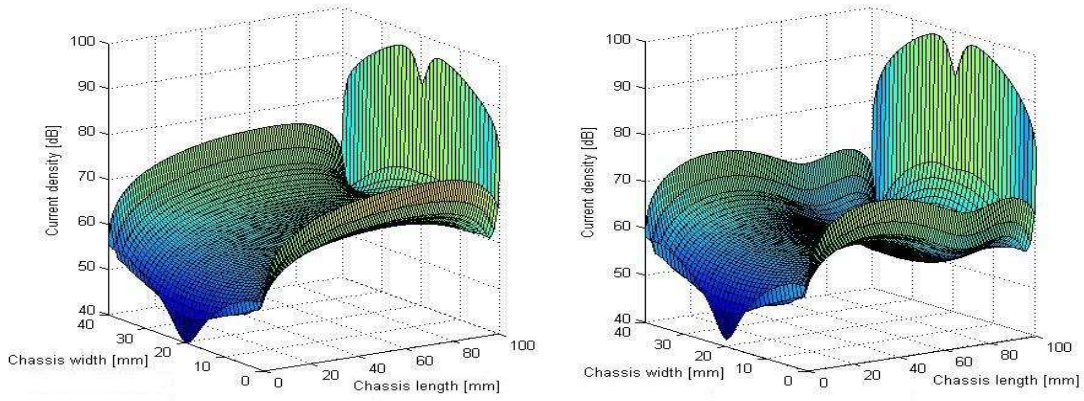

a) **b)**

Figure 2.3 Current densities on the surface of the back side of the chassis at a) 900 MHz and b) 1800 MHz. The chassis wavemodes are seen by the sinusoidal dipole-type distribution and also the concentration of current for the antenna element is clear. Strong currents appear on the edges of the chassis, as well.

As discussed earlier in this chapter, reducing the size of an antenna leads to an increase in radiation quality factor and thus to a decrease in relative bandwidth. With antennas whose size is that of a typical handset antenna element, such bandwidths - while maintaining feasible efficiency - as required for mobile terminals can not be achieved. A larger current distribution is needed and that can be attained for example by effectively utilizing the chassis wavemode. Depending on whether the chassis is at resonance or not, it is possible to reach up to 30 times wider maximum bandwidths compared to the minimum [6].

The current distributions on the chassis surface were examined in [16]. Based on those results, it is clear that at chassis resonant frequencies the currents caused by the dipole-type chassis wavemodes are most significant. The chassis current distribution has also a clear relation to bandwidth: When the contribution of the chassis currents to the overall current distribution is high, also the bandwidth reaches a local maximum. However, as the frequency increases, the effect of the chassis decreases steadily and at the same time the contribution of the antenna element wavemodes to the radiation increases. Figure 2.4 [16] shows the effect of the resonant frequencies of the chassis on the bandwidth potential of the antenna and on the surface integrals of chassis current distributions. By “bandwidth potential” it is in this context meant the maximum relative bandwidth that can be achieved by using two lumped elements (critical coupling) in the matching circuit. The simulations in [16] were executed by using two coupling element based antenna models of which the antenna model 2 (red curves) had a considerably stronger coupling to the chassis wavemode. This is seen

by the stronger resonances in the reflection coefficient curves of Figure 2.4a); also the bandwidth potential (Figure 2.4b)) of antenna model 2 is clearly larger than that of antenna model 1.

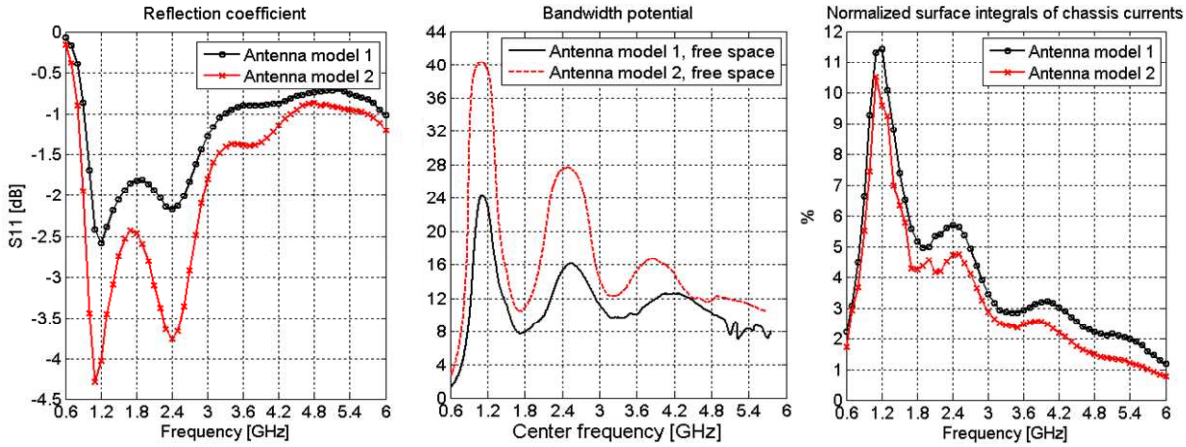

a) **b)** **c)**

Figure 2.4 a) Reflection coefficients, b) relative bandwidths ($|S_{11}| \leq$ -6 dB) and c) normalized surface integrals of chassis current distributions as a function of frequency in free space [16].

2.7.2 Planar inverted-F antenna

A planar inverted F antenna (PIFA) is an antenna that consists of radiating antenna element placed on top of a conducting ground plane. The antenna element is typically rectangular in shape, placed parallel to the ground plane and short-circuited at one corner. In comparison to traditional whips and helices, PIFAs offer two major advantages: They are easy to place fully within the housing of a mobile phone, and have reduced backward radiation towards the user's head. Other advantageous features of PIFAs are the inexpensive manufacturing, simplicity in structure and low profile. No additional matching networks are needed because the matching is achieved by varying the feed location and the length of the patch. The main disadvantage of PIFAs is their narrow impedance bandwidth compared to the size of the antenna structure. The impedance bandwidth can be increased by resistive loading, but this would decrease the efficiency. Another way of enhancing the impedance bandwidth is to use parasitic elements or matching circuits, which would naturally increase the complexity of the antenna structure [20], [21].

With the help of varying patch configurations, such as using multiple separate patches or meandered patch, PIFAs are capable of multiband operation. Such configurations have been under intensive investigation. As an example, an internal PIFA (presented in Figure 3.3) covering the E-GSM (880-960 MHz), GSM1800 (1710 – 1880 MHz), DECT (1880 – 1900 MHz), PCS1900 (1850 – 1990 MHz) and UMTS (1900 -2170 MHz) frequencies with a return loss $L_{retn} \geq 6$ dB was

reported in [22]. In [23], a PIFA for WLAN operation in both the 2.4 GHz and 5.2 GHz bands was presented.

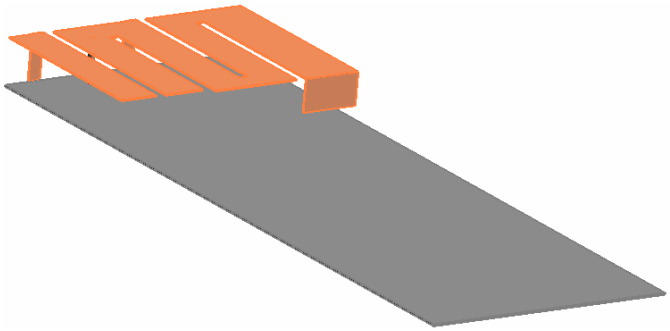

Figure 2.5 A multiband PIFA presented in [22].

An example of a dual-band (GSM 900/1800) PIFA inside a Nokia 7650 mobile phone is presented in Figure 2.5. The antenna element, the EMC shielding and the printed circuit board can be observed. The dimensions of the antenna element are about 40 x 45 mm (length x width) so it occupies a relatively large space inside the device.

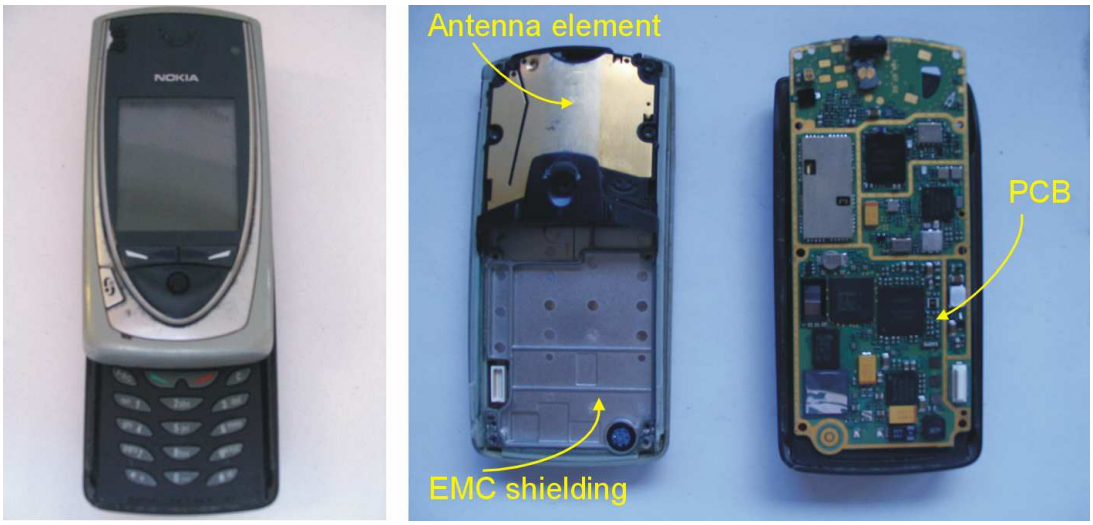

Figure 2.6 Nokia 7650 mobile phone and components inside the phone.

2.7.3 Dielectric resonator antenna

A dielectric resonator antenna (DRA) is a resonant antenna which consists of a piece of dielectric material placed on top of a ground plane. The resonant frequency of the dielectric piece is a function of its size, shape and permittivity. A wide range of permittivity values can be used: typically ε_r' varies from about 6 to 100, which makes it possible to control the size and the bandwidth of the structure. In general, wide bandwidth is reached using low permittivity material, and compact size is attained using high permittivity material. The dielectric piece can, in addition,

have various shapes, which brings flexibility to the design. Other attractive features that DRAs offer are their low cost, simple structure and light weight. Also the radiation efficiency of DRA structures is very high (>95%) [17].

In [18] a small wideband dual-resonant DRA for mobile phones was presented. The center frequency of the operating band was 2.36 GHz and the resulting relative bandwidth (with $L_{retn} \geq 6$ dB matching criterion) 28.4 %. In [19] a two-segment DRA for WLAN applications was introduced. The used frequency band was 5-6 GHz and the obtained bandwidth 19 % ($L_{retn} \geq 10$ dB), which easily satisfies the requirements in IEEE 802.11a standard for wireless LANs. These studies, among many others, suggest that DRAs are attractive candidates for wireless communication systems operating in various systems.

2.7.4 Chip antenna

The so called chip antennas usually comprise a ceramic base and metal line patterns printed on or embedded within the base. Chip antennas are extremely small in size and can be directly mounted on a circuit board of a communication device. They are suitable especially for WLAN applications that operate in 2.4 GHz and 5.2 GHz regions. There are two major types of ceramic chip antennas: one is with a ground plane printed on the bottom of the ceramic base, and the other is without a ground plane. For the former type, the chip antenna can be directly mounted on the ground plane of the system circuit board, but on the other hand, because of the large permittivity of the ceramic base (usually larger than 7), the impedance bandwidth and radiation efficiency are considerably decreased. For the chip antenna without the ground plane the effects of the ceramic base on antenna's bandwidth and efficiency are much smaller. For both kinds of ceramic chip antennas a common drawback is that they tend to break up easily due to the fragile nature of ceramic materials [20], [24].

2.7.5 Coupling element based antennas

Antenna structures that are based on coupling elements, rest their operation on the features of the phone chassis, which were explained above in Section 2.7.1; the usage of the chassis as the primary radiator has made the implementation of very low-profile and low-volume antenna structures possible. As coupling element structures enable the usage of very small and high-Q antenna/coupling elements, they even seem to ridicule the fundamentals of small antennas that have been thought to set the ultimate limits in the size reduction of a mobile terminal antenna. Figure 2.7 illustrates a typical and simple coupling element structure.

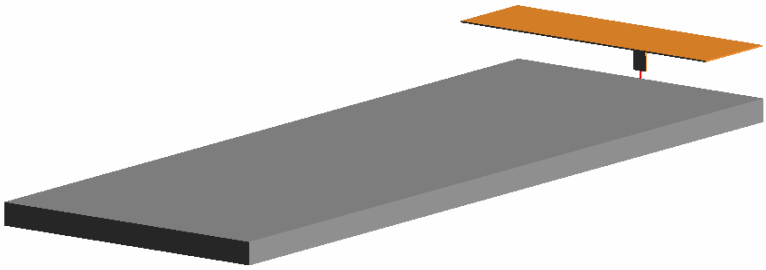

Figure 2.7 A typical coupling element based antenna structure. The antenna element is non-resonant and used for coupling signals to chassis wavemodes.

The bandwidth of an antenna-chassis combination can be increased by enhancing coupling from antenna element to the dominant wavemode of the chassis. The coupling can be done either via electric (capacitive coupling) or magnetic fields (inductive coupling). Coupling to the electric fields can be done with e.g. a capacitive plate, aperture or probe so that its electric field direction is parallel to that of the chassis wavemode. Coupling to the magnetic fields, in turn, can be enabled with e.g. an inductive loop or aperture so that its magnetic field coincides with that of the chassis wavemode. In this work, only antennas with capacitive coupling are treated [6].

According to the research results presented in [6], [15] and [26], it is clear that a self-resonant antenna element structure like PIFA is not optimal in terms of efficient coupling: the electric field maximum of a planar antenna element should be located near the electric field maximum of the chassis, and the electric field strength should also be as high as possible all around the antenna element. In fact, especially at frequencies around 1 GHz, a traditional self-resonant antenna element mainly works as a matching element between the feed of the antenna element and the chassis. In coupling element based antenna structures, the self-resonant antenna element is replaced with a non-resonant coupling element that efficiently excites the chassis wavemodes. A separate matching circuit is then used to tune the antenna to the desired frequency [6], [26].

Although the effect of the chassis is strongest at its resonances, it is significant at other frequencies, as well. As far as adequate coupling to the chassis wavemodes is obtained, large bandwidths with high enough efficiency can be achieved with non-radiating and non-resonant coupling elements. Since the necessary matching circuitry is fully separated from the coupling element, the size, shape and location of the coupling element can be individually optimized to achieve the best possible coupling to chassis wavemodes. In addition, what makes coupling element based antennas promising especially in the future multisystem environments is that the same structure can be used in a wide range of different frequencies and thus systems, as far as the matching circuitry is properly designed [6].

Even if the concept of coupling element based antenna structures and the effects of the phone chassis to the antenna performance is already quite widely studied, an extensive study on the general user interaction at a wide frequency range seems to be lacking. As mentioned in Section 2.7.1, in [14] and [15] it was suggested that the maximum bandwidth is reached at chassis resonances and at the same time an increase is *SAR*s and a decrease in radiation efficiency occur. In [25] a totally opposite result concerning *SAR*s was obtained. In [16] the earlier-mentioned trend seemed to hold at low-order chassis resonances, but at higher frequencies no clear trend was brought into light. The area of wide band user interaction of small handset antennas thus still remains, mildly speaking, somewhat unclear. One of the main goals of this work is to attack the questions left open in [14], [15], [16] and [25], and to hunt for a deeper and more thorough understanding of the causes and effects of the issue.

3 INTERACTION BETWEEN ANTENNA AND USER

3.1 Introduction

As in personal mobile communications a human using the device is always present, the effect of the user needs to be considered in order to design antennas with proper performance. The user of a mobile terminal can actually be considered as a part of the radiating system, as the nearby human tissue affects the electromagnetic fields generated by the device. When radio waves propagate in a dielectric material, such as human tissue, electric field is generated inside the material. The frictional forces between the particles that start to move due to the electric field cause losses, which results in absorption of energy. It is quite well known how these electrical fields inside a dielectric material interact with the material, but the connection between the original external fields and the generated internal fields has remained slightly unclear. Since the total efficiency of a system including the antenna and the user is strongly affected by the energy absorbed into the user, the topic of energy absorbing mechanisms in human body tissue is an important one from antenna efficiency point of view. Therefore, for an antenna designer, it would be extremely useful to know and understand these mechanisms and thus to be able to predict the trends of bandwidth, efficiency and *SAR*. In this chapter, the interaction between the fields generated by the antenna and the nearby dielectric tissue of a user is studied.

3.2 Radiowave in a lossy dielectric material

When an electromagnetic wave propagates in a material whose electrical conductivity σ differs from zero, as is the case in all human tissues, losses are caused by the current generated according to Ohm's law,

$$\vec{J} = \sigma \vec{E} . \quad (3.1)$$

Part of the power in the electric field thus turns into heat. With high-conductivity materials the losses are high and, conversely, losses in low-conductivity materials are low. Conductivity, on the other hand, increases as the water content of the tissue increases. Thus, in tissues with high water content, such as muscle, blood, skin and nerve, losses caused by conductivity are higher than in dryer tissue types, like fat and bone. However, it is worth noticing, that the effect of conductivity is related to frequency; the same material can be a good insulator at high frequencies, but a good conductor at low frequencies [27].

In a dielectric material, losses caused by the conductivity are not the only loss mechanism: Also the response of polar molecules to the oscillating electric field results in absorption of energy. An example of such material is water, whose hydrogen atoms are asymmetrically located around the oxygen atom. When an electric field is situated in water, it causes a rotative moment in a molecule, which forces the molecules to result parallel to the electric field. The losses in this process cause dielectric energy absorption, which clearly is an entirely different kind of a loss mechanism from the conductivity losses [27].

The dielectric properties of a material are fully characterized by its complex permittivity ε, defined in the following way [1]:

$$\varepsilon = \varepsilon_0 \varepsilon_r = \varepsilon_0 (\varepsilon_r' - j\varepsilon_r'') \quad (3.2)$$

$$\varepsilon_r = \varepsilon_r' - j(\varepsilon_{rd}'' + (\sigma / \omega \varepsilon_0)) , \quad (3.3)$$

where ε_0 is the free space permittivity, ε' the real part of complex permittivity, ε'' the imaginary part of complex permittivity and $\omega = 2\pi f$ the angular frequency; ε_{rd}'' represents the dielectric losses and σ the ionic conductivity. The imaginary part of the relative permittivity ε_r can be considered to represent all the losses in the material:

$$\mathrm{Im}\{\varepsilon_r\} = \frac{\sigma_{eff}}{\omega \varepsilon_0} \quad (3.4)$$

All the losses, including (ionic) conductivity losses and dielectric losses are therefore described by the effective conductivity σ_{eff}. Because all human tissues are non-magnetic materials, no losses due to permeability μ occur.

As a reminder from Chapter 2, *SAR* - a measure to quantify the amount of radiowave energy absorbed in the dielectric human tissue - is directly proportional to the effective conductivity of the tissue and to the electric field inside the tissue (see Equation (2.20)). Accordingly, *SAR* is evidently generated by the loss mechanisms - conductive and dielectric losses - described above.

3.3 Dielectric properties of human body tissues

To be able to predict and model the behavior of radiowave propagation inside dielectric material, accurate knowledge of the values of dielectric parameters of the material must be available. In case of a human, tissues inside the body can be roughly divided into two categories. Tissues that have high water content, like muscle or skin, have high values of real part of permittivity ε_r' and losses caused by the effective conductivity σ_{eff} are high, as well. In materials that have low water content and low ε_r' and σ_{eff} losses are low, and also other effects on the propagating fields are remote. Examples of such materials are bone and fat.

The frequency dependence of dielectric parameters of human tissues was studied in [28]. A model for determining the tissue parameters at frequency range of 10 Hz - 100 GHz was presented in that paper. In Table 3.1 values of ε_r' and σ_{eff} for tissues that are relevant in studies that consider interaction between mobile terminal antenna and user are presented in frequency range 600 MHz - 6 GHz. Values given in Table 3.1 are based on the parametric model described in [28] and will be used in simulations later in the thesis. Values for tissue densities are also given in Table 3.1.

Table 3.1 Values of tissue parameters in frequency range 600 MHz - 6 GHz.

	brain		**muscle**		**bone**		**fat**		**skin**	
ρ (kg/m^3)	1040		1050		1645		1100		1090	
Frequency (MHz)	ε_r'	σ_{eff}	ε_r'	σ_{eff}	ε_r'	σ_{eff}	ε_r'	σ_{eff}	ε_r'	σ_{eff}
600	47.49	0.66	55.96	0.85	17.18	0.19	5.52	0.04	43.63	0.76
700	46.77	0.70	55.87	0.88	16.97	0.21	5.50	0.05	42.70	0.80
800	46.25	0.73	55.29	0.91	16.78	0.22	5.48	0.05	41.98	0.83
900	45.81	0.77	55.03	0.94	16.62	0.24	5.46	0.05	41.41	0.87
1000	45.43	0.80	54.81	0.98	16.47	0.26	5.45	0.05	40.94	0.90
1100	45.11	0.84	54.61	1.02	16.34	0.28	5.43	0.06	40.54	0.93
1200	44.82	0.88	54.43	1.06	16.21	0.30	5.42	0.06	40.21	0.97
1300	44.56	0.92	54.27	1.10	16.09	0.32	5.41	0.06	39.92	1.00
1400	44.33	0.97	54.11	1.14	15.98	0.34	5.40	0.06	39.66	1.04
1500	44.11	1.01	53.96	1.19	15.87	0.36	5.38	0.07	39.43	1.07
1600	43.91	1.06	53.82	1.24	15.76	0.38	5.37	0.07	39.23	1.11
1700	43.72	1.10	53.68	1.29	15.66	0.41	5.36	0.07	39.04	1.15
1800	43.55	1.15	53.55	1.34	15.56	0.43	5.35	0.08	38.87	1.18
1900	43.38	1.20	53.42	1.40	15.46	0.46	5.34	0.08	38.71	1.22
2000	43.21	1.26	53.29	1.45	15.37	0.48	5.33	0.09	38.57	1.27

2100	43.05	1.31	53.16	1.51	15.28	0.51	5.32	0.09	38.43	1.31
2200	42.90	1.37	53.04	1.58	15.19	0.53	5.31	0.09	38.30	1.35
2300	42.75	1.42	52.91	1.64	15.10	0.56	5.30	0.10	38.18	1.39
2400	42.61	1.48	52.79	1.71	15.01	0.59	5.29	0.10	38.06	1.44
2500	42.47	1.54	52.67	1.77	14.92	0.61	5.27	0.11	37.95	1.49
2600	42.33	1.60	52.55	1.84	14.84	0.64	5.26	0.11	37.84	1.54
2700	42.19	1.67	52.42	1.91	14.75	0.67	5.25	0.12	37.74	1.58
2800	42.06	1.73	52.30	1.99	14.67	0.70	5.24	0.12	37.64	1.64
2900	41.93	1.80	52.18	2.06	14.59	0.73	5.23	0.13	37.54	1.69
3000	41.80	1.86	52.06	2.14	14.50	0.76	5.22	0.13	37.45	1.74
3100	41.67	1.93	51.94	2.22	14.42	0.79	5.21	0.13	37.36	1.79
3200	41.54	2.00	51.81	2.30	14.34	0.82	5.20	0.14	37.27	1.85
3300	41.41	2.08	51.69	2.39	14.27	0.85	5.19	0.15	37.18	1.91
3400	41.28	2.15	51.57	2.47	14.19	0.88	5.18	0.15	37.09	1.97
3500	41.15	2.22	51.44	2.56	14.11	0.91	5.17	0.16	37.01	2.02
3600	41.03	2.30	51.32	2.65	14.04	0.94	5.16	0.16	36.92	2.09
3700	40.90	2.38	51.20	2.74	13.96	0.97	5.15	0.17	36.84	2.15
3800	40.78	2.45	51.07	2.83	13.89	1.00	5.14	0.17	36.75	2.21
3900	40.65	2.53	50.95	2.92	13.81	1.03	5.13	0.18	36.67	2.27
4000	40.53	2.61	50.82	3.02	13.74	1.06	5.12	0.18	36.59	2.34
4100	40.40	2.70	50.69	3.11	13.67	1.10	5.12	0.19	36.51	2.41
4200	40.28	2.78	50.57	3.21	13.59	1.13	5.11	0.19	36.42	2.47
4300	40.16	2.86	50.44	3.31	13.52	1.16	5.10	0.20	36.34	2.54
4400	40.03	2.95	50.31	3.41	13.45	1.19	5.09	0.21	36.26	2.61
4500	39.91	3.03	50.19	3.51	13.38	1.22	5.08	0.21	36.18	2.69
4600	39.79	3.12	50.06	3.62	13.31	1.26	5.07	0.22	36.10	2.76
4700	39.66	3.21	49.93	3.72	13.25	1.29	5.06	0.22	36.02	2.83
4800	39.54	3.30	49.80	3.83	13.18	1.32	5.05	0.23	35.94	2.91
4900	39.42	3.39	49.67	3.94	13.11	1.35	5.04	0.24	35.85	2.98
5000	39.30	3.48	49.54	4.04	13.04	1.39	5.03	0.24	35.77	3.06
5100	39.17	3.57	49.41	4.16	12.98	1.42	5.02	0.25	35.69	3.14
5200	39.05	3.66	49.28	4.27	12.91	1.45	5.01	0.25	35.61	3.22
5300	38.93	3.76	49.15	4.38	12.85	1.49	5.00	0.26	35.53	3.30
5400	38.80	3.85	49.02	4.49	12.78	1.52	4.99	0.27	35.45	3.38
5500	38.68	3.95	48.88	4.61	12.72	1.55	4.98	0.27	35.36	3.46
5600	38.56	4.04	48.75	4.73	12.66	1.58	4.97	0.28	35.28	3.55
5700	38.44	4.14	48.62	4.84	12.60	1.62	4.96	0.29	35.20	3.63
5800	38.31	4.24	48.48	4.96	12.53	1.65	4.95	0.29	35.11	3.72
5900	38.19	4.34	48.35	5.08	12.47	1.68	4.95	0.30	35.03	3.80
6000	38.07	4.44	48.22	5.20	12.41	1.72	4.94	0.31	34.95	3.89

3.4 Radiation regions of an antenna

3.4.1 Definitions

The ultimate feature, or the mission, of an antenna is to create an electromagnetic field into the surrounding space. The properties of this particular field are by their very nature dependent on the distance from the antenna. The field that is generated by the antenna can be roughly divided into three regions.

Closest to the antenna stands the so called reactive near field, where the reactive fields, generated by the reactive part of the antenna input impedance, dominate over the radiating fields. If the eyes of a human being could be able to see the power in the reactive near field, it could be noticed with ease that, the power is actually just bumping back and forth, instead of radiating anywhere [3].

The role of the radiating fields becomes more dominant when moving away from the antenna. The distance, where the reactive and radiating powers become equally strong, determines the border of reactive and radiating near fields. For an antenna, whose maximum extent is D_a, the radiating near field region begins at distance r_1 from the antenna [3]:

$$r_1 = 0.62\sqrt{\frac{D_a^{\,3}}{\lambda}}, \tag{3.5}$$

where λ is the wavelength in free space. The radiating near field region is historically called the Fresnel region. In the Fresnel region, the field pattern is still dependent on the distance from the antenna. For comparison, the near field distance for an infinitely small current element can be calculated from $\lambda/2\pi$.

The region where the field pattern is no more distance-dependent is called the far field region, or more elegantly, the Fraunhofer region. The far field region can be considered to begin at distance [3]:

$$r_2 = \frac{2D_a^{\,2}}{\lambda}. \tag{3.6}$$

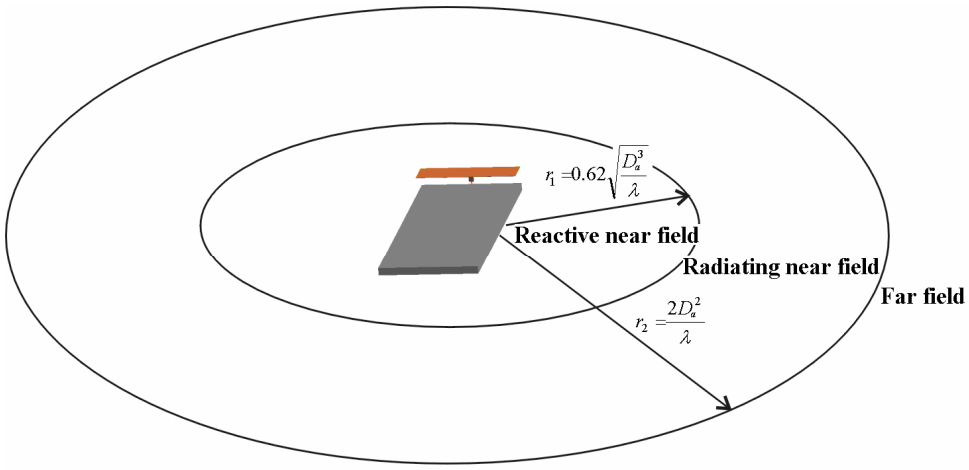

Figure 3.1Radiation regions of an antenna. D_a is the largest extent of the antenna.

Looking from this thesis' point of view, the interesting question is what actually happens when an object is situated in the different radiation regions of an antenna. It is quite intuitive that, it has no significance on the antenna operation, if an object stands in the far field region of the antenna. However, if dielectric material is brought to the close near field, it is certain, that not only the fields of the antenna affect the object substantially, but also the fundamental characteristics of the antenna are disturbed by the material. The object can be considered to be a part of the radiating system, as it alters the current distribution, and accordingly all the other parameters, of the antenna.

3.4.2 Radiation regions of handset antennas

In the case of the antenna-chassis combination of a mobile handset, the distances to near and far field from the antenna structure can be difficult to define. Although the largest dimension of the antenna element itself is in the order of 40 mm at frequencies not substantially higher than 1 GHz, the chassis, whose length is about 100 mm, works as the main radiator. At this point, it might be worth reminding that, in this thesis the dimensions of the studied antenna structures are 40 mm x 100 mm (width x length). Distances to near- and far field boundaries – when the largest dimension of the antenna is considered to be 40 or 100 mm - are plotted in Figure 3.2. The contributions of powers radiated by chassis and antenna element are strongly dependent on the used frequency, which, in turn, decides whether to regard 40 or 100 mm as the largest extent of the antenna. From Figure 3.2 it is easy to see that in a normal talk-position situation the user is always situated in the close near field of the antenna.

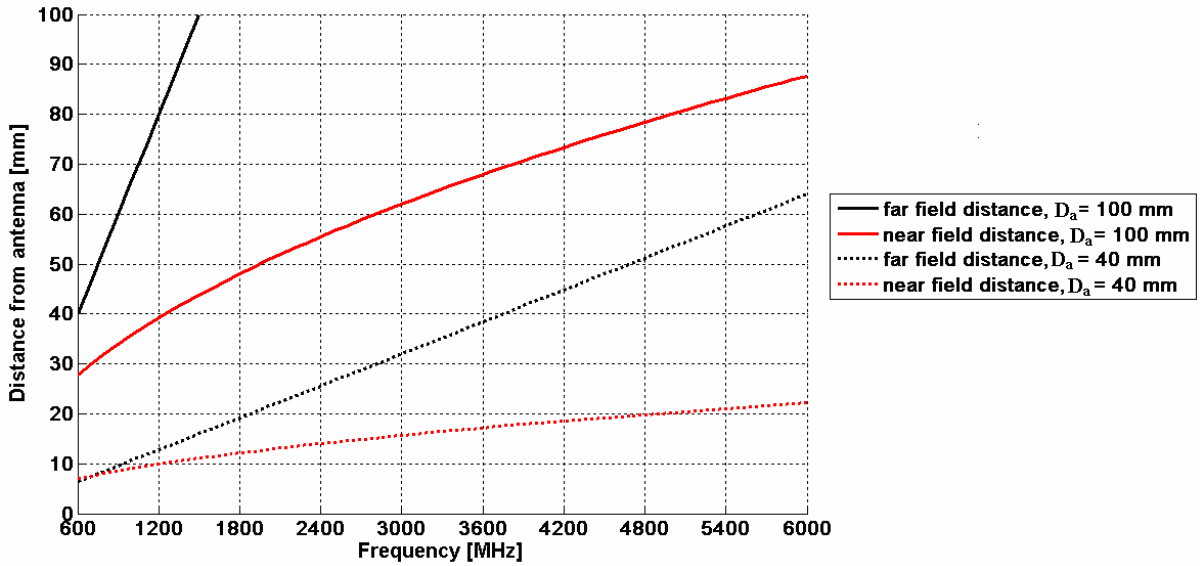

Figure 3.2 Distances to near field and far field boundaries from the antenna. D_a is 40 or 100 mm.

3.5 Antenna parameters in the vicinity of a user

From the graphs presented in Figure 3.2 it can be concluded that in mobile communications the user is commonly situated in the reactive near field of the antenna, meaning that the parameters of the antenna are very likely to be disturbed. In most cases these disturbances are very much case-specific, and an exact prediction of the problem is difficult. Nevertheless, some theoretical background of how the dielectric loading would affect the antenna operation can be found. In this section the treatment proceeds as follows: At first, an extension to the equivalent resonant circuit presented in Chapter 2 is introduced. This is followed by discussion about the fundamentals of the so called "perturbation theory", which was used also in [29] to predict the fields generated inside a human tissue.

3.5.1 Equivalent circuit including the effect of the user

The effect of the user can be modeled as an extension to the standard circuit model of a resonator (presented in Figure 2.2). In the extended model (Figure 3.3), losses caused by the user are modeled as the conductance G_{user}, while the parallel capacitance C_{user} symbolizes the reactive effects of the user; the existence of C_{user} can cause, for instance, disturbances in the resonant frequency of the antenna structure. A quick look at the definition of the resonant frequency of a resonator - commonly known to be $f_r = 1/2\pi\sqrt{LC}$ - leads to the trivial conclusion that the resonant frequency is lowered by the additional, user-originated, parallel capacitance C_{user}.

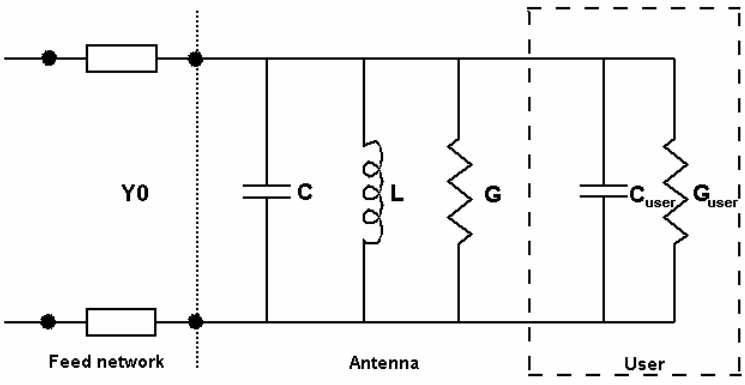

Figure 3.3 Equivalent circuit model of an antenna, including the effect of the user.

According to the new extended circuit model, losses caused by the power absorbed into the user can be considered to be described as a reduction in the unloaded quality factor Q_0, for which the definition can thus be re-written as

$$\frac{1}{Q_0} = \frac{1}{Q_{rad}} + \frac{1}{Q_d} + \frac{1}{Q_c} + \frac{1}{Q_{user}}, \tag{3.7}$$

where Q_{user} represents the losses caused by the user. Accordingly, the effect of the user can furthermore be included in Equation (2.18), which defines the radiation efficiency in terms of quality factors:

$$\eta_{rad} = \frac{Q_0}{Q_{rad}} = \frac{{Q_{rad}}^{-1}}{{Q_{rad}}^{-1} + {Q_c}^{-1} + {Q_d}^{-1} + {Q_{user}}^{-1}}. \tag{3.8}$$

3.5.2 Perturbation theory

The word "perturb" means to disturb or to change slightly. Perturbational methods are useful for calculating changes in some quantity due to small changes in the problem. Usually two problems are involved: the "unperturbed" problem for which the solution is known, and the "perturbed" problem, which slightly differs from the unperturbed one. Generally, the perturbation theory is used for example to describe the interaction between the fields of an electromagnetic resonator and materials inserted into it [2], [30].

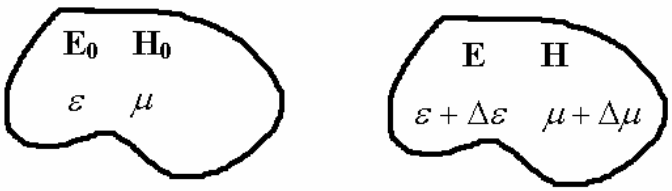

Figure 3.4 Perturbation of matter in a cavity. a) Original cavity, b) perturbed cavity.

The change of resonant frequency of a cavity due to a perturbation of the material in the cavity can be investigated by using perturbation theory. Figure 3.4a) represents the original cavity containing material with parameters ε and μ and Figure 3.4b) the same cavity with parameters $\varepsilon + \Delta\varepsilon$ and $\mu + \Delta\mu$. If E_0, H_0 and ω_0 represent the field and resonant frequency of the original cavity, and E, H and ω the corresponding quantities of the perturbed cavity, the change in the resonant frequency can be presented as [30]

$$\frac{\omega - \omega_0}{\omega} = -\frac{\int_V \left[\Delta\varepsilon\vec{E}\cdot\vec{E}_0^* + \Delta\mu\vec{H}\cdot\vec{H}_0^*\right]dV}{\int_V \left[\varepsilon\vec{E}\cdot\vec{E}_0^* + \mu\vec{H}\cdot\vec{H}_0^*\right]dV}. \tag{3.9}$$

Equation (3.9) states, that any increase in permittivity ε and/or in permeability μ can only decrease the resonant frequency. A further inspection of Equation (3.9) implies, that in case of non-magnetic materials ($\Delta\mu = 0$), such as human body tissue, the magnetic field term in the numerator disappears. On the other hand, at resonance, the stored electric energy equals the magnetic energy, and the denominator can be substituted by twice the value of the first term in the integral. These observations justify the consideration of only electric fields in problems, where all the materials are both low-conductivity and non-magnetic [2].

Equation (3.9) gives an exact formula for the change in resonant frequency, due to a change in ε and/or μ within a cavity. The major drawback of the formula is that it assumes zero losses, in other words requiring ε and μ to be real. The general formulation in the lossy case is given by

$$\frac{\omega-\omega_0}{\omega} = -\frac{\int_V \left[\left(\Delta\varepsilon - j\Delta\sigma_{eff}/\omega\right)\vec{E}\cdot\vec{E}_0 + \Delta\mu\vec{H}\cdot\vec{H}_0\right]dV}{\int_V \left[\left(\varepsilon - j\sigma_{eff}/\omega\right)\vec{E}\cdot\vec{E}_0 + \mu\vec{H}\cdot\vec{H}_0\right]dV}, \qquad (3.10)$$

where σ_{eff} denotes the original effective conductivity of the material and $\Delta\sigma_{eff}$ the perturbed conductivity. Obviously, if both σ_{eff} and $\Delta\sigma_{eff}$ are not identically zero, ω and ω_0 are complex [30]. The change in the imaginary part of the resonant angular frequency can be interpreted as a change in the loaded quality factor of the resonator, and therefore the loss mechanisms for the interaction can be defined [2].

3.6 SAR generation - suggested theories

Even if the theory of how radiowaves propagate in a lossy material is quite well known, the connection between the original external electric field generated by a mobile terminal antenna and the field inside a dielectric tissue is not fully explained. The related studies have mostly focused on determining the *SAR* characteristics related to a certain problem, while the general energy absorption mechanism has been left with less consideration. In addition, results of studies concerning the issue [29], [31], [32] are quite diverging.

The general energy absorption mechanism in the close near field of dipole antennas above 300 MHz was studied in [31]. The goal of this study was to find a relation between the free space field strengths of the antenna and the corresponding *SAR* values. The starting point was to examine the behavior of magnetic fields, since electric fields suffer from structural changes in the vicinity of dielectric material, while the current distribution was considered to be less affected. Research results in this paper suggested that the main absorption mechanism can be described by surface

currents induced by the magnetic fields. *SAR* values were found to be mainly proportional to the square of the incident magnetic field strength, which led to the conclusion that the spatial peak *SAR* is related to the antenna current. Consequently, it was concluded that coupling of electric fields would be of minor importance.

The conclusions presented in [31] were only partly confirmed in [32], where the effects of the fat layer on microwave near-field radiation to the abdomen of a full-scale human body model were studied by placing a dipole antenna operating at 915 MHz beside a homogenous muscle phantom with and without a covering fat layer. Without the fat layer, the peak *SAR* was located near the antenna feed point, which followed the assumptions of [31]. However, with the 0.8 and 2.6 cm fat layers on top of the muscle phantom, high *SAR* values were found close to the ends of the dipole, which could not be explained by the theory presented in [31]. Due to the dielectric properties of muscle (high ε_r and σ_{eff}) and fat (low ε_r and σ_{eff}), *SAR* values without the fat layer were shown to be clearly higher than with the fat layer. Nevertheless, no reason for the different peak *SAR* locations was suggested.

Furiously seeking for a deeper understanding of the issue, partly motivated by the controversial results of [31] and [32], the general absorption mechanism in the human tissue was further investigated in [29]. The initial approach was – contrary to the one used in [31] - to pay the main attention to the behavior of the electric fields of small antennas nearby lossy materials. A half-wave dipole and a patch antenna at 900 MHz were placed beside a lossy dielectric half-space that consisted of several materials with different dielectric parameters. The interaction between the fields of an antenna, and the material inserted in it, was described by using perturbation theory, which is commonly used for determining changes in the resonant frequency of a resonator due to a perturbation of the material inside or close to the resonator cavity. The change in the resonant angular frequency from the original resonant frequency to the perturbed one can be interpreted as a change in the loaded quality factor of the antenna, and hence the loss mechanism for the interaction can be defined. As a starting point, it was concluded that because all the tissues in human body are non-magnetic (the relative permeability $\mu_r = 1$) and because magnetic fields do not interact with non-magnetic materials, the treatment of electrical fields alone was considered adequate.

The main message of [29] was that the interaction of electric fields and dielectric materials can be described by the boundary conditions derived from Maxwell's equations: at a dielectric boundary, the electric field components normal to the surface are related as

$$\varepsilon_1 \vec{E}_{1n} = \varepsilon_2 \vec{E}_{2n} . \qquad (3.11)$$

On the other hand, the tangential field components are equal on adjacent sides of the boundary:

$$\vec{E}_{1t} = \vec{E}_{2t}. \tag{3.12}$$

The application of the boundary conditions of electrical fields to the process in question led to a conclusion that the peak *SAR*, in fact, is not related to antenna current, which had pretty much been the dominant conception. Instead, the locations of *SAR* maximums were explained by exploring the real part of the tissue permittivity ε_r and its effect on the electric field components perpendicular and parallel to the surface of the tissue. In general, the process was divided into two basic cases: for tissues whose ε_r is high, such as muscle, the electric field components perpendicular to tissue surface is significantly attenuated at the tissue surface, and thus the *SAR* maximums were found in a location where the total original electric field was moderate, but the component parallel to the surface was significant. For low-permittivity tissues, like fat, the *SAR* maximums were found close to locations where the electric field was at strongest also in free space, because in low- ε_r tissues the attenuation of the perpendicular components is small.

4 SIMULATION STUDIES ON NEAR-FIELD DISTRIBUTIONS

4.1 Introduction

A review of studies ([29], [31], [32]) concerning the general mechanisms of interaction between antenna and user was given in Chapter 3. As explained, results from these studies don't provide us with a fully consistent explanation about the issue. Especially conclusions made concerning the general energy absorption mechanism in human tissue have been quite diverging. Results obtained in [31] suggested that the main absorption mechanism can be described by currents induced to the surface of human tissue by magnetic fields. *SAR* values were found to be mainly proportional to the square of the incident magnetic field strength, which led to the conclusion that the spatial peak *SAR* is related to antenna currents. Consequently, it was concluded that dielectric losses due to the coupling of electric fields would be of minor importance. In [29], it was concluded that that the peak *SAR*, in fact, is not related to antenna currents, which had pretty much been the dominant conception. Instead, the locations of *SAR* maximums were explained by exploring the real part of tissue permittivity ε_r' and its effect on the electric field components perpendicular and parallel to the surface of the tissue.

In addition to the limited understanding on the general energy absorption mechanism in human tissue, studies that are related to user interaction have most commonly been very case-specific, concentrating simply on determining certain parameters related to a specific problem. As a rare exception, work done in [16] provided results from an extensive simulation study on the behavior of bandwidth, *SAR* and efficiency of a mobile terminal antenna in a wide frequency range. Many important and interesting conclusions were given in that paper. However, many things were still left without a proper explanation. The main reason for the difficulties in explaining each and every

phenomenon in [16] was considered to be the excessive complexity of the used simulation models, which included two different antenna models, two different hand models and the SAM phantom as the head model. Also the wide frequency range in question made things more complicated.

The studies that are reported in this chapter are motivated by the lack of full understanding on the mechanisms of how antennas actually interact with the user. The main goal is to improve the understanding on the basic absorption mechanisms of microwave energy in human tissues. On the basis of the achieved knowledge, the behavior of different user interaction-related parameters of an antenna is further studied (later in Chapter 5); these studies are in many respects a continuation of the work reported in [16].

This chapter is organized in the following way. First, in Section 4.2, the used antenna model is introduced, and properties of this particular antenna in free space are discussed to provide the reader with a sufficient background and points of comparison with the user interaction studies reported in the later parts of the thesis. In Section 4.3, the effects of dielectric material on the field distributions of the antenna are studied by a very simple model; field distributions inside and nearby a dielectric half space situated beside the antenna are studied as a function of different parameters. All the presented results in this chapter (as well as in all the coming chapters) are based on simulations that have been carried out with a commercial FDTD-based software SEMCAD-X [33].

4.2 Antenna model for the simulations

The versatility and on the other hand the simplicity of the structure provided motivation for the use of a coupling element based antenna structure in the user interaction studies of this thesis. Coupling element structures offer at least two significant features that are advantageous in studies that concern interaction with user: The effect of phone chassis can be seen in the results and separated from other factors with ease, since the antennas are from the very beginning designed to optimize coupling between antenna element and chassis. On the other hand, coupling element based antennas provide a unique chance to study user interaction in a wide frequency range using a single antenna, because the same structure can and is actually meant to operate in numerous systems and frequencies.

The coupling element of the antenna model that is used in the basic user interaction studies of this chapter is placed fully on top of the ground plane, whose dimensions are 3 x 40 x 100 mm^3 (Thickness x width x length). The coupling element is simply rectangular in shape, has a height of

6.6 mm and occupies a volume of only 2.9 mm^3. The geometry of the antenna model is presented in Figure 4.1. The same antenna model was used in [16], so results obtained in this work can be straightforwardly compared with the results presented in that paper.

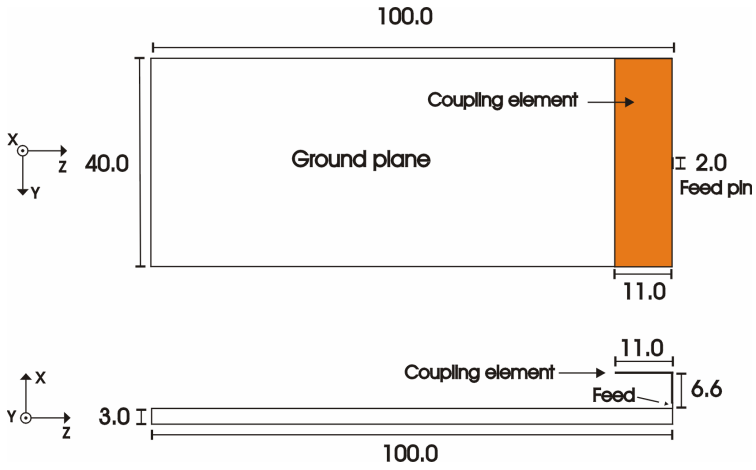

Figure 4.1 Geometry of the antenna model. Dimensions are in millimeters.

To get a reasonable background and points of comparison for studies on interaction between antenna and user, properties of the antenna model in free space are first introduced in this section (4.2). The treatment includes discussion about the behavior of reflection coefficient, bandwidth potential, current distribution and distributions of electric and magnetic near fields. Radiation efficiency, which is an important factor in user interaction studies, is left out from the discussion of this section, since in free space the used antenna model has always radiation efficiency of 100 % due to the fact that all parts of the antenna are modeled as PEC (Perfect Electrical Conductor), meaning that no losses occur anyway. As the basis for this thesis is in many respects formed on the results presented in [16], the results in this section haven been partly presented already in that paper.

4.2.1 Reflection coefficient

Broadly speaking, reflection coefficient describes how big share of the signal that is fed into the input port of an antenna is accepted by the antenna. In case of internal mobile phone antennas, a feasible reflection coefficient is typically achieved by either shaping the antenna element to resonate at the operating frequency, or by using a separate matching circuit to tune the resonance to the desired frequency. The latter option is applied with coupling element antennas, since the antenna element is not designed to be self-resonant. However, in this thesis matching circuits are excluded from the antenna model mainly for two reasons. The first reason is that matching circuits would increase the complexity of the model, and the second is that most of the parameters that are

interesting from the user interaction point of view don't even take mismatching into account by their definition.

Even if said that matching is not a great issue of interest in this thesis, inspecting the reflection coefficient without the matching circuitry provides valuable information about the performance of the antenna, since many important parameters are strongly dependent on whether the chassis is at resonance or not. Reflection coefficient of the used antenna without matching is presented in Figure 4.2. Notches at 1200 MHz and 2400 MHz are caused by the first and the second order resonances of the chassis of the antenna. Higher order resonances are not clearly seen in this curve.

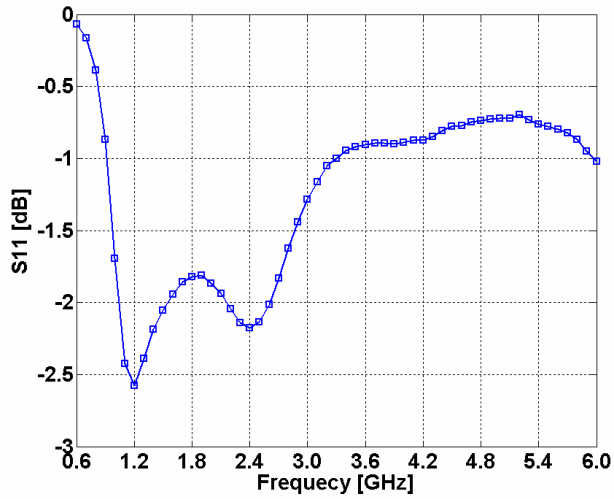

Figure 4.2 Reflection coefficient of the used antenna model in free space.

4.2.2 Bandwidth

As already mentioned, coupling of signals to chassis wavemodes is most significant when the operating frequency is close to the resonant frequency of the chassis. At these frequencies most of the radiated power is radiated by the chassis, meaning that from the radio frequency signal point of view, the antenna seems to be somewhat larger in size than just the antenna/coupling element. From the basis of the theory presented in Chapter 2, we know that with larger antennas wider impedance bandwidths are possible to achieve. These thoughts are supported by Figure 4.3, where the impedance bandwidth that can be achieved, or in other words the bandwidth potential of the antenna, with different center frequencies is presented. The bandwidth potential curve in Figure 4.3 is obtained by first matching the input impedance of the antenna with two lumped elements (i.e. single resonant matching) and then calculating the relative bandwidth according to $|S_{11}| \leq -6$ dB matching criterion. Especially at low frequencies, the effect of the chassis to the achievable

bandwidth is extremely high. For example, around the first resonance of the chassis at 1200 MHz, the achievable relative bandwidth is about 24 %, and at 1800 MHz only about 8 %.

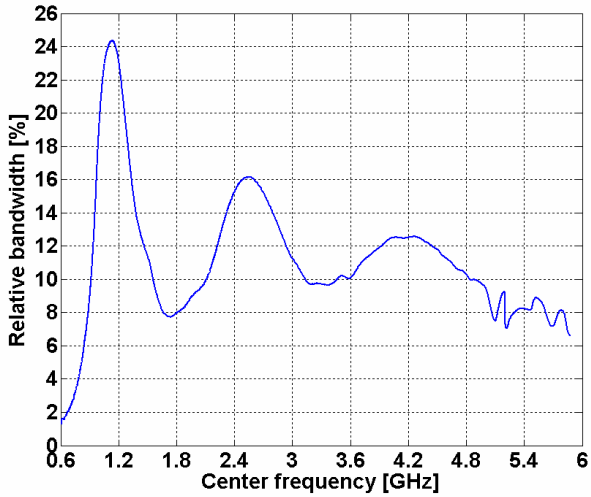

Figure 4.3 Bandwidth potential of the antenna model [16].

4.2.3 Current distributions

Before going deep into the details of the distributions of electric and magnetic fields, let us spend a while looking at the current distributions of the antenna in question. After all, fields generated by any antenna can be characterized by the current distribution of the antenna [3]. In general, current distribution of the chassis of a mobile phone is known to be largely of similar kind to that of a thick dipole. Figure 4.4 illustrates current densities in free space on the surface of the chassis backside at 1200 MHz, 2400 MHz and 5000 MHz (compare with Figure 2.3). To clarify what is meant by chassis backside, see the top picture of Figure 4.5. At 1200 MHz, the current density has one maximum in vertical direction corresponding to a half wave dipole-type current distribution. At 2400 MHz, the effective length of the chassis is close to a full wave length, meaning that two current maxima fit into the chassis. At 5000 MHz, two current maxima are clear at the lower half of the chassis, but in the upper half, the contribution of the coupling element to the current distribution is already very large somewhat obscuring the wavemodes of the chassis. At each frequency, the concentration of current to the edges of the chassis is clear, as well.

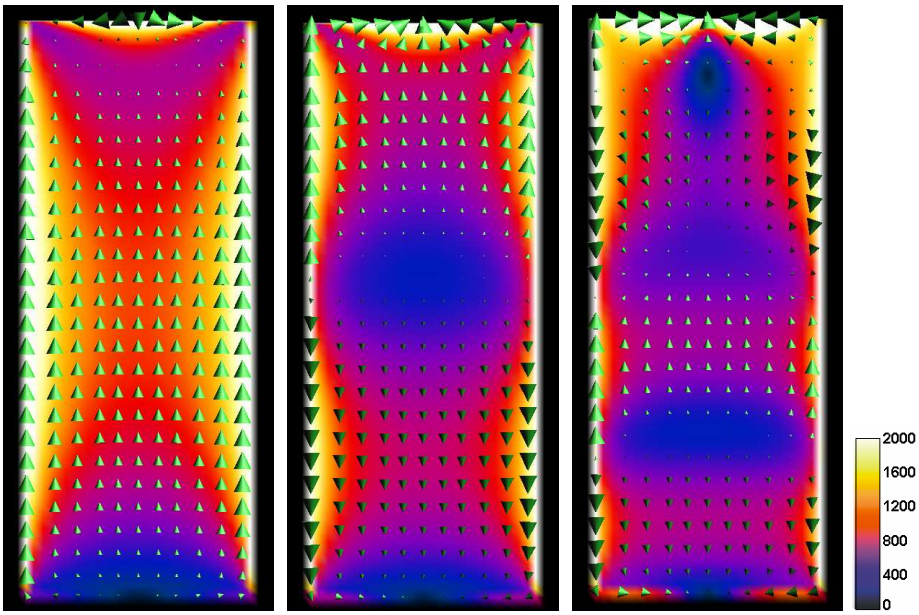

Figure 4.4 Current densities [A/m^2] on the surface of the chassis backside (opposite to the coupling element, see Figure 4.5 for clarification) in free space at 1200 MHz, 2400 MHz and 5000 MHz.

Due to strong coupling of signals at chassis resonances, also amplitudes of current integrals on the surface of the chassis have maxima at the resonance frequencies. The normalized surface integral of chassis current is plotted in Figure 4.5. The current integral was first calculated on the lower half of the chassis backside, and then the results were normalized separately at each frequency point to the integral calculated over the whole backside of the chassis ($I_{normalized} = I_{half} / I_{whole} \times 100\%$). This way, the effect of coupling element originated currents could be minimized. With the used coupling element based antenna, the largest value for normalized surface current integral is a little bit more than 12 % at the first order resonance (1200 MHz). Also the second, the third and even the fourth order resonances can be separated from the curve at frequencies around 2400 MHz, 3800 MHz and 5400 MHz, respectively. However, as the wavemodes of the coupling element grow into the main contributor at higher frequencies, the high-order resonances get less significant accordingly.

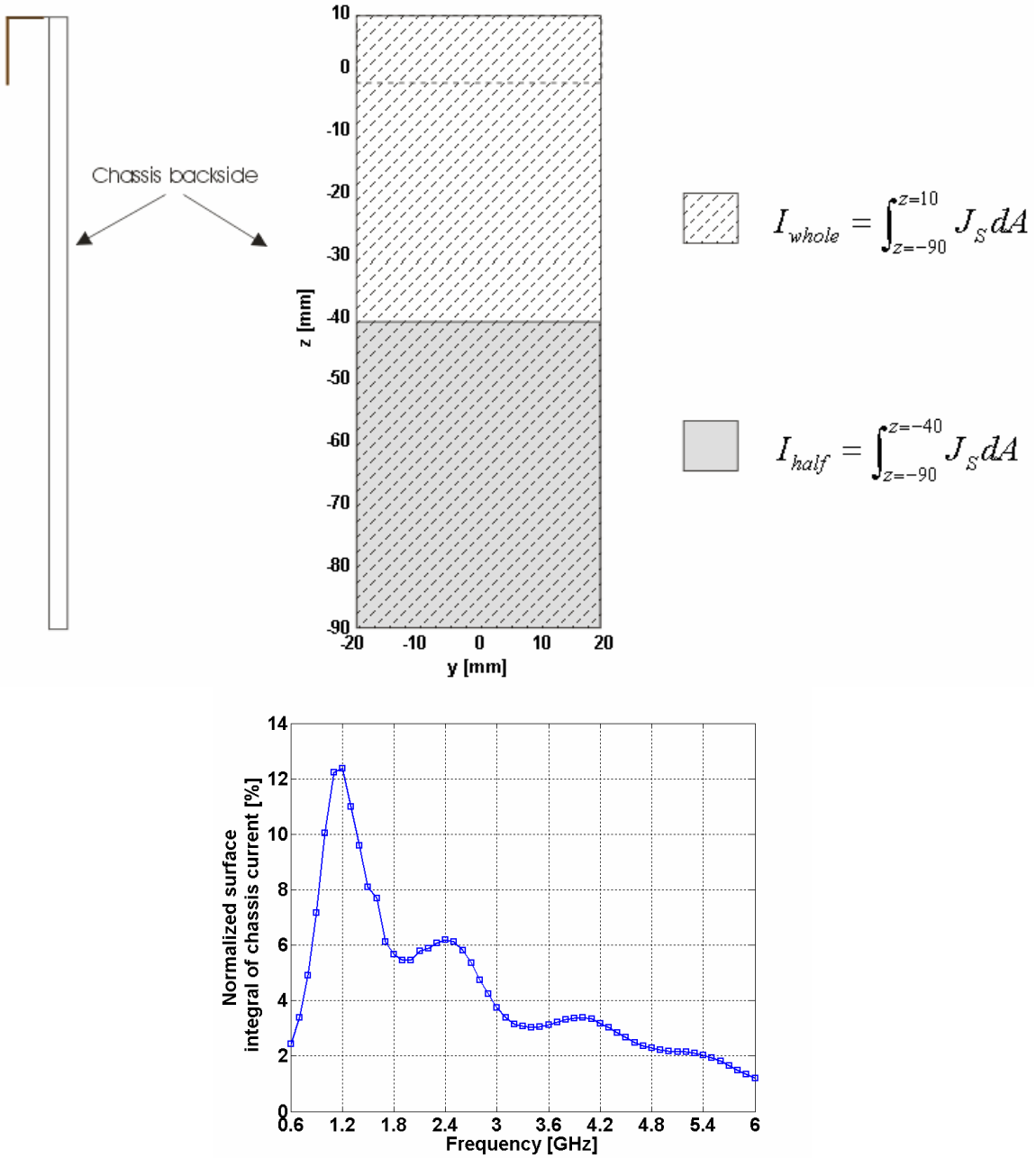

Figure 4.5 Normalized surface integral of chassis current [16]. $I_{normalized} = I_{half}/I_{whole}$ *x 100%.*

4.2.4 Near field distributions

The issue of how electromagnetic fields and dielectric materials interact with each other was discussed in Chapter 3. Losses inside dielectric material were said to be caused by the electric field that is generated inside the material. However, even if the general mechanisms of how electromagnetic fields inside a dielectric material interact with the material are quite well known, clear connections between the original external fields and the fields that are generated inside the material have still been left without an extensive explanation. Conclusions drawn in related studies

(reviewed earlier in Section 3.6) have been quite diverging, some of them telling that antenna current and the incident magnetic field are the main interaction mechanism while conclusions from other studies ignore the inspection of magnetic fields paying the whole attention to examination of electric fields alone. In the following sections the issue is re-examined to extend the understanding of the process. As a starting point, in this section the field distributions are studied in free space. The treatment is then extended to examination of fields when objects with different material parameters are placed nearby the antenna.

The distributions of electric and magnetic fields in free space on a plane parallel to antenna chassis (*xz*-cut) are plotted in Figure 4.6. The magnitudes of the fields are illustrated in colors, and the arrows show the direction of the corresponding components. In each field distribution figure in this section as well as in each of the preceding sections, colors that illustrate magnitudes of the fields are fully comparable. In electric field plots, 0 dB corresponds to 2 kV/m field strength and in magnetic field plots 0 dB corresponds to 20 A/m field strength.

All values are normalized to 1 W input power. The fields are recorded at 1200 MHz, 2400 MHz and 5000 MHz. 1200 MHz is the first and 2400 MHz the second resonant frequency of the chassis and at those frequencies the contribution of chassis wavemodes to total radiated power is most significant and thus the thick dipole type operation is clearly seen. At 5000 MHz the main contributor are the wavemodes of the antenna/coupling element.

E-field at 1.2 GHz, 0 dB = 2 kV/m

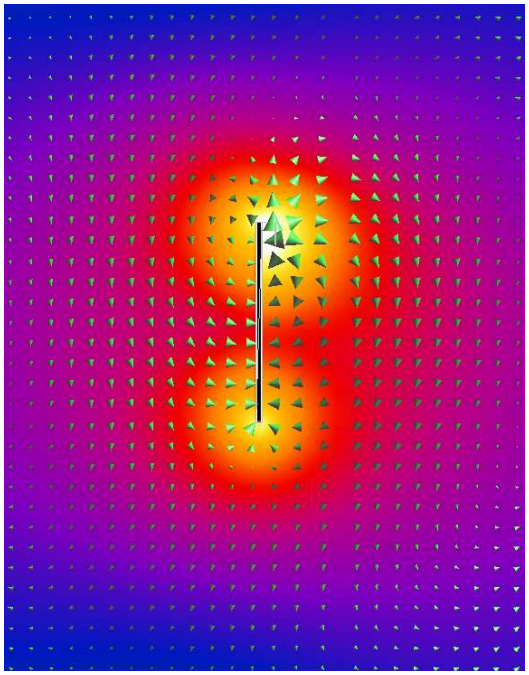

H-field at 1.2 GHz, 0 dB = 20 A/m

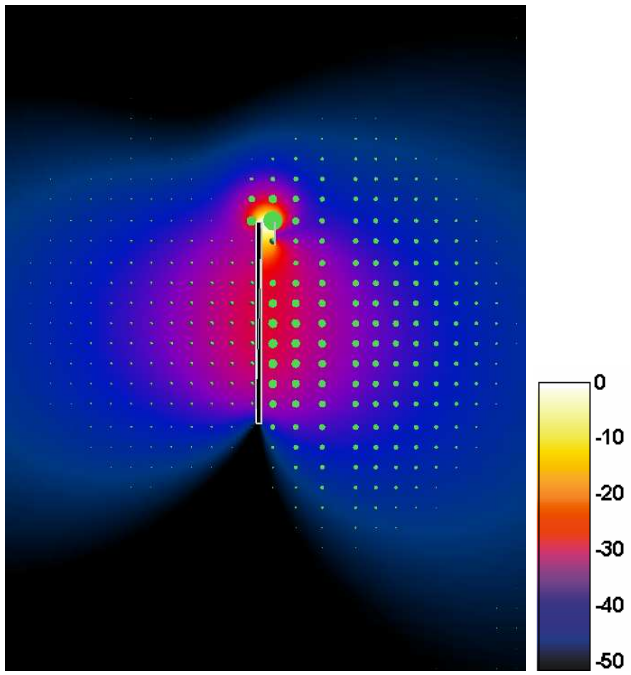

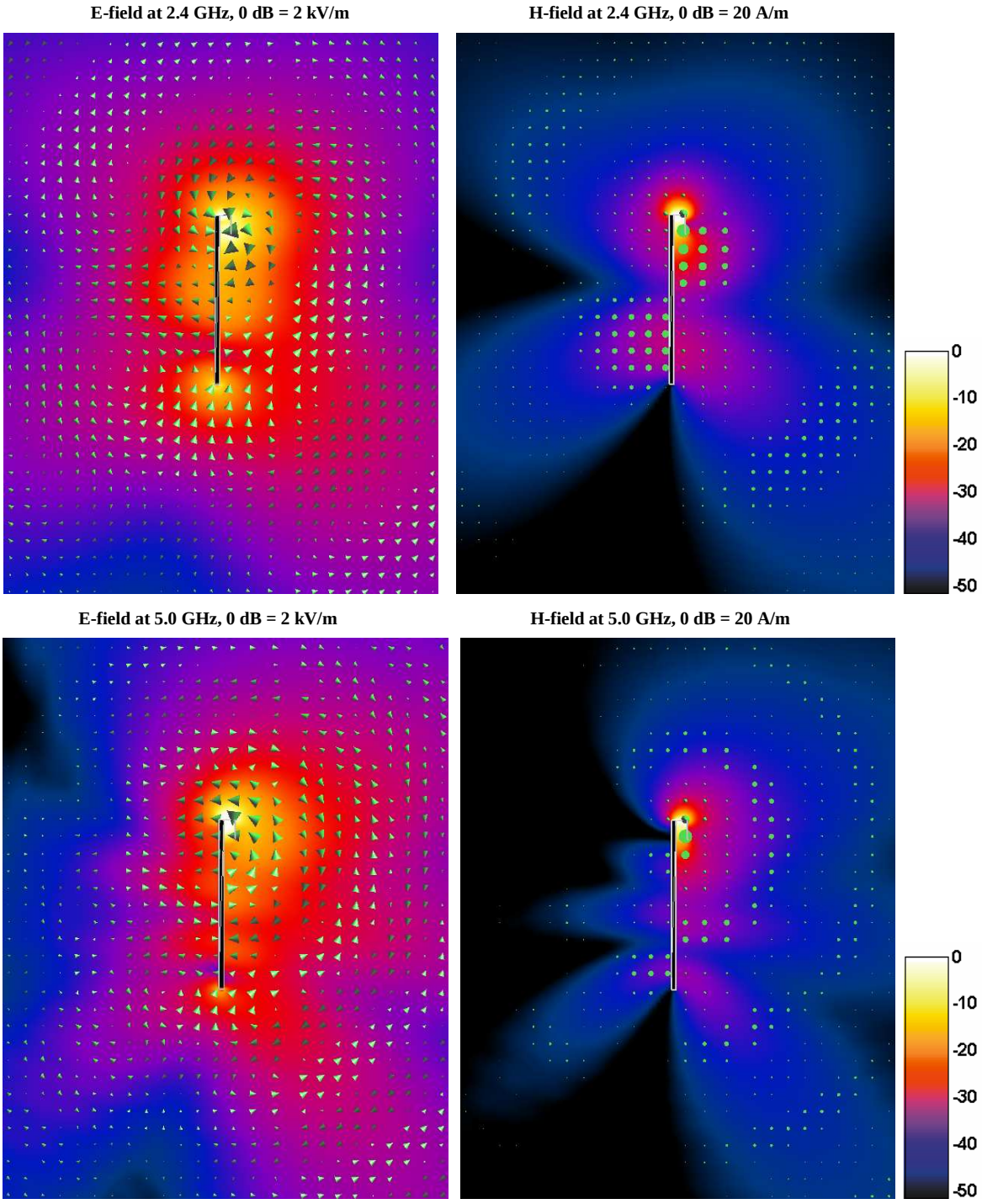

Figure 4.6 Field distributions on xz-cut (y=0 mm) in free space. The magnitudes of the fields are illustrated in colors, and the arrows show the direction of the corresponding components. All values are normalized to 1 W input power.

At 1200 MHz the electric field is strong around both ends of the chassis and also the directions of the electric field are similar to those of a half-wave dipole. Magnetic field, in turn, is significant around the vertical (*z*-direction) center point of the chassis. At 2400 MHz the length of the chassis is rather close to a full wavelength, meaning that current has two maxima in *z*-direction along the

chassis and a minimum close to the center point of the chassis. Accordingly, electric field has a strong area around the center point of the chassis in addition to the strong areas at the ends of the chassis, and magnetic field high values around areas in which the current in the chassis is high. At 5000 MHz both electric and magnetic fields are strongest around the coupling element while the influence of the chassis wavemodes is already quite weak. Connections between currents and fields of the antenna can be noticed by comparing Figures 4.4 and 4.6.

4.3 Field distributions inside and near dielectric material

Studies on interaction between the fields of an antenna inside and near dielectric material were started with exploring the electric and magnetic fields when a half space filled with material having different dielectric parameters was placed beside the antenna. In the beginning, the simulation model was kept as simple as possible to ease the understanding of the process. On the contrary, for instance in [16], it was found too difficult to understand and explain all the phenomena that came out in the studies; realistic talk-position model including head and hand models was considered somewhat too complex to be able to understand causes for each and every phenomena. So, partly motivated by the unclear issues of [16], the simulation models were simplified as much as possible.

As the first step, the effect of dielectric material on the parameters of the antenna was studied by a simple simulation model which consisted of the antenna and a dielectric block placed near the antenna. The geometry of the simple simulation model is presented in Figure 4.7. Dimensions of the dielectric block are 200 x 322 x 360 mm^3 ($x \times y \times z$). Distance between the ground plane of the antenna and the dielectric block is denoted by d. Different values for the real part of permittivity ε_r' and effective conductivity σ_{eff} of the block were used. In the beginning, values for ε_r' and σ_{eff} didn't model any "genuine" human tissues (see Section 3.3). At first in Section 4.3.1, effects of changes in ε_r' of the material are examined by keeping effective conductivity zero. In Section 4.3.2 results of simulations made with different values of σ_{eff} are analyzed. The frequency dependence of values for human tissues was not considered in simulations made in this section.

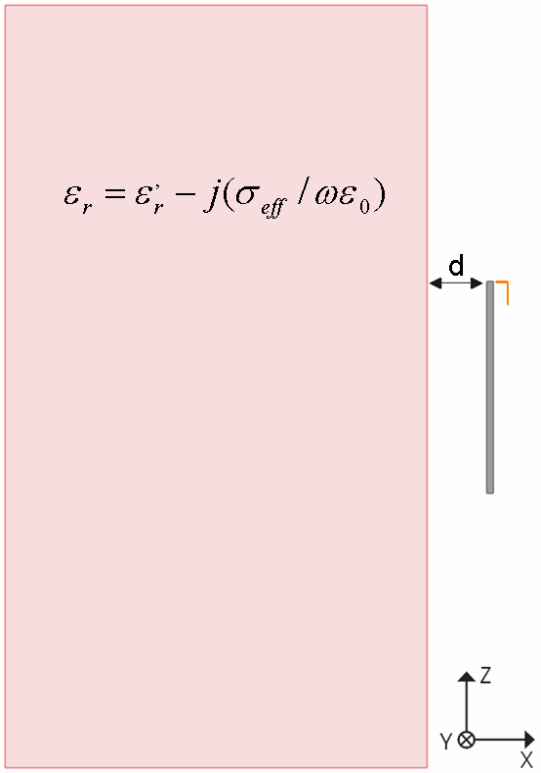

Figure 4.7 Geometry of the simulation model Dimensions of the dielectric block are 200 x 322 x 360 mm^3 ($x \times y \times z$).

4.3.1 Effect of real part of permittivity ε_r'

The effect of the dielectric block on the field distributions of the antenna was first studied by changing the permittivity of the block but keeping the distance between the block and the ground plane of the antenna fixed. In order to study purely the effects of permittivity, conductivity was set to zero, meaning that no losses occurred. Distributions of electric and magnetic fields when the distance between the dielectric block and the ground plane of the antenna was 5 mm, are plotted in Figures 4.8 - 4.13 (at frequencies 1200 MHz, 2400 MHz and 5000 MHz, respectively) with four different values of permittivity (ε_r' = 1, 5, 20 and 50). The case when the value of permittivity equals unity (i.e. ε_r' = 1) corresponds to free space situation and it is also plotted with the outline of the dielectric block to ease the comparison between the fields with different permittivity values.

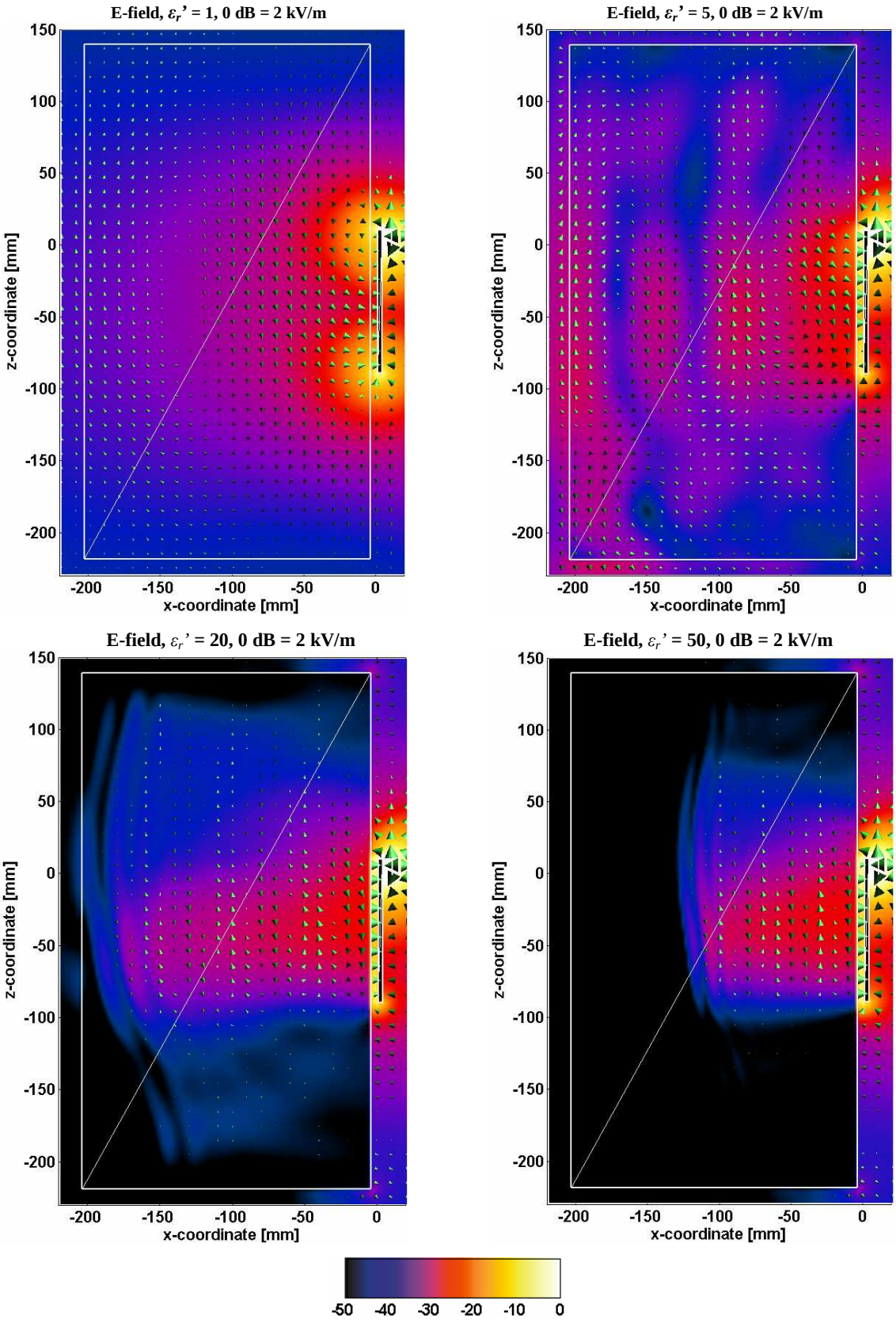

Figure 4.8 E-field distributions at 1200 MHz on xz-cut (y=0 mm) when a dielectric block is placed at a distance d = 5 mm from the antenna. Real part of permittivity ε_r' is 1, 5, 20 and 50. Effective conductivity σ_{eff} = 0.

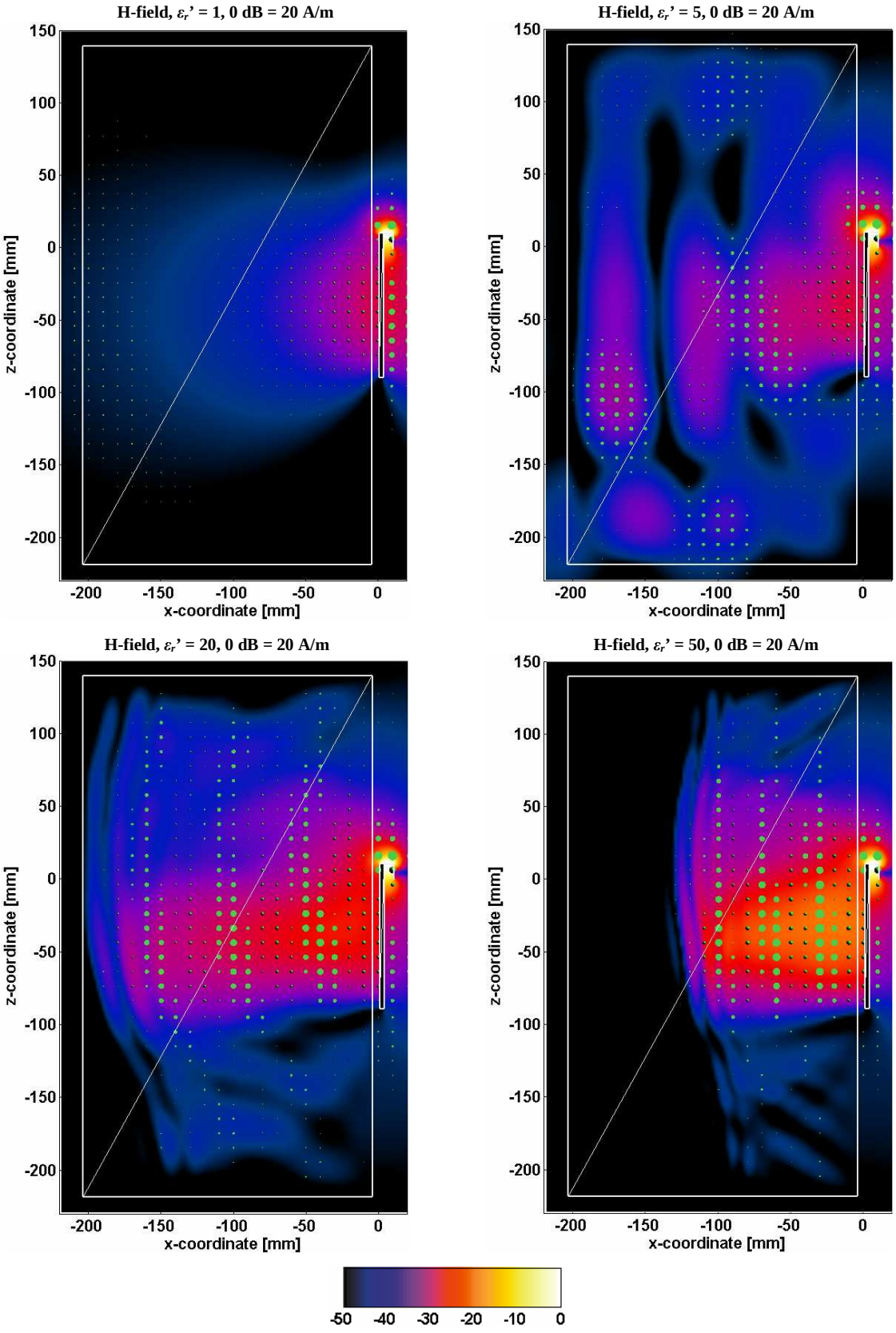

Figure 4.9 H-field distributions at 1200 MHz on xz-cut (y=0 mm) when a dielectric block is placed at a distance d = 5 mm from the antenna. Real part of permittivity ε_r' is 1, 5, 20 and 50. Effective conductivity σ_{eff} = 0.

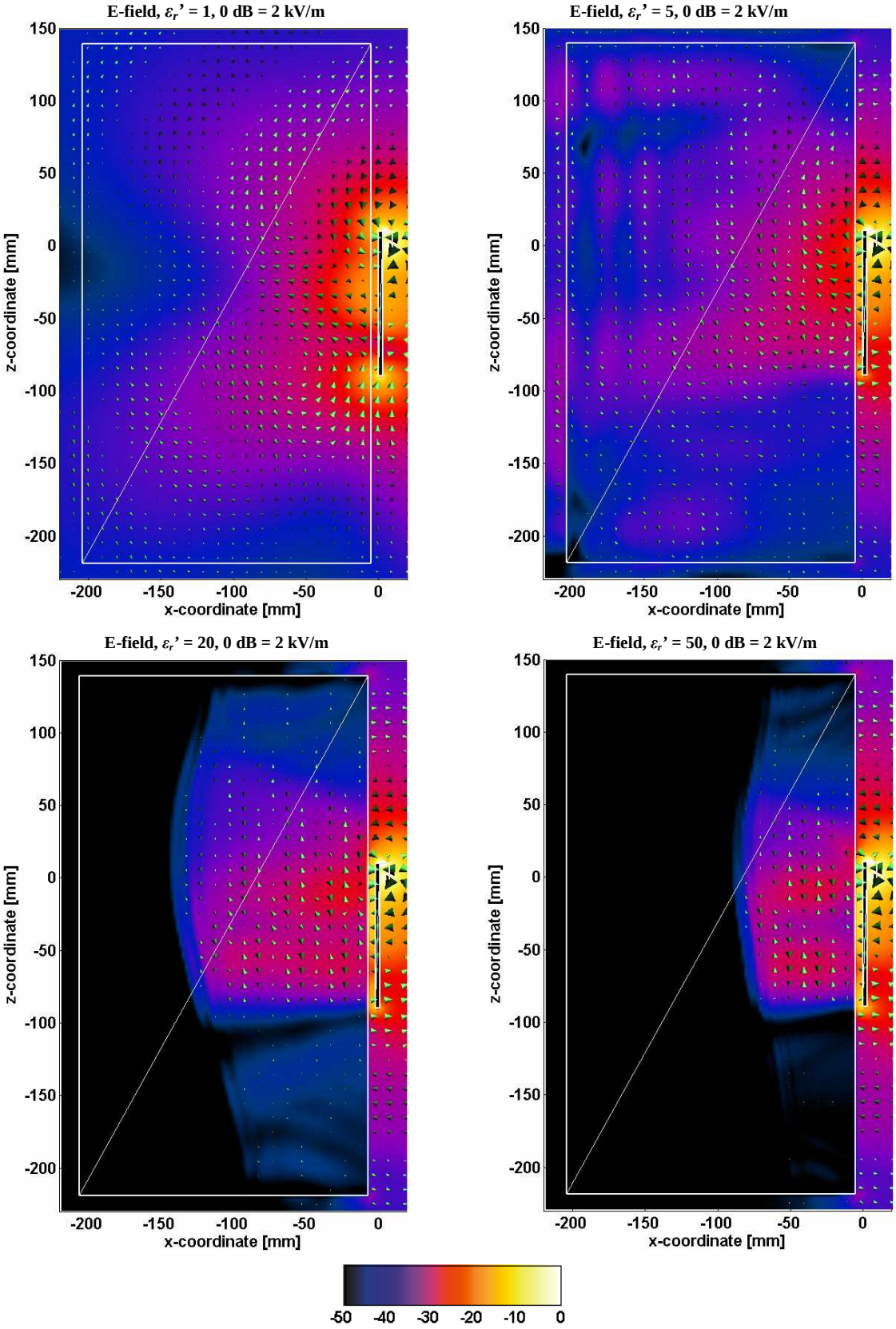

Figure 4.10 E-field distributions at 2400 MHz on xz-cut (y=0 mm) when a dielectric block is placed at a distance d = 5 mm from the antenna. Real part of the permittivity ε_r' is 1, 5, 20 and 50. Effective conductivity σ_{eff} = 0.

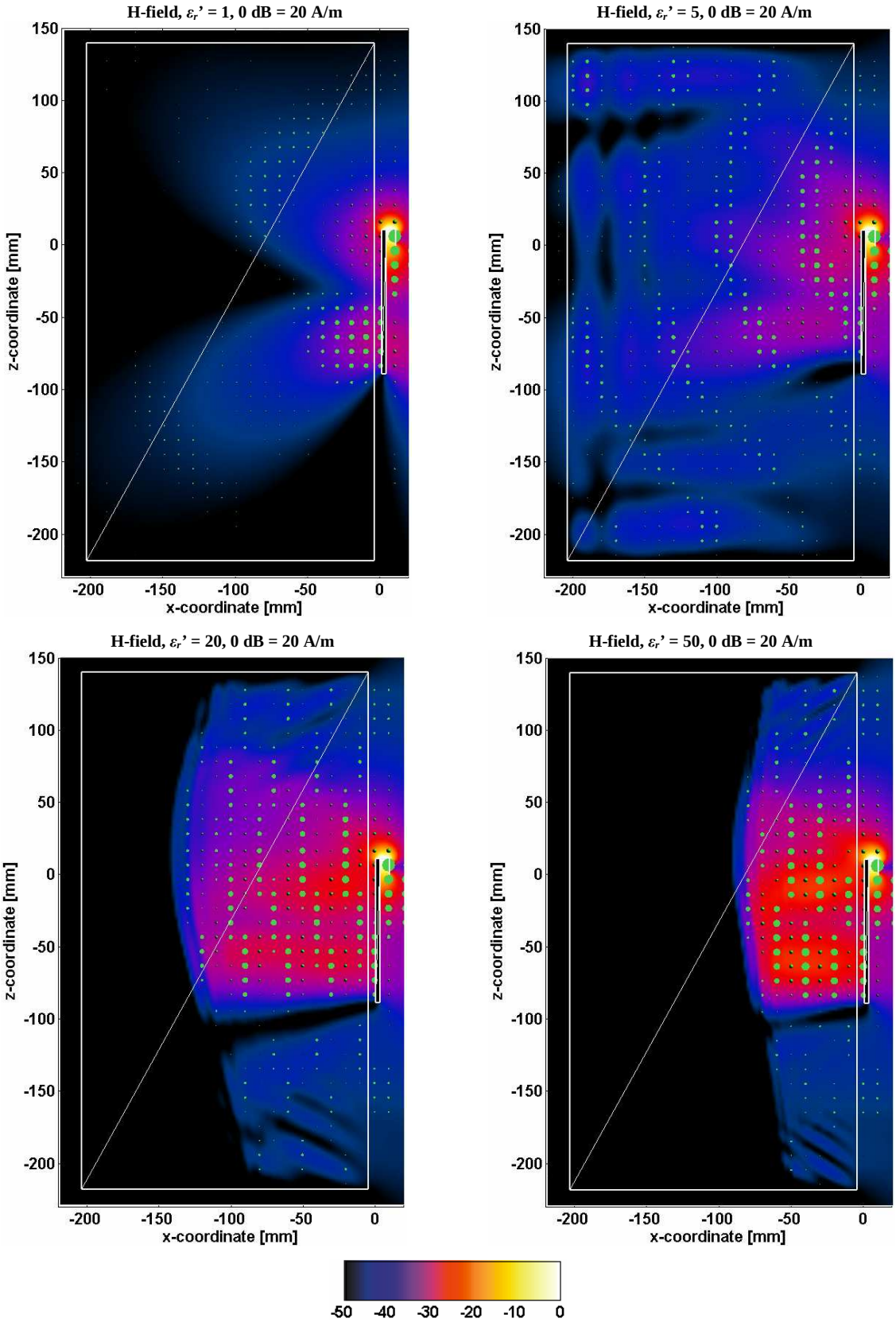

Figure 4.11 H-field distributions at 2400 MHz on xz-cut (y=0 mm) when a dielectric block is placed at a distance d = 5 mm from the antenna. Real part of the permittivity ε_r' is 1, 5, 20 and 50. Effective conductivity σ_{eff} = 0.

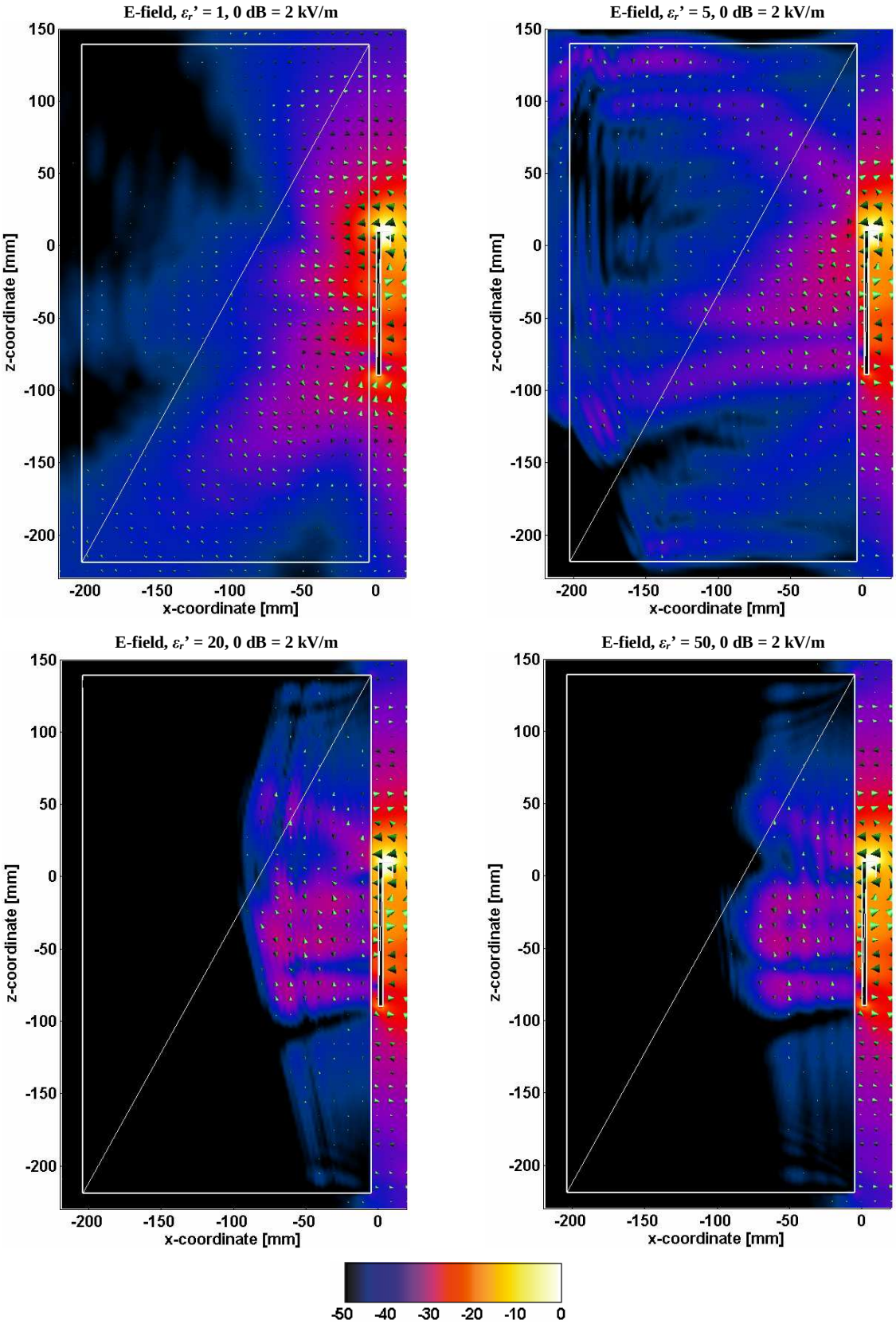

Figure 4.12 E-field distributions at 5000 MHz on xz-cut (y=0 mm) when a dielectric block is placed at a distance d = 5 mm from the antenna. Real part of the permittivity ε_r' is 1, 5, 20 and 50. Effective conductivity σ_{eff} = 0.

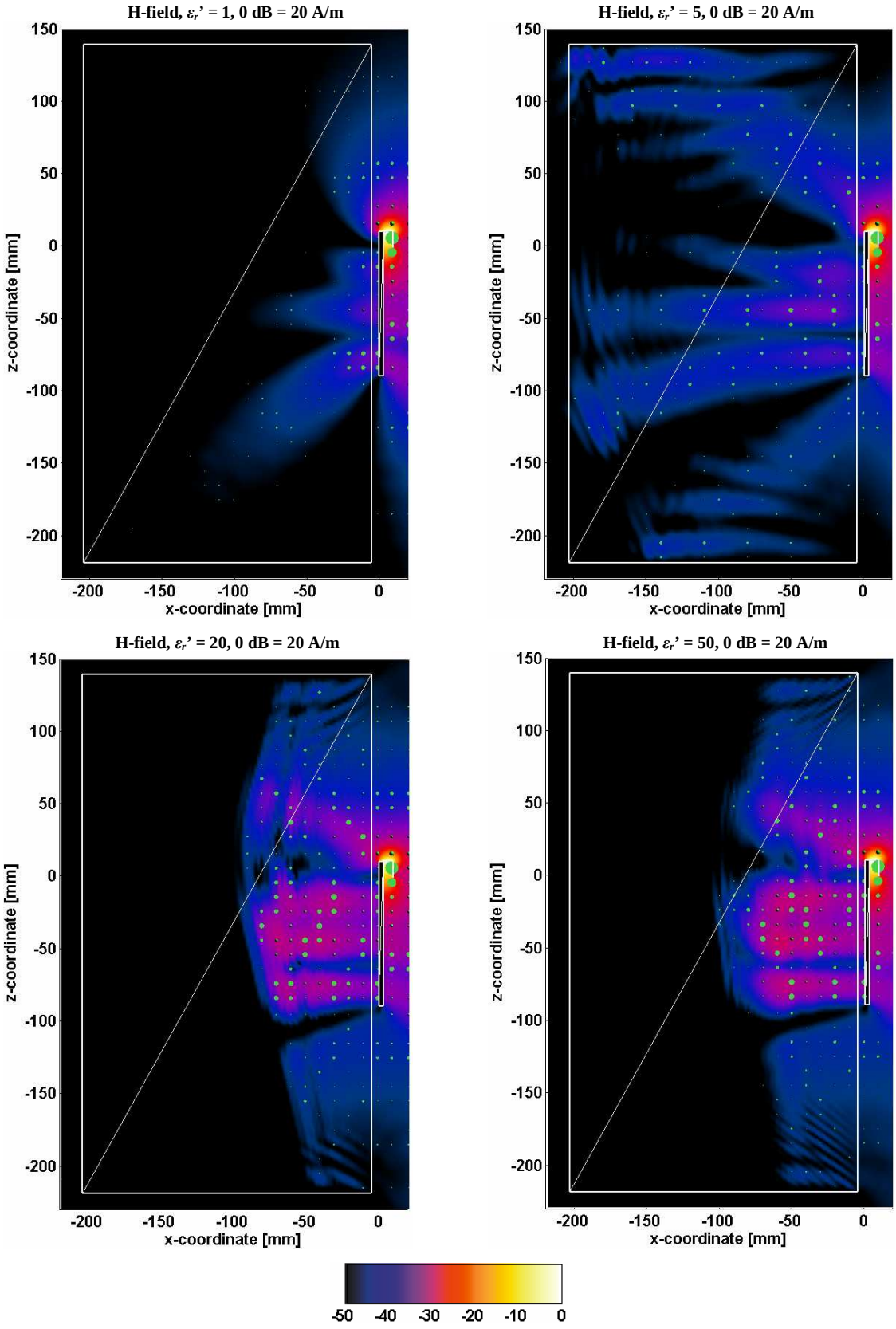

Figure 4.13 H-field distributions at 5000 MHz on xz-cut (y=0 mm) when a dielectric block is placed at a distance d = 5 mm from the antenna. Real part of the permittivity ε_r' is 1, 5, 20 and 50. Effective conductivity σ_{eff} = 0.

Two important observations can be made based on Figures 4.8 - 4.13: at first, as the permittivity of the dielectric block increases, the directions of the electric fields inside the block are forced to turn more and more parallel to the surface of the block. This can be explained by Maxwell's boundary conditions (shown in Equations (3.11) and (3.12)) for electric field components parallel and normal to the surface. As the permittivity of the material increases, the electric field component perpendicular to the surface of the block is more and more attenuated at the boundary. Although the *x*-component (perpendicular to the surface of the material) of the electric field is very strong between the antenna and the dielectric block, it doesn't penetrate through the material when the permittivity of the material is high. For example, according to Equation (4.5), using the value $\varepsilon_r' = 50$ the *x*-component of the electric field strength is approximately 34 dB lower inside the material than outside it. On the other hand, components parallel to the surface of the material are not attenuated substantially at the boundary; the tangential field components are equal on adjacent sides of the boundary (Equation (3.12)).

The second observation made on the basis of Figures 4.8 - 4.13 is that as the permittivity of the dielectric block increases, distributions of the magnitudes of electric and magnetic fields inside the block start to be more and more alike. This observation means that electric and magnetic fields both have strong values in areas which are vertically (in *z*-direction) located close to locations where the currents on the surface of the ground plane of the antenna are high, as well. The behavior in free space, in turn, is notably different; in free space, electric field has minima near the locations where the current in the chassis is strong. Additionally, magnitude of the magnetic field inside the dielectric block seems to increase substantially as the permittivity of the block increases.

Based on the observations made above, it can be concluded (supporting the results of [29]) that as a function of the real part of the permittivity, the generation of the electric field inside dielectric material located in the close vicinity of an antenna acts as follows:

1. With materials whose ε_r' is low, electric field inside the material is strong close to locations where also the original electric field in free space was strong.

2. With materials whose ε_r' is high, electric field components inside the material are significant close to locations where the antenna current is strong.

4.3.2 Effect of effective conductivity σ_{eff}

In the previous section (4.3.1), the conductivity of the materials inside the dielectric block was in all cases set to zero. In this section, the effects of the effective conductivity on the fields inside and near dielectric material are studied. Once again, the simulation model comprises the basic coupling element antenna situated beside the simple dielectric block. The results are presented only for electric fields, since no new information in addition to Section 4.3.1 was found from magnetic fields. Also the number of frequencies has been limited from the previous section: only results at 1200 MHz are presented.

The electric near fields at 1200 MHz are presented in Figures 4.14 and 4.15 with materials having two different values for permittivities (5 and 50) and four different conductivities. For the high-permittivity case (ε_r' = 50), the fields are plotted in Figure 4.14 with conductivities 0, 0.2, 1 and 5 S/m, and for the low-permittivity case (ε_r' = 5) in Figure 4.15 with conductivities 0, 0.05, 0.1 and 0.5 S/m. For comparison, real values based on the parametric model presented in [28] (see Table 3.1) for example for muscle tissue at 1200 MHz are about ε_r' = 54 and σ_{eff} = 1 S/m and for fat tissue about ε_r' = 5 and σ_{eff} = 0.5 S/m, respectively.

From Figures 4.14 and 4.15 it can be seen that increasing the conductivity doesn't change the directions of the fields inside the dielectric material. However, as the conductivity of the material increases, the fields inside the material attenuate very quickly. This can be understood by looking at the definition for the penetration depth [27]:

$$\delta = \frac{1}{\left|\mathrm{Im}\{k\}\right|}, \tag{4.1}$$

$$k = \omega\sqrt{\mu_0\varepsilon_0}\sqrt{\varepsilon_r' - j\frac{\sigma_{eff}}{\omega\varepsilon_0}}. \tag{4.2}$$

It is easily seen, that as the effective conductivity of the material increases, the (absolute value of the) imaginary part of k also increases, which consequently decreases the penetration depth.

From Figures 4.14 and 4.15 it can also be seen that the attenuation of the field inside the material is faster in the case of the low-ε_r' material.

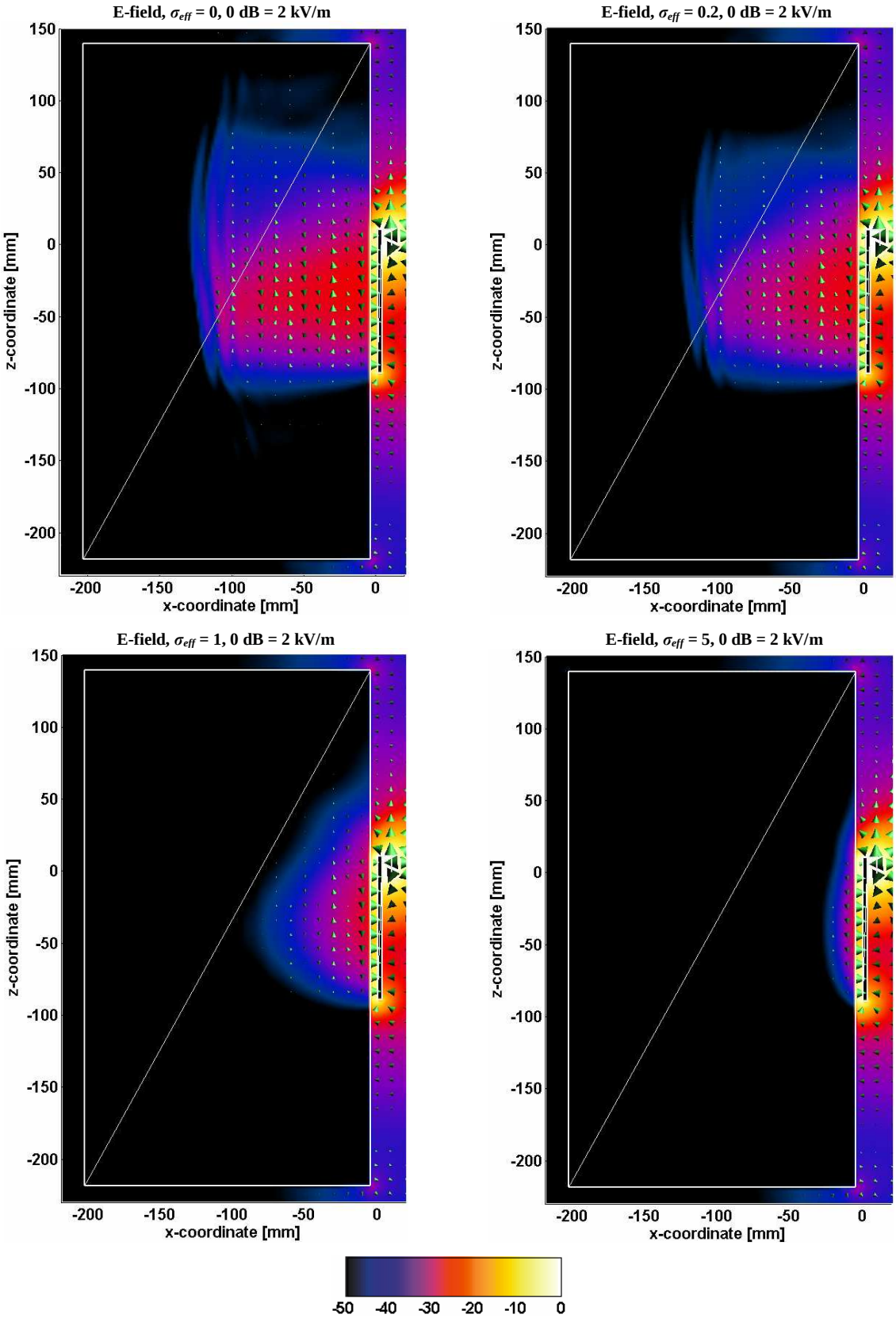

Figure 4.14 E-field distributions at 1200 MHz on xz-cut (y=0 mm) when a dielectric block is placed at a distance d = 5 mm from the antenna. Effective conductivity σ_{eff} = 0, 0.2, 1 and 5. Real part of permittivity ε_r' = 50.

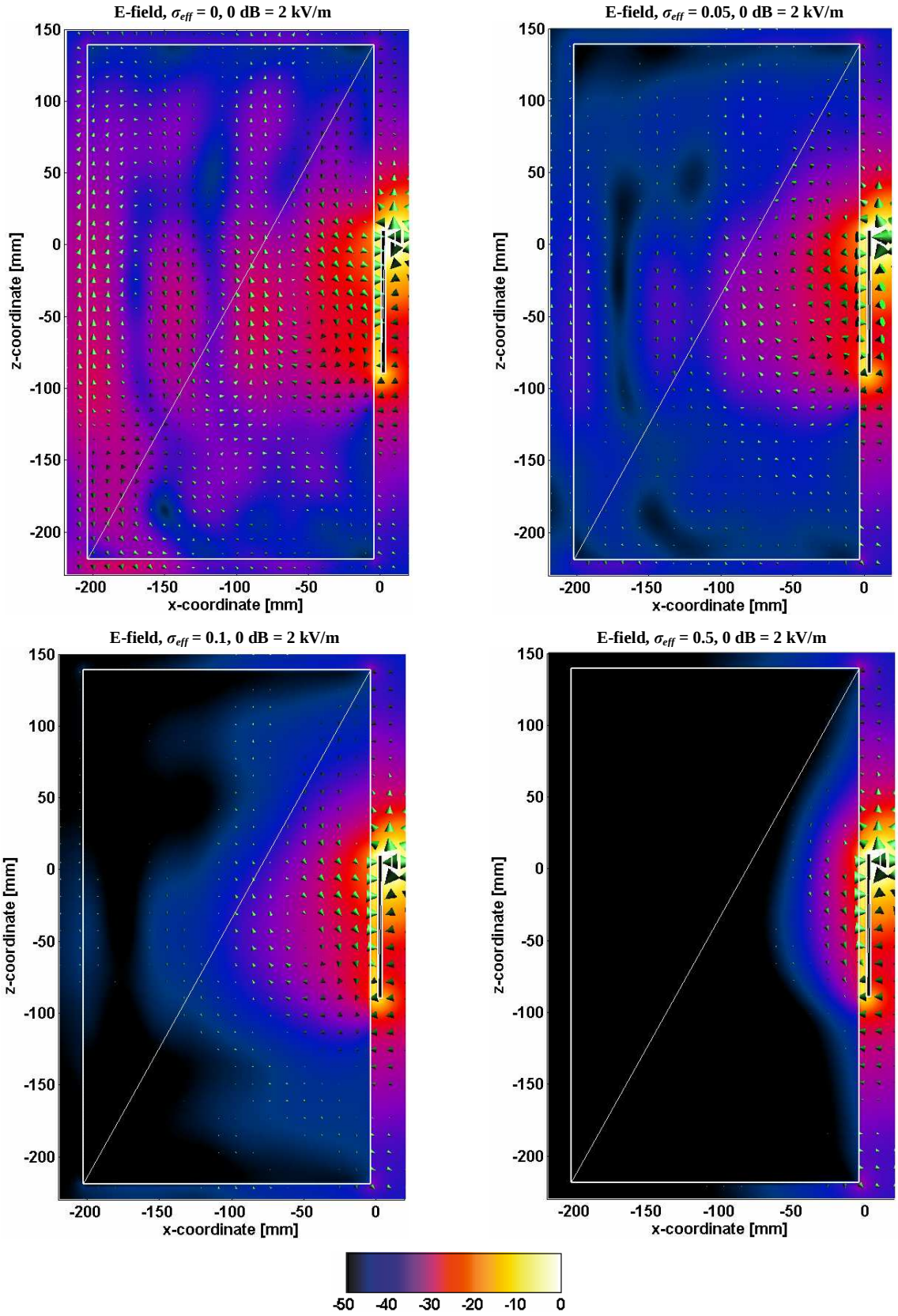

Figure 4.15 Field distributions at 1200 MHz on xz-cut (y=0 mm) when a dielectric block is placed at a distance d = 5 mm from the antenna. Effective conductivity σ_{eff} =0, 0.05, 0.1 and 0.5. Real part of permittivity ε_r' = 5.

5 FREQUENCY DEPENDENCE OF ANTENNA PARAMETERS

5.1 Introduction

The frequency dependence of the bandwidth, *SAR* and radiation efficiency of coupling element antennas was studied in [16]. The main message of that paper was that clear connections can be found between these parameters: as was already concluded e.g. in [2] and [14], at chassis resonances the bandwidth reaches a local maximum, and at the same time an increase in *SAR*s and a decrease in efficiency occur. However, it was also said that this trend is not anymore followed at higher order resonances (above 3 GHz) of the chassis.

In this chapter the interrelations between bandwidth, *SAR* and radiation efficiency are further studied. At first in Section 5.2 the simulations are carried out by using the same simple block model that was used earlier in Chapter 4. In Section 5.3, the simulations are repeated with the SAM phantom head model. In addition to the parameters that were studied in [16], the behavior of the resonance frequency of the chassis nearby dielectric material is studied. The locations of the maximum *SAR* values are also investigated.

5.2 Simulations with a dielectric block

In Chapter 4 the materials that were used in simulations didn't model any authentic tissues of human body. Values for permittivities and conductivities as such were fictitious not representing any true values; neither was the frequency dependence of the material parameters taken into account. To take the first step towards a more realistic user interaction situation, in this chapter the materials inside the dielectric half space are substituted to represent real human tissues. Two

tissues are treated: the first tissue is muscle which is a typical example of a tissue with high values of permittivity ($\varepsilon_r' \approx 50$) and conductivity ($\sigma_{eff} \approx 1$ - 5 S/m in the frequency range in question). The second tissue, fat, is an example of a tissue with low permittivity ($\varepsilon_r' \approx 5$) and conductivity ($\sigma_{eff} \approx$ 0.05 - 0.3 S/m). The frequency dependence of tissue parameters (exact values given in Table 3.1) is also taken into account in simulations from this point on.

In contrast to the very fundamental and basic nature of studies so far in this thesis, this section is a point where the considerations start to be more related to certain parameters of the antenna-user combination. This section, together with the next one (5.3), deals with determining the behavior of the resonance frequency, bandwidth, radiation efficiency and *SAR* in a wide frequency range. The simulation models in this section are the same as above in Section 6.3, containing the antenna and the dielectric block. In Section 5.3, the presented analysis is further extended to a more realistic case as the same simulations are executed by replacing the dielectric half space with a SAM (Specific Anthropomorphic Mannequin) phantom modeling the human head.

5.2.1 Resonance frequency

Resonance frequency is one of the most fundamental parameters that characterize an antenna; without proper impedance matching the antenna neither radiates nor is able to receive power. Furthermore, matching of the antenna is possible only with certain values of (complex) reflection coefficients, or in other words when the input impedance of the antenna is in a certain location in the Smith chart. Therefore, detuning caused by the user can possibly produce tricky business for the antenna designer. Even if the details of impedance matching are still excluded from the considerations of this thesis, some conclusions about the behavior of reflection coefficient of the antenna in the vicinity of dielectric objects are provided.

The theory presented back in Section 3.5 included discussion about the behavior of the resonance frequency of a resonator when dielectric material is located nearby or inside the resonator. The first assumption - according to general resonator theory and perturbation theory - was that whenever a resonator is loaded with dielectric material, the resonance frequency of the resonator would be shifted downwards. This assumption was pretty easy to believe in; intuitively, in dielectric material the wavelength of the propagating signal is smaller than in free space, meaning that the effective length of the dielectric material increases as the permittivity of the material increases. This would of course decrease the resonant frequency, respectively.

Reflection coefficients with the dielectric block at different distances from the antenna (d = 60 mm, 20 mm, 10 mm and 5 mm) are plotted in Figure 5.1. Figure 5.1a) illustrates the high-

permittivity case (muscle) and Figure 5.1b) the low-permittivity case (fat). With distance d = 60 mm, the first resonance lies at 1100 MHz in both cases. As the dielectric block is brought closer to the antenna, the first order resonance shifts upwards. In the case of the muscle tissue (Figure 5.1a)) with d = 20 mm and d = 30 mm, the first resonances are slightly increased, being 1200 MHz and 1300 MHz, respectively. With d = 5 mm (in the muscle tissue), the first resonance can be found at 1800 MHz. With the fat tissue (Figure 5.1b)), already with d = 10 mm the first resonance is around 1800 MHz. It is rather surprising that in the low-permittivity case, the movement of the resonance seems to start already at a larger distance compared to the high-permittivity case.

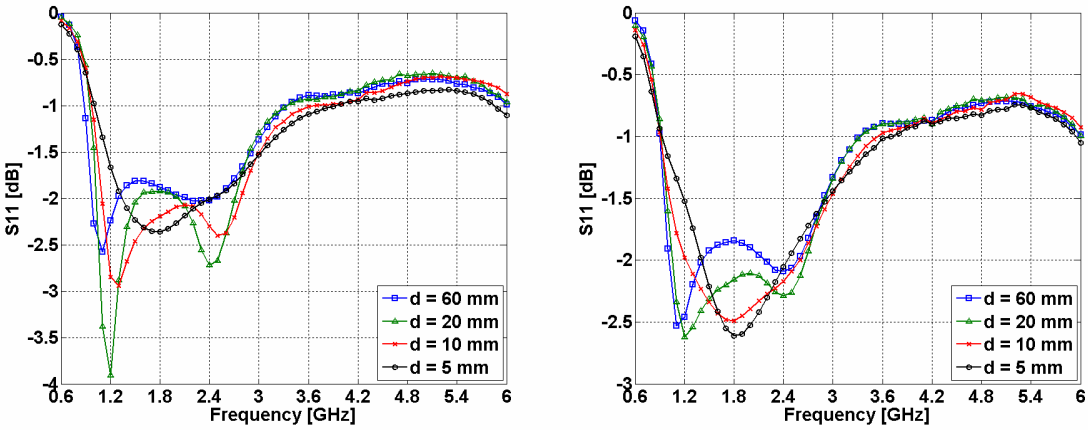

Figure 5.1 Magnitude of reflection coefficient with dielectric block at distances d = 60 mm, 20 mm, 10 mm and 5mm. Tissue inside the block is a) muscle b) fat.

In order to get more convinced about the reason for the slightly unexpected behavior of the resonance frequency, the *z*-component (tangential to the surface of the dielectric block) of the electric field strength at 1200 MHz with distances d = 5 mm and d = 60 mm is plotted in Figure 5.2. Based on that figure it is pretty obvious that when the dielectric block is brought closer to the antenna, the electric field at the lower edge of the chassis is forced to direct steeper towards the surface of the block. It should be noted that in Figure 5.2, the green arrows show the direction of the overall E-field, and that the colors illustrate the magnitude of the corresponding z-component. The bending of the electric field towards the block decreases the effective length of the antenna, which further causes the increase in the resonant frequency. However, this result is rather case-specific, and doesn't include any information for example about a case where the chassis would be covered with dielectric material from the other side of it. An example of a case like this would be a hand holding the antenna.

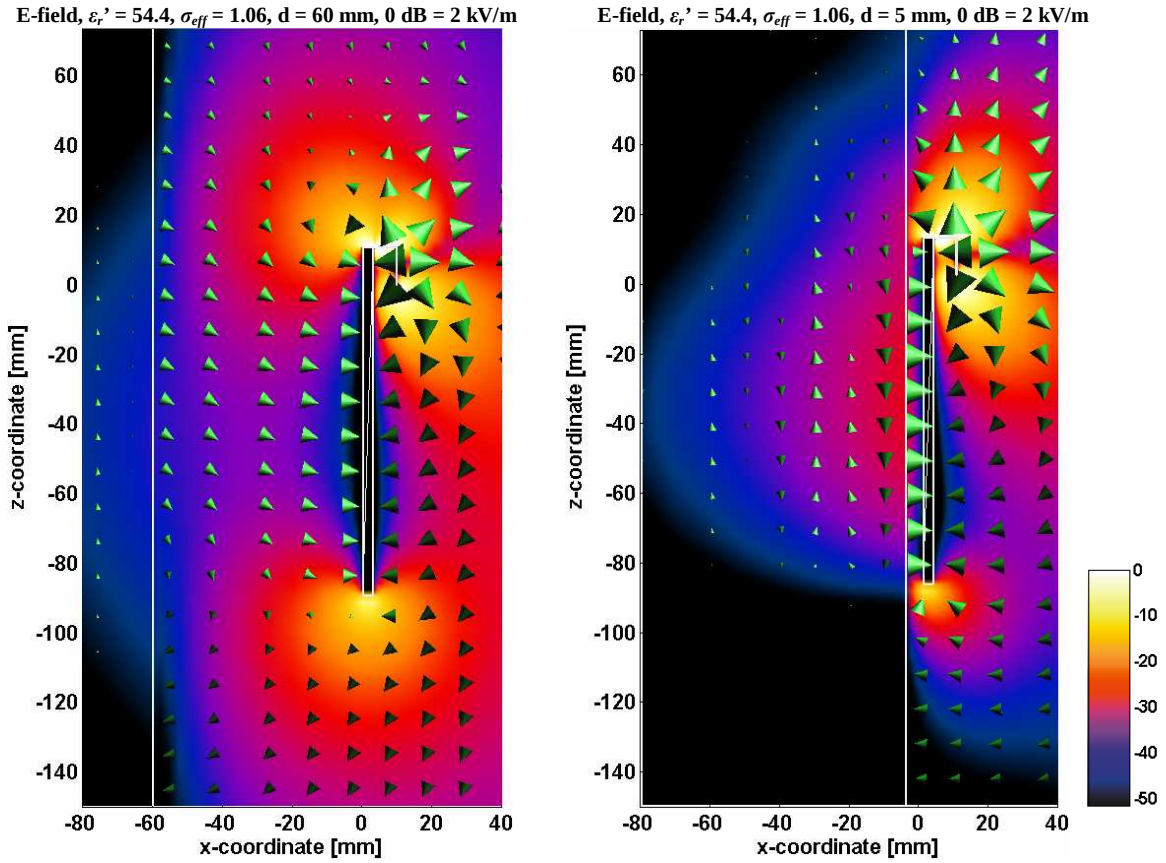

Figure 5.2 E-field at 1200 MHz with the antenna at distances d = 60 and d = 5 mm from the dielectric block (muscle; ε_r' = 54.4, σ_{eff} = 1.06). The green arrows show the direction of the overall E-field, and the colors the magnitude of the corresponding z-component. The white line left from the antenna is the outline of the surface of the dielectric block. (P_{in} = 1 W, 0 dB = 2 kV/m).

5.2.2 Bandwidth

The bandwidth potential is known to be strongly interrelated with the resonance frequencies of the chassis. To be more precise, the bandwidth is largest at the chassis resonances due to the strong coupling of signals to the chassis wavemodes [2], [14], [16]. This trend can be seen by comparing Figures 5.1 and 5.3. It should be noted that the curves in Figure 5.3 have been obtained by first matching the impedance of the antenna (critical coupling) at a single frequency with two lumped elements and then calculating the relative bandwidth according to - 6 dB matching criterion. This procedure has been repeated separately for each value of *d*. In this way, we apply a single resonant matching and larger bandwidths could be easily obtained by utilizing multiple resonances. However, the possible trends in the behavior of the achievable bandwidth can be seen in a simple manner.

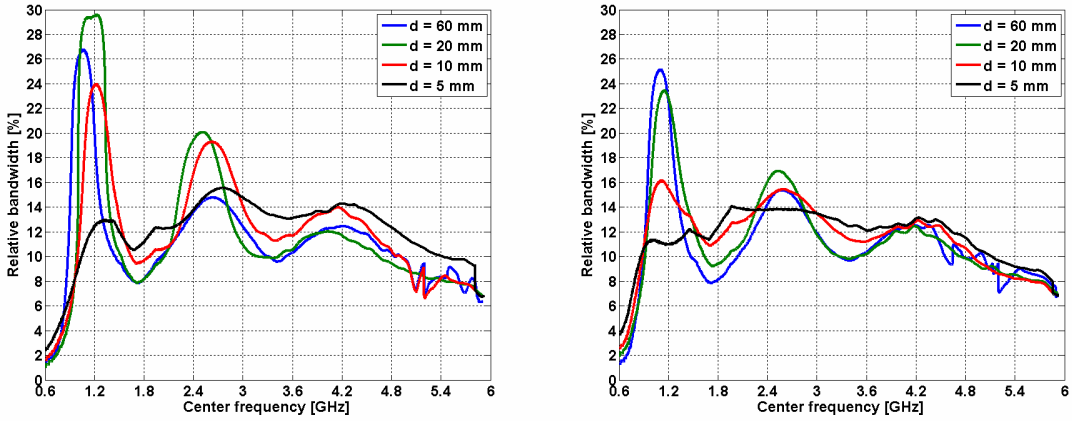

Figure 5.3 Bandwidth potential. Tissue inside the block is a) muscle b) fat.

The curves in Figure 5.3a) suggest that the bandwidth potential around the first resonance of the chassis (around 1.2 GHz) is lowered when the antenna is brought closer to the dielectric block. However, the bandwidth potential with d = 20 mm is somewhat larger than with d = 60 mm. Around the second resonance, the bandwidth potential is largest with d = 20 mm and d = 10 mm, but even with d = 5 mm a larger bandwidth than with d = 60 mm can be obtained. As a general note, it can be said that the bandwidth potentials especially around the chassis resonances in the low-permittivity case (Figure 5.3b)) are somewhat lower than in the high-permittivity case (Figure 5.3a)). Otherwise, no big differences between these two cases can be observed.

5.2.3 Radiation efficiency

Radiation efficiencies with different distances between the antenna and the dielectric block are plotted in Figure 5.4.

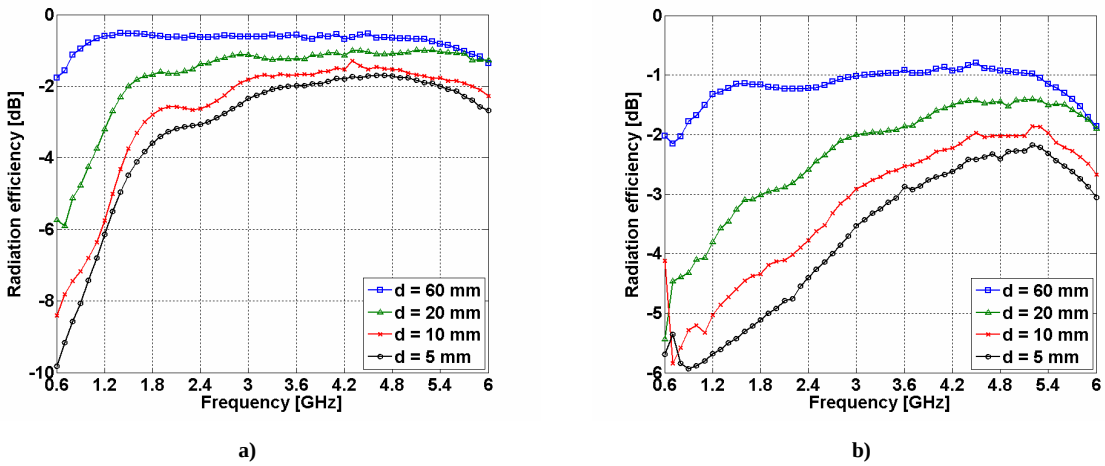

Figure 5.4 Radiation efficiency. Tissue inside the block is a) muscle b) fat.

From Figure 5.4a) it can be seen that when the dielectric block is filled with the high-permittivity material (muscle), the radiation efficiencies are very low at low frequencies, but as the frequency increases, they start to increase rapidly. The maximum is reached around 5 GHz. As could be expected, the radiation efficiencies decrease in the whole range, when the distance between the antenna and the block is decreased. However, the difference between d = 10 mm and d = 5 mm is quite small.

In the low-permittivity case (fat; Figure 5.4b)) the radiation efficiencies increase steadily up to about 5 GHz. The starting values in the low-permittivity case at low frequencies are much higher than in the high-permittivity (muscle) case, but as the frequency increases, the radiation efficiencies increase more rapidly in the high-permittivity case.

5.2.4 SAR

The general trend according to earlier studies [2],[14] is that the peak *SAR* occurs at chassis resonances, and that at the same time a minimum in efficiency and a maximum in bandwidth are reached. This rule of thumb was refined in [16]; as the frequency increases, the wavemodes of the antenna/coupling element start to dominate over the chassis wavemodes, and the behavior of bandwidth, *SAR* and efficiency can no longer be predicted by the chassis resonances.

SAR values (averaged over 10 g) in the dielectric block are plotted in Figure 5.5. In Figure 5.5a), where the tissue inside the block is muscle, the above-mentioned trend is quite clearly followed. High values of *SAR* occur at chassis resonances around 1.2 and 2.4 GHz. Above 3 GHz, *SAR*s increase steadily, as the radiation of coupling element becomes more and more significant. With fat (Figure 5.5b)), the trend is not so clear. However, a small increase in the *SAR* values is found around the resonant frequencies with distances 5 mm and 10 mm. As a surprising observation, it can be seen that although the *SAR*s below 3 GHz are substantially higher in the high-permittivity tissue, with the low-permittivity tissue, *SAR* values are higher above 3 GHz. The reason for this behavior is yet to be found. Another surprising thing is that at frequencies 1.2 GHz - 1.8 GHz, in the case of the high-permittivity material, the *SAR*s are higher with d = 10 mm than with d = 5 mm.

By comparing Figures 5.1 and 5.5 it can be seen, that even if the first resonance of the chassis shifts to a higher frequency, the frequency behavior of the *SAR*s is not following the same trend. The first maximum with d = 5 mm (in Figure 5.5a)) seems to be even at a lower frequency than with the larger distances. Furthermore, in the same curve (d = 5 mm, in Figure 5.5a)), there is a minimum in *SAR*s at the same frequency (1.8 GHz) where on the other hand is a resonance frequency according to the reflection coefficient curve in Figure 5.1a).

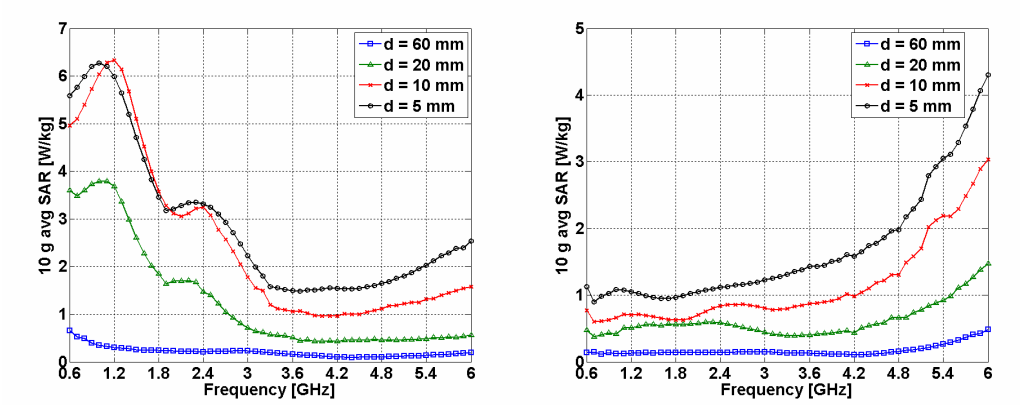

Figure 5.5 10 g avg SAR in dielectric block. Tissue inside the block is a) muscle b) fat.

In addition to the magnitudes of *SAR*s, it was found interesting to study the locations of the maximum *SAR* values. The assumption that at low order resonances high *SAR*s are caused by the chassis radiation and that at higher frequencies the main contributor are the coupling element wavemodes is fully supported by Figures 5.6a) and 5.6b) where the *z*-coordinates of the peak *SAR* locations are plotted. The basic behavior is that at low frequencies, peak *SAR* is generated quite close to the vertical center point of the chassis. As the frequency increases, the peak *SAR* location follows the location of the current maximum on the chassis surface thus moving downwards. At some point (for example at 2.6 GHz with d = 10 mm in Fig 5.6a)) the highest *SAR* value jumps under the second current maximum. To ease the understanding of the process, current density on the chassis is plotted in Figure 5.6c). The frequency in question is 2.4 GHz. If we compare Figures 5.6a) and 5.6b) with 5.6c) it is relatively easy to see, how the two current maxima have the battle over the highest *SAR* value. Only one of them can win, and that explains the discontinuities in 5.6a) and 5.6b). The operation is similar at other frequencies, as well.

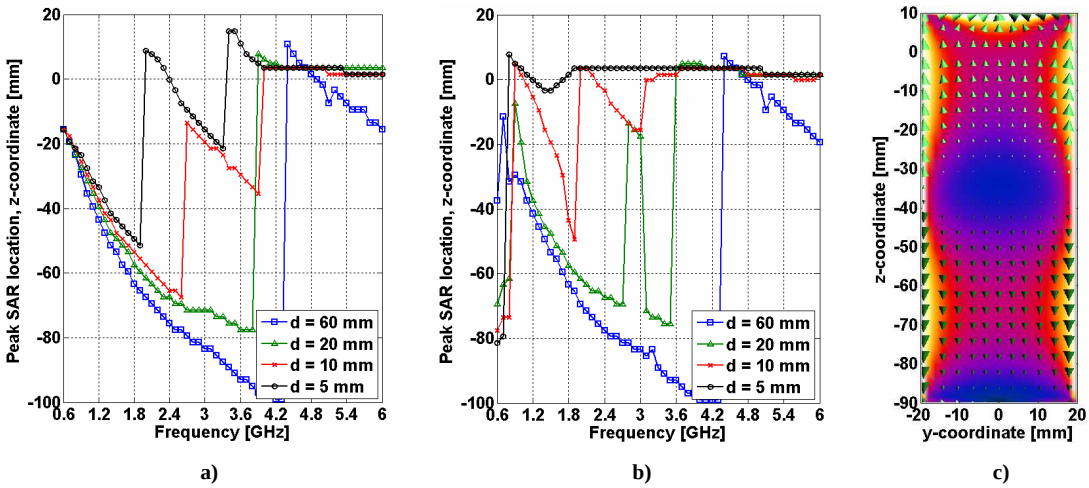

Figure 5.6 The Z-coordinate of the peak SAR location in the dielectric block. Tissue inside the block is a) muscle b) fat. c) Antenna placement and chassis current density at 2.4 GHz.

5.3 Simulations with the SAM phantom head model

In the previous section (5.2), the behavior of the resonance frequency, bandwidth, radiation efficiency and *SAR* was studied in a wide frequency range by modeling the user with a simple block model. The cases when the block consisted either of fat (low-permittivity case) or muscle (high-permittivity case) were analyzed.

In this section, the simulations are repeated by replacing the dielectric block with a SAM phantom head model. Two different distances between the head and the chassis of the antenna are used (d = 3 mm and d = 7 mm). The tissue inside the head models the brain tissue, for which the exact values for the dielectric parameters are given in Table 3.1. It is worth noticing that the values of ε_r' and σ_{eff} for the brain tissue are fairly close to those of the muscle tissue which was used in Section 5.2 as the high-permittivity tissue.

5.3.1 Resonance frequency

In Section 5.2, it was noticed that when the antenna is brought closer to the dielectric material, the first resonance of the chassis shifts upwards in frequency, which was considered to be a somewhat surprising result. However, from Figure 5.7 it can be seen that the same thing happens in the case where the antenna is placed beside the head model. With d = 7 mm, the first resonance is around 1.2 GHz, but as soon as the antenna is brought closer (d = 3 mm), the resonance shifts to 1.8 GHz. In addition, the second resonance more or less seems to disappear. In Section 5.2, the increased resonance frequency was concluded to be caused by the decreased effective length of the chassis (see Figure 5.2). The same thing is very likely to be happening also in this case.

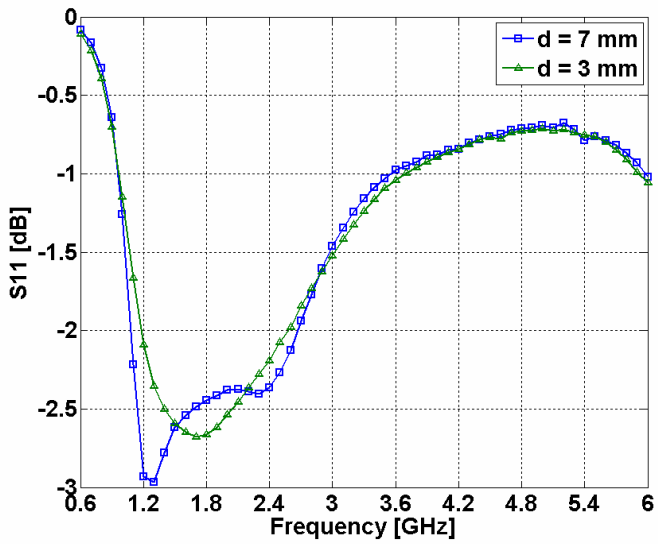

Figure 5.7 Magnitudes of reflection coefficients beside the head model.

As mentioned, in the simulations with the head model, the distance between the head and the chassis of the antenna is d = 3 mm or d = 7mm. It should be noted that the distances that were used in the previous section (5.2) in the case of the block model (d = 5, 10, 20 and 60 mm) can note be straightforwardly compared with the distances that are used in this section. At first, the surface of the head is not completely flat, which means that the distance between the head and the antenna changes slightly depending on the location. The second difference between the two models is that in the block model the high-permittivity brain tissue starts immediately at the surface, while in the head model the brain tissue simulating liquid starts after a few millimeter-thick low-permittivity shell. However, as far as the reflection coefficients are concerned, the results of Section 5.2 and the results of this section (5.3) largely seem to follow a similar trend.

5.3.2 Bandwidth

The bandwidth potential of the antenna beside the head model is presented in Figure 5.8. Again, the results follow a similar trend than in the case when the antenna was placed beside the block model. With the greater distance (d = 7 mm), the achievable bandwidth is larger than with d = 3 mm around the resonances; between the resonances, in turn, the bandwidth potential seems to be even higher with d = 3 mm. As an interesting observation, it could be noticed that even if the resonance frequency - in terms of the reflection coefficient - increases as the antenna is brought closer to the head (d decreases from 7 mm to 3mm), the locations of the bandwidth maxima are not shifted accordingly. This trend was already noticed in the previous section (5.2), and it clearly is an issue which would require further examination.

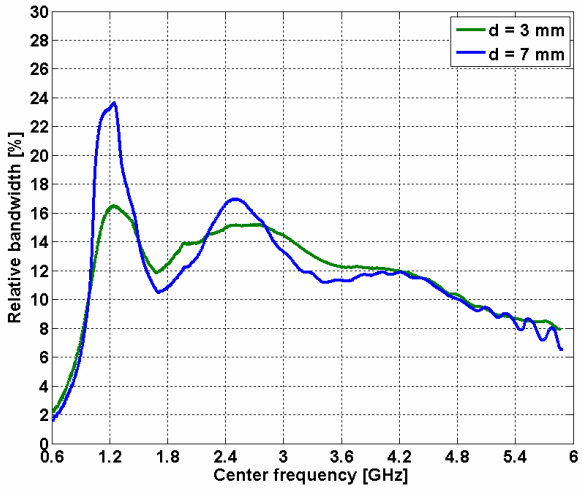

Figure 5.8 Bandwidth potential beside the head model.

5.3.3 Radiation efficiency

The radiation efficiencies beside the head model are presented in Figure 5.9.

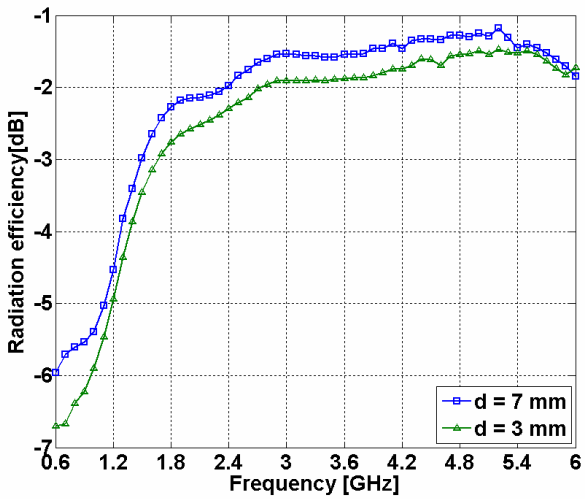

Figure 5.9 Radiation efficiency beside the head model.

It can be seen by comparing Figures 5.4a) and 5.9 that the radiation efficiencies beside the head model agree fairly well with the efficiencies in the case when the dielectric block was filled with the high-permittivity material (muscle). The radiation efficiencies are very low at low frequencies, but as the frequency increases, they start to increase rapidly. The rapid increase goes on up to about 3 GHz due to the decreased contribution of the radiation of the chassis. Above 3 GHz, the radiation efficiency stays nearly constant as the main radiator at those frequencies is the coupling element.

5.3.4 SAR

In Section 5.2, the trend in *SAR*s in the case of the high-permittivity block followed the assumptions made in the earlier studies ([2], [14], [16]); the peak *SAR* occurs at the low-order resonances of the chassis, but at higher frequencies the chassis resonances are not seen in *SAR* values, since the coupling element becomes the main radiator. As a new observation, it was found that even if the first resonance of the chassis is shifted to a higher frequency, the frequency behavior of the *SAR*s is not following the same trend.

The behavior of *SAR* when the antenna is placed beside the head model follows the same trend to some extent. From Figure 5.10 it can be seen, that the first order resonances are located around 1.2 GHz with both distances. By comparing Figures 5.5a) and 5.10 it can be seen that, on the other hand, the second resonance of the chassis is not that clearly seen in the *SAR*s inside the head model

than inside the high-permittivity block. This is very likely to be caused by the fact that the high *SAR* values around 2.4 GHz are located around $z \approx$ -10 mm or $z \approx$ -70 mm (see Figure 5.6a) and 5.6c)); around this range, the head model is not completely flat (see for example Figure 6.21 on page 93), meaning that the distance between the antenna and the surface of the head gets larger. On the other hand, the increase in the *SAR* values above 3 GHz is stronger in the head model than in the block model. This phenomenon is also probably caused by the shape of the head model.

The *SAR* values are almost through the whole frequency range higher with d = 3 mm than with d = 7 mm, which is an expected result. Between 1.2 GHz and 1.8 GHz, however, the *SAR* values are almost equal in both cases, and between 1.8 GHz and 2.4 GHz even higher with d = 7 mm.

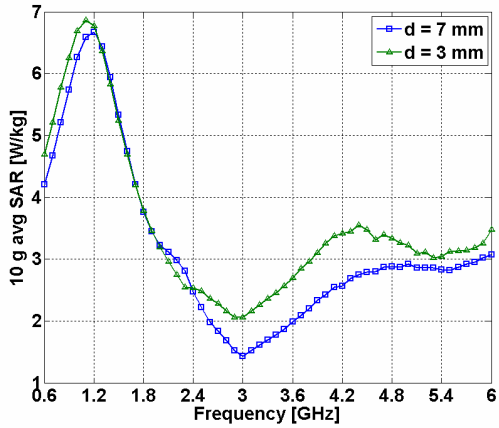

Figure 5.10 10 g avg SAR in the head model.

The z-coordinate of the peak *SAR* location is plotted in Figure 5.11. It can be seen that in contrast to the case of the block model (see Figure 5.6a)), only in very few cases the peak *SAR* is located around z = -30…0 mm. This can be expected to be caused again by the shape of the head model.

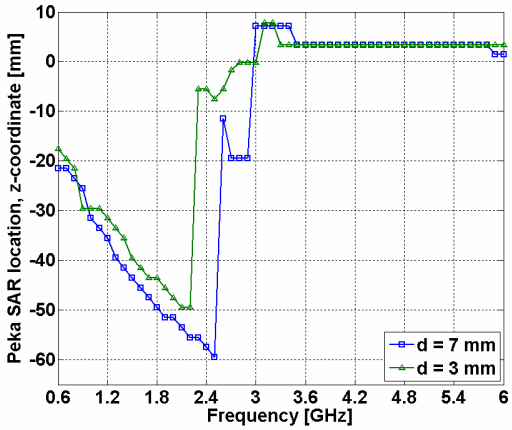

Figure 5.11 Z-coordinate of the peak SAR location in the head model.

5.4 Summary of the simulation results

The frequency dependence of the user-related parameters of the antenna was studied in the simulations of this chapter. The frequency range in question was from 600 MHz to 6 GHz.

At first, the interrelations between the resonance frequency, bandwidth, radiation efficiency and *SAR* were studied by modeling the user with a simple block model. Two human tissues (muscle and fat) were analyzed. In the simulations, it was found that the resonance frequency of an antenna/chassis combination can increase when dielectric material is brought beside the antenna. As a possible explanation to this rather surprising result, it was shown that the effective electrical length of the chassis can decrease when the distance between the antenna and the dielectric object is decreased. The bandwidth, *SAR* and radiation efficiency in many respects behaved as could be expected based on the earlier studies concerning the issue. In addition, it was found that especially with the high-permittivity material, even if the resonance frequency changed when the material was brought closer to the antenna, neither the high values of *SAR* nor the maxima in bandwidth shifted accordingly. The inspection of the peak *SAR* locations showed that in high-permittivity material, the locations of the high *SAR* values accurately follow the current distribution of the chassis. However, this trend was not evident in the low-permittivity case.

The results that were obtained from simulations when the antenna was placed beside the head model were of similar kind to the results that were obtained with the high-permittivity (muscle) block model. This was quite expected, since the dielectric parameters of the brain tissue are rather close to those of the muscle tissue. However, small differences in the results were noticed and concluded to be caused by the non-flat shape of the head model. For example, the *SAR* maximum around the second resonance of the chassis was much weaker in the case of the head model than in the case of the block model.

6 SAR CONTROL MECHANISMS

6.1 Introduction

As we already know, the strong radiation of the chassis at the low cellular frequencies causes high *SAR* values and accordingly low radiation efficiency, which especially at the GSM900 band is quite often problematic. As a possible solution to the problem, a technique to increase the total efficiency of an antenna by reducing its *SAR* values was presented in [34]. The used method comprised a dual-band (900/1800 MHz) PIFA and a parasitic radiator placed on the backside of the ground plane. It was shown that *SAR* reached a minimum when the length of the parasitic radiator was 45 mm (at 900 MHz). Compared to the case when no parasitic radiator was attached to the ground plane, the *SAR* reduced by approximately 5 dB in the simulations (from 1.5 W/kg to 0.5 W/kg for 0.25 W input power). In measurements, the reported reduction in *SAR* was 6 dB. Total efficiency in talk-position was approximately 1 dB higher with the 45 mm long parasitic radiator compared to the reference case (no parasitic radiator).

Even if the *SAR* control method that was proposed in [34] seems to be working quite nicely, the operating principle of the parasitic radiator was left somewhat unclear. It was only mentioned that the effect of the parasitic radiator would be to cancel a part of the near field that is coupled inside the head. Furthermore, it was concluded that the cancellation of the near field would be caused by the currents of the parasitic radiator, which are opposite in direction to the currents on the chassis. The purpose of this chapter is to improve understanding on the proposed *SAR* control method by applying the concept to coupling element antennas. At first, an antenna model including the parasitic plate as a *SAR* shield is presented and analyzed in free space. Examination of the antenna configuration as a *SAR* control mechanism is started by studying the *SAR* values, radiation

efficiencies, bandwidth potentials and near field distributions with the same simple block model that was used earlier in Chapters 4 and 5 (see Figure 4.7). After that, the method is tested with a SAM phantom head model. Finally, a summary of the studied *SAR* control method is given and possible interrelations between the *SAR*, radiation efficiency and bandwidth are discussed.

6.2 Antenna with parasitic radiator as a SAR shield

The antenna configuration consists of the same coupling element antenna that has been used throughout the thesis and of a metallic plate mounted on the backside of the chassis. The metallic plate works as a parasitic radiator, which should cancel a part of the near field coupling to the head [34]. The coupling element antenna with the parasitic radiator is presented in Figure 6.1.

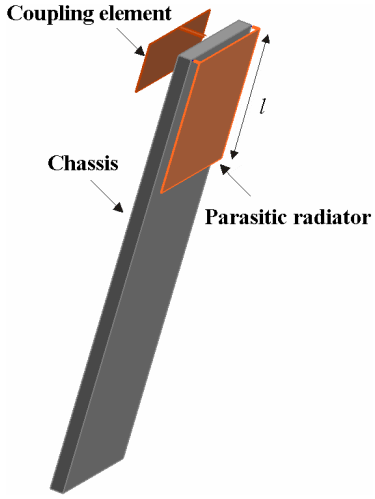

Figure 6.1 Coupling element antenna and a parasitic radiator as a SAR shield. The distance between the parasitic radiator and the chassis is 1.8 mm. The length of the parasitic plate is denoted by l.

The length of the parasitic plate is denoted by *l* and the distance between the chassis and the plate is 1.8 mm. The thickness of the plate is 0.2 mm, as well as that of the coupling element. The parasitic plate is shorted from two upper corners with 2 mm wide shorting posts.

6.3 Free space simulations

6.3.1 Near fields

The largest impact on *SAR* values (reduced approximately from 1.5 W/kg to 0.5 W/kg, P_{in} = 0.25 W) in the studies of [34] was reported to occur in case when the antenna had a 45 mm long parasitic radiator attached to the chassis. Based on those results, it was found interesting to study

the near fields and the current distributions of the antenna without the parasitic plate and with the 45 mm long plate in free space. The total (*RMS*) electric near field is plotted in Figure 6.2, where the colors illustrate the magnitude of the field, and the green arrows show the direction.

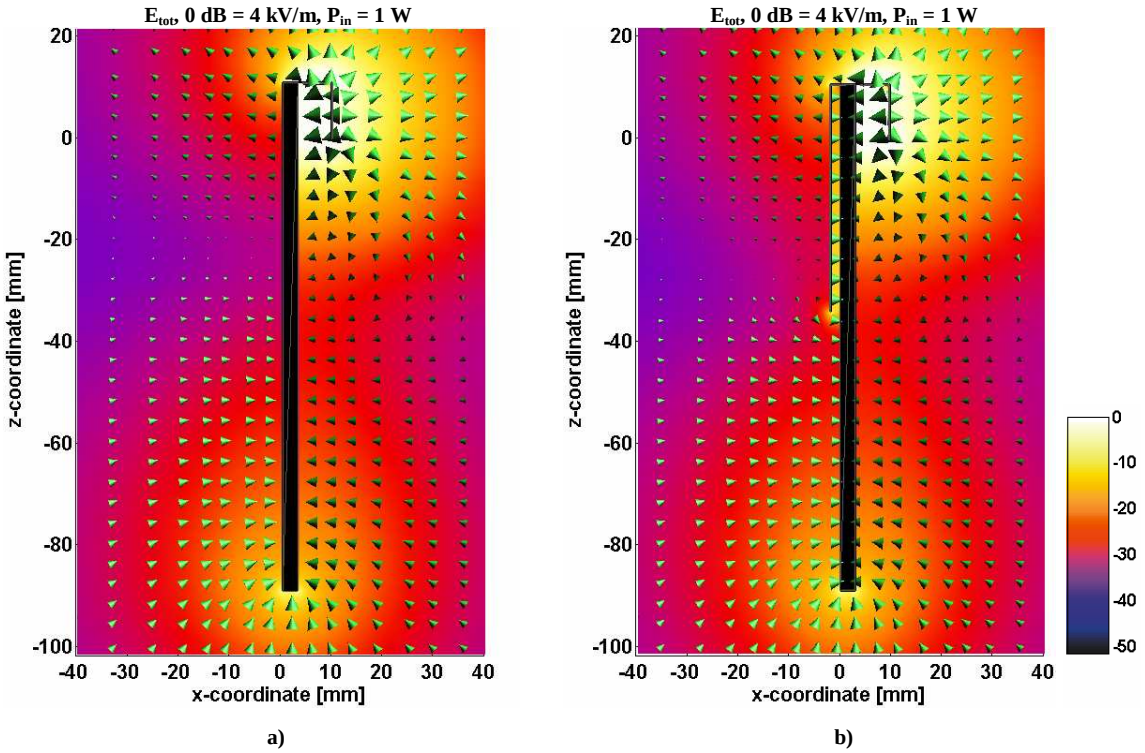

Figure 6.2 Total E-field in free space at 900 MHz. a) Antenna without the parasitic plate b) antenna having a 45 mm long parasitic plate attached to the chassis.

From Figure 6.2, no remarkable differences in the near fields can be observed around the lower half of the chassis or in the space right from the chassis; the cancellation of the electric field radiating towards the head (which would be located left from the antenna) can not be seen. As a slightly confusing result, it can be noticed that the electric field seems to be even somewhat stronger near the parasitic plate, around locations where the x-coordinate is -2…-10 mm and the z-coordinate -35…10 mm. However, due to the fact that the x-component of the electric field is very dominating, it is quite difficult to say anything conclusive from the *SAR* plots in Figure 6.2; we know from earlier parts of this thesis that electric field components normal to the surface of the tissue are very strongly attenuated on the boundary (see Equation 3.11) of a high-permittivity material, and thus do not cause high *SAR* values. On the contrary, electric field components that are parallel with respect to the surface of the tissue are not that strongly attenuated on the boundary of the material (see Equation 3.12), meaning that they penetrate more easily inside the material and cause the absorption of energy. To see the effect of the parasitic plate on the different components of the electric field, the magnitudes of the x- and z-components of the electric field are plotted in Figures 6.3 and 6.4, respectively.

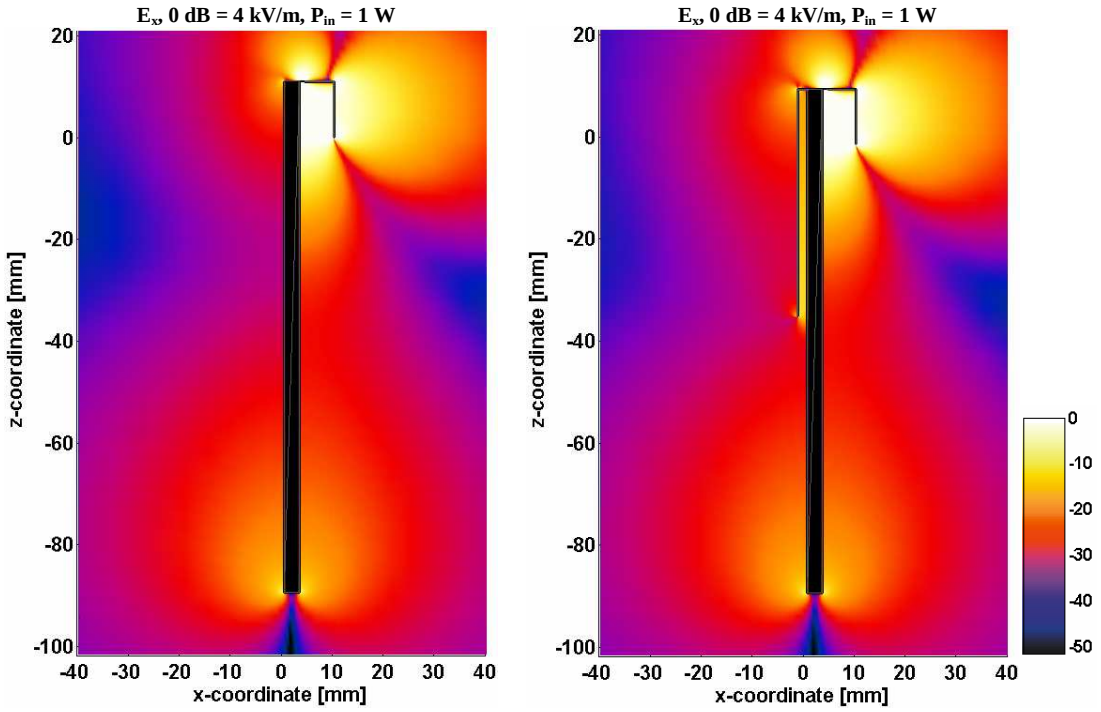

Figure 6.3 X-component of the E-field in free space at 900 MHz. a) Antenna without the parasitic plate and b) antenna with a 45 mm long parasitic plate.

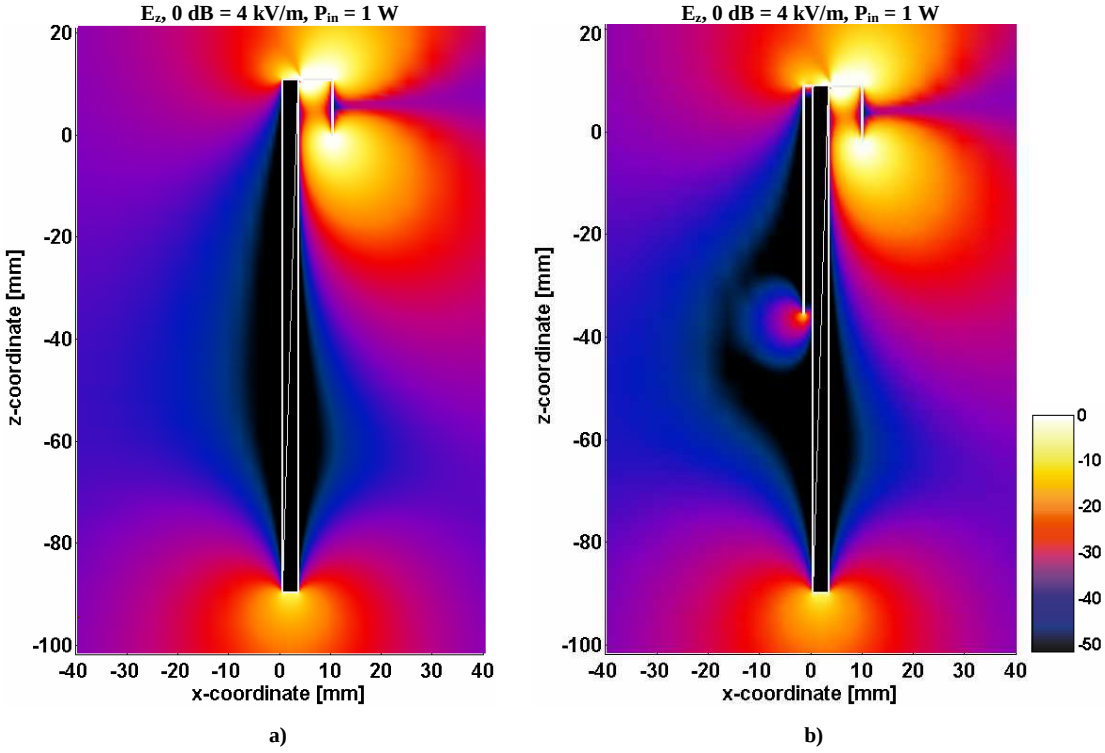

Figure 6.4 Z-component of the E-field in free space at 900 MHz. a) Antenna without the parasitic plate and b) antenna with a 45 mm long parasitic plate.

From Figure 6.3, it can be seen that the x-component of the electric field around z = -35…10 mm gets much stronger when the parasitic plate is added to the antenna. Elsewhere, no large differences in the x-component can be seen. The magnitude of the z-component of the electric field (Figure 6.4) is on the other hand significantly lower around z = -60…-30 mm with the antenna having the 45 mm long plate. Remembering (from Chapter 7) that at frequencies around 1 GHz with the basic coupling element antenna (without any parasitic plate) the *SAR* maximum is generated to locations that are close to the vertical center point of the chassis, provides us with a hint that this might cause the reduction in the *SAR* values.

From Figures 6.2-6.4, it can be concluded that the total electric field that is coupled inside the head around the upper parts of the chassis (z = -40…10 mm) seems to be stronger when the parasitic plate is added to the antenna; However, the increase in the field strength is mostly caused by the strong x-components of the electric field, but at the same time the z-components of the electric field get less significant, especially around z = -60…-30 mm. This can be expected to have a decreasing influence on the *SAR*s and consequently also on the radiation efficiency of the antenna.

6.3.2 Current distributions

In Chapter 5, it was shown that with the basic coupling element antenna (without the parasitic plate), the locations of high *SAR* values pretty much follow current distribution maxima on the chassis at least at frequencies below 3 GHz (see Figure 5.6 for an example). Furthermore, from the curves presented in Figure 5.6a), it can be seen that at 900 MHz the peak *SAR* is located at z = -30 mm, at which location the current on the backside surface of the chassis has also a maximum (Figure 6.5).

The plots in Figure 6.5 show that above z = -40 mm the current distribution is very strongly affected by the parasitic plate. The current density on the chassis under the parasitic plate (Figure 6.5b)) is very much stronger than without the plate (Figure 6.5a)) and the direction of the current has also changed to the opposite. The current distribution on the outside surface of the plate (Figure 6.5c)) is similar (but much stronger) to the current on the chassis of the antenna without the plate (Figure 6.5a)). The strong currents on the plate together with the fact that the plate is located closer to the head than the chassis could lead us to predict that extremely high *SAR* values are generated under the parasitic plate. Apparently, this was not anyway the case at least in [34].

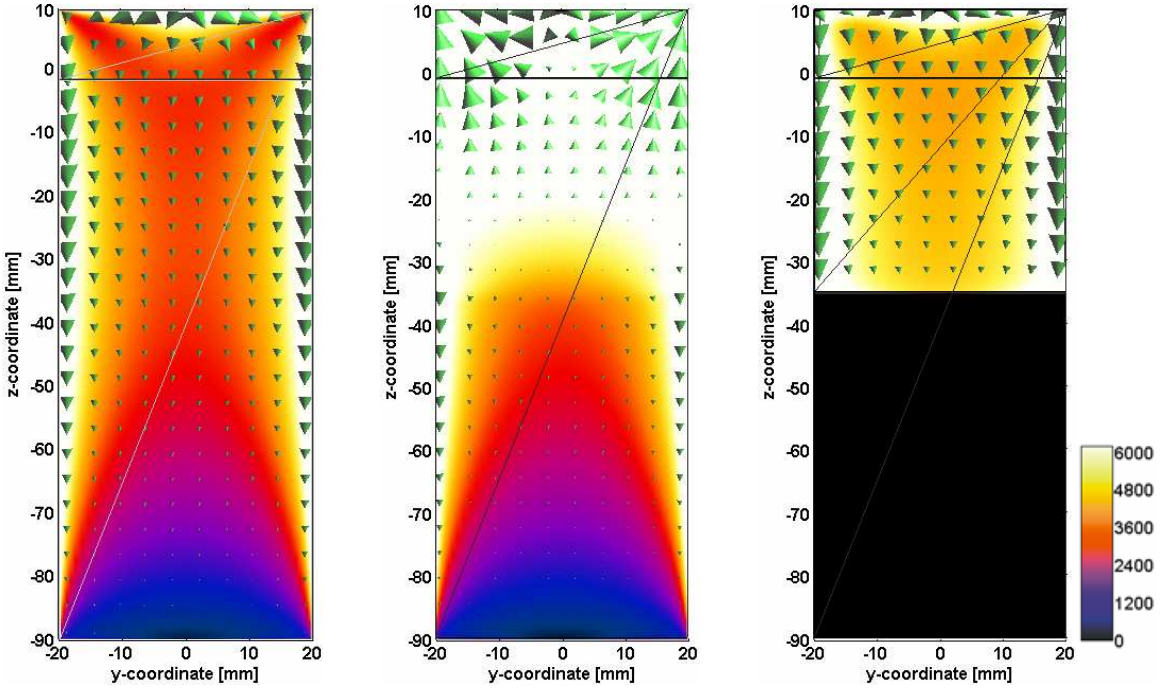

Figure 6.5 Current densities [A/m^2] at 900 MHz on chassis backside and on the parasitic plate. Current distribution on the chassis backside with a) antenna without the parasitic plate b) antenna with the 45 mm plate. c) Current distribution on the outside surface of the parasitic plate.

6.4 Simulations with the block model

In the previous section (6.3), it was shown that in free space the electric field that is coupled inside the head, gets stronger when a 45 mm long parasitic radiator is attached to the chassis of the antenna. Also the currents on the parasitic plate where shown to be much higher on the parasitic plate than on the chassis when no plate was attached to it. These observations would easily make one suspect that the introduced method of using the parasitic plate as a *SAR* control method would only increase the amount of absorption of energy to the head. However, it was also found that even if the total (*RMS)* electric field radiating towards the head gets stronger when the plate is added to the antenna, the electric field components that are parallel to the surface of the head get less significant, especially at locations that are close to the vertical center point of the chassis, with the antenna having the 45 mm long parasitic plate attached to the chassis. This can be expected to have a positive influence on the *SAR* values, and consequently on the radiation efficiency, of the antenna.

In this section, the antenna is placed beside the same dielectric block model that was introduced in Chapter 4. The length of the parasitic plate is increased in 5 mm steps. The *SAR* curves are

presented for two frequencies, 900 MHz and 1800 MHz, but the analysis concentrates in other respects on the more problematic E-GSM900 band. The dielectric block is filled with material having the same dielectric parameters as the brain tissue.

In addition to the behavior of *SAR* and radiation efficiency, the effect of the parasitic radiator on the achievable bandwidth, and on the near field distributions inside and nearby the material, are studied. Later, in Section 6.5, the same simulations are repeated by replacing the dielectric block with a SAM phantom head model.

6.4.1 SAR

The simulations with the dielectric block were done at two different distances between the chassis and the surface of the dielectric block (d = 3 mm and d = 7 mm). One should note here, that the respective distances between the parasitic plate and the dielectric block are 1 mm and 5 mm, since the distance between the chassis and the plate is 2 mm. The *SAR*s in the whole range (l = 0…100 mm) are presented in Figures 6.6a) (at 900 MHz) and 6.6b) (at 1800 MHz).

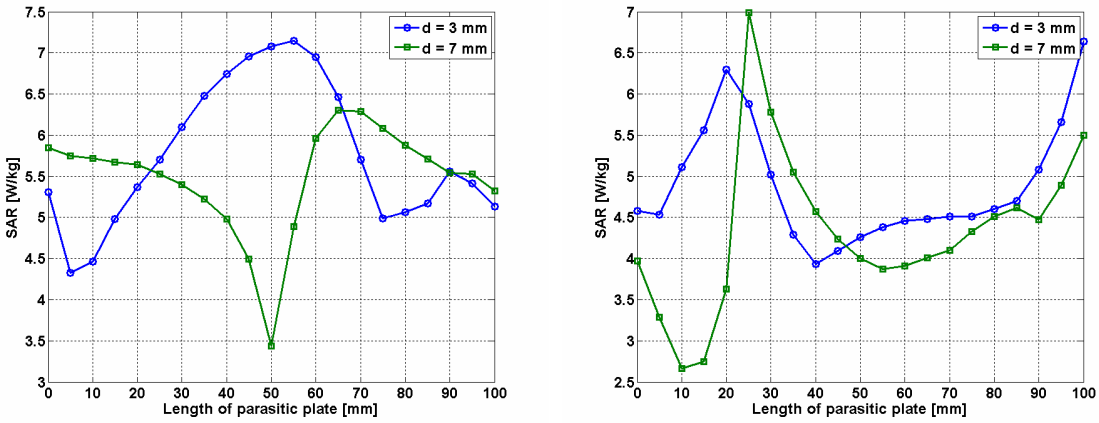

Figure 6.6 SAR (10 g average) in dielectric block at a) 900 MHz and b) 1800 MHz. The distance between the chassis of the antenna and the block is 3 mm (blue curve) and 7 mm (green curve). P_{in} = 1 W.

At 900 MHz, the effect of the parasitic plate on the *SAR* values is pretty much as could be expected (based on the results of [34]) when the distance between the chassis and the dielectric block is 7 mm. This case corresponds to the green curve in Figure 6.6a). *SAR* decreases from about 5.9 W/kg to about 3.4 W/kg when the length of plate changes from 0 mm to 50 mm. The reduction in *SAR* is thus approximately 42 % compared to the reference case (l = 0 mm, antenna without the plate). With plate lengths larger than 50 mm, *SAR* starts to increase rapidly, being even higher than the

original one already with a 60 mm plate. When the antenna is brought closer to the dielectric block (d = 3 mm, blue curve in Figure 6.6a)), the behavior of *SAR* changes completely. First of all, a somewhat surprising result is that with plate lengths l = 0…20 mm *SAR* values are lower with the smaller distance. When the parasitic plate is added to the antenna, *SAR* already at l = 5 mm has decreased from 5.3 W/kg to 4.3 W/kg, i.e. about 19 %. When the length of the plate is further increased, the *SAR* increases, reaching a maximum around the length at which there was a minimum in the case of d = 7 mm. This maximum is clearly higher than the original value of *SAR*. The behavior of *SAR* at 900 MHz shows that even if the used method works pretty well in some cases, even a small change in the system can completely change the performance.

*SAR*s at 1800 MHz are presented in Figure 6.6b). In this case, the differences in *SAR* behavior at different distances between the antenna and the dielectric block are not significant. Around l = 25 mm there is a high maximum with both cases. Around l = 40…70 mm, the *SAR* values are again lowered to the original level.

A significant reduction (42 % in the case of d = 7 mm) in *SAR*s can be obtained when a 50 mm long plate is added to the chassis of the antenna. The *SAR* distribution in this case is plotted in Figure 6.7.

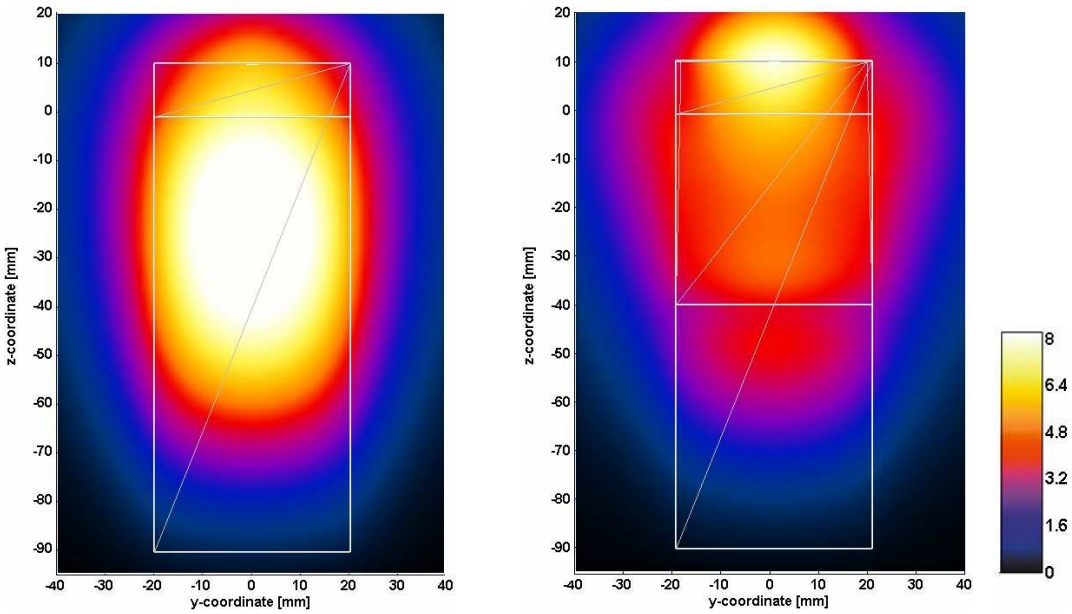

Figure 6.7 SAR distribution [W/kg] on the surface of the dielectric block at 900 MHz. a) antenna without the parasitic plate, b) antenna with 50 mm long parasitic plate. The distance between the chassis of the antenna and the block is 7 mm. P_{in} *= 1 W.*

From Figure 6.7 it can be seen that the 50 mm long plate strongly affects the distribution of the *SAR*. In Figure 6.7a) the *SAR* distribution is plotted without the parasitic plate. In that case, the maximum *SAR* lies around z = - 30 mm. When the 50 mm long plate is added to the antenna (Figure 6.7b)), the high *SAR* values around this area attenuate significantly, and at the same time high *SAR* values are generated around the upper edge of the chassis, under the coupling element (z ≈ 10 mm). In addition to the reduction in the maximum *SAR*, it is easy to see that the size of the area where the *SAR* is high is much larger in Figure 6.7a). This could be expected to have an increasing influence on the radiation efficiency.

6.4.2 Radiation efficiency

As a function of frequency, radiation efficiency and *SAR* are in general terms interrelated so that at chassis resonances *SAR* has a maximum and at the same a minimum in radiation efficiency occur ([14], [16]). In this case, however, the simulations have been made at single frequency points, changing the length of the parasitic plate. The radiation efficiencies as a function of the length of the parasitic plate are presented in Figure 6.8.

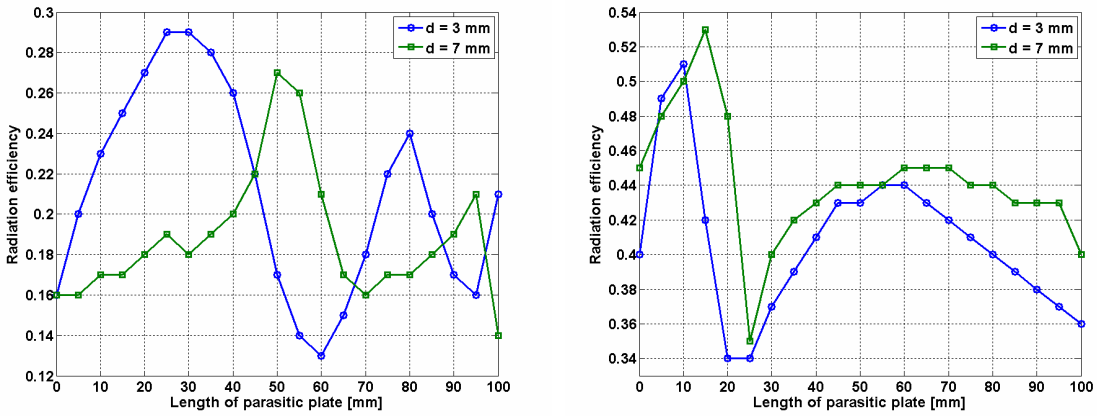

Figure 6.8 Radiation efficiency beside the dielectric block at a) 900 MHz and b) 1800 MHz. The distance between the chassis of the antenna and the block is 3 mm (blue curve) and 7 mm (green curve).

At 900 MHz with distance d = 7 mm between the antenna and the dielectric block (the green curve in Figure 6.8a)), the trend in radiation efficiency is such that when the length of the plate is increased, the radiation efficiency increases and reaches a maximum at l = 50 mm. Compared to the reference case (l = 0 mm), the radiation efficiency increases from 16 % to 27 %. After l = 50 mm, the radiation efficiency decreases rapidly close to the original value. A small increase can be seen again when the length of the plate exceeds 70 mm, until the radiation efficiency decreases

rapidly to 14 % at l = 100 mm. By comparing Figures 6.6a) and 6.8a), it can be seen that at 900 MHz and with d = 7 mm, radiation efficiency and *SAR* are pretty closely related. The best performance is achieved when the length of the parasitic plate is 50mm: a 42 % decrease in *SAR* and an increase of 11 %-unit in radiation efficiency are simultaneously obtained compared to the reference case.

With the smaller distance between the chassis of the antenna and the dielectric block (d = 3 mm, blue curve in Figure 6.8a)) the trend in the radiation efficiency at 900 MHz is very different from the case when d = 7 mm. At first, compared to the case d = 7 mm, the radiation efficiency is much higher at plate lengths 0…45 mm with d = 3 mm. The maximum in radiation efficiency (29 %) is obtained around l = 30 mm. This maximum is not seen in the *SAR* curve in Figure 6.6a). At plate lengths longer than 30 mm, radiation efficiency and *SAR* start to (inversely) follow each other. Around l = 60 mm, the minimum in radiation efficiency is at the same place as the corresponding maximum in *SAR*. At l = 80 mm, a minimum in *SAR* and a maximum in radiation efficiency can be seen.

At 1800 MHz, the radiation efficiencies are quite similar with both distances. In both cases a high maximum can be seen around l = 10…15 mm, after which the radiation efficiency decreases rapidly reaching a minimum already at l = 20…25 mm. The radiation efficiencies in the whole range (l = 0…100 mm) are considerably higher at 1800 MHz than at 900 MHz.

6.4.3 Bandwidth

In the previous two sections (6.4.1 and 6.4.2) it was shown that at the problematic GSM900 band it is possible to significantly reduce *SAR* and at the same time increase the radiation efficiency by adding a parasitic plate to the chassis of the coupling element antenna. In general, the price that has to be paid for high efficiency and low *SAR* is that at the same time the matching of the antenna becomes more difficult. In other words, the achievable bandwidth gets narrower [14], [16]. The bandwidth potential curves in Figure 6.9 show that unfortunately this rule of thumb is valid also in this case. The curves have been obtained by first matching the impedance of the antenna (critical coupling) at a point frequency with two lumped elements and then calculating the relative bandwidth according to - 6 dB matching criterion. This procedure is repeated separately for each plate length. It should be noted that in this way we apply a single resonant matching and that larger bandwidths could be easily obtained by utilizing multiple resonances. However, in this way we can see the possible trends in the behavior of the achievable bandwidth in a simple manner.

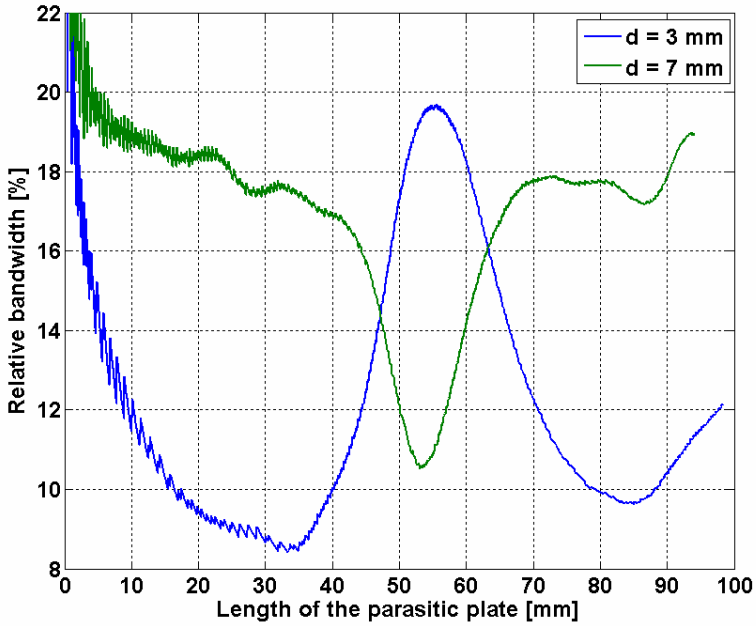

Figure 6.9 Bandwidth potential at 900 MHz.

When the antenna is placed at d = 7 mm from the dielectric block, the relative bandwidth is commonly between 16 % and 20 % except for the range where the length of the parasitic plate l = 45…65. In this range, the achievable relative bandwidth decreases and has a minimum of about 11 % at l = 55 mm. Unfortunately, this bandwidth minimum occurs close to the same plate length where the best performance in the radiation efficiency and *SAR* point of view was obtained. The same trend is evident also in the case when d = 3 mm. However, as was the case also with the radiation efficiency and *SAR*, the minima and maxima of the bandwidth potential are obtained with completely different plate lengths when the two cases, d = 3 mm or d = 7 mm, are compared. For example, at l = 55 mm there is a minimum in relative bandwidth in the case d = 7 mm, but a high maximum with d = 3 mm.

6.4.4 Near field distributions

Earlier in this chapter (in Section 6.3) it was shown how the different components of the electric field behave in free space when a 45 mm long parasitic plate or no plate at all is added to the chassis of the antenna. The effect of the plate was that the x-component (normal to the surface of the dielectric material) gets stronger around the plate, but at the same time the z-component (parallel to the surface of the dielectric material) is significantly reduced around the vertical center point of the chassis. This was considered to have a positive impact on *SAR*s and consequently on the radiation efficiency.

In the beginning of Section 6.4 it was then shown with a simple block model representing the user that significant improvement can indeed be obtained in terms of *SAR* and radiation efficiency with certain plate lengths. The best performance was obtained when the dielectric block was placed at a distance d = 7 mm from the antenna that had a 50 mm long plate attached to the chassis. In this section, in order to achieve a better understanding on the reason for this behavior, the electric near fields are studied inside and nearby the dielectric block. As a starting point, the overall (*RMS*) electric field without the plate and with a 50 mm plate (at 900 MHz, with d = 7 mm) is plotted in Figure 6.10.

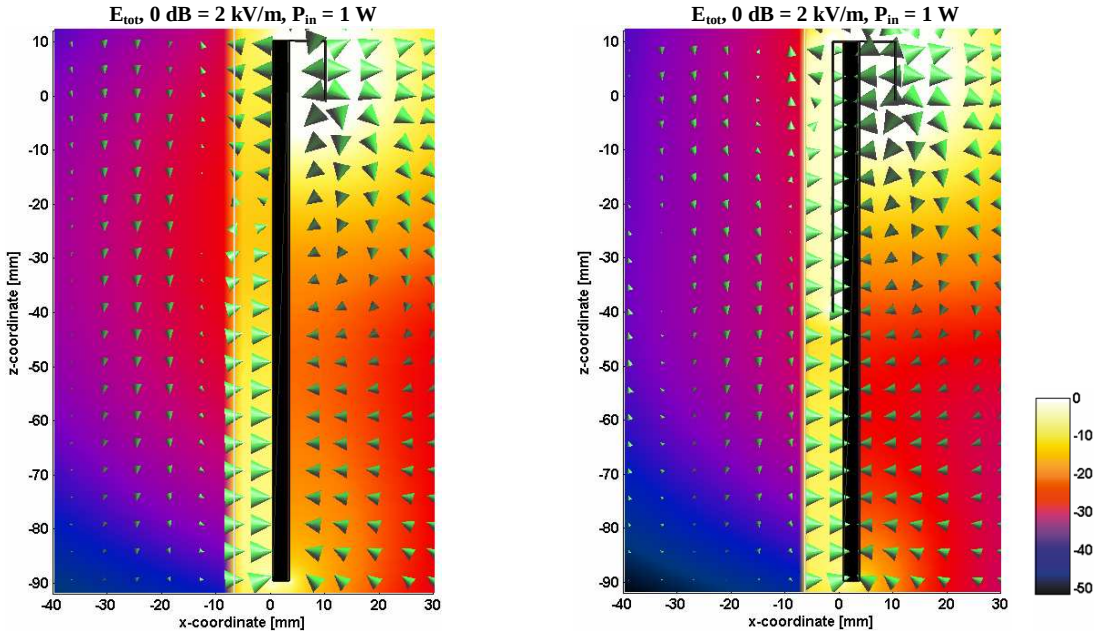

Figure 6.10 Total E-field at 900 MHz. a) Antenna without a parasitic plate b) antenna having a 50 mm long parasitic plate attached to the chassis. The distance between the chassis and the dielectric block is 7 mm.

Although the electric field gets stronger between the plate and the dielectric block (around z = -40…10 mm, compared to the case without the plate), the electric field that is coupled inside the dielectric material is clearly decreased when the plate is present. Since the increase in field strength outside the material is mostly caused by the increase in the x-component of the electric field, it doesn't result in significant increase in the electric field that is generated inside the block. In the case when no plate is added to the antenna (Figure 6.10a)), the electric field inside the block is strongest around z = -30 mm. In this range, the electric field is significantly decreased when the 50 mm long plate is added to the antenna (Figure 6.10b)). To see the reason for this behavior more clearly, plots of the different components of the electric fields are presented next in Figures 6.11 and 6.12.

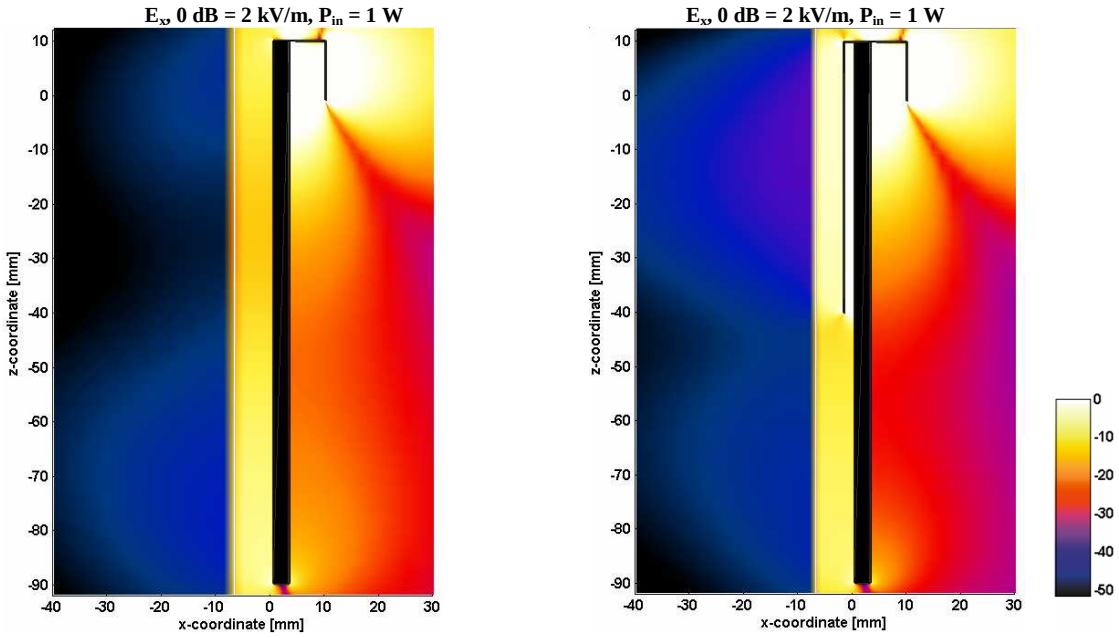

a) b)

Figure 6.11 The x-component of the E-field at 900 MHz. a) Antenna without a parasitic b) antenna having a 50 mm long parasitic plate attached to the chassis. The distance between the chassis and the dielectric block is 7 mm.

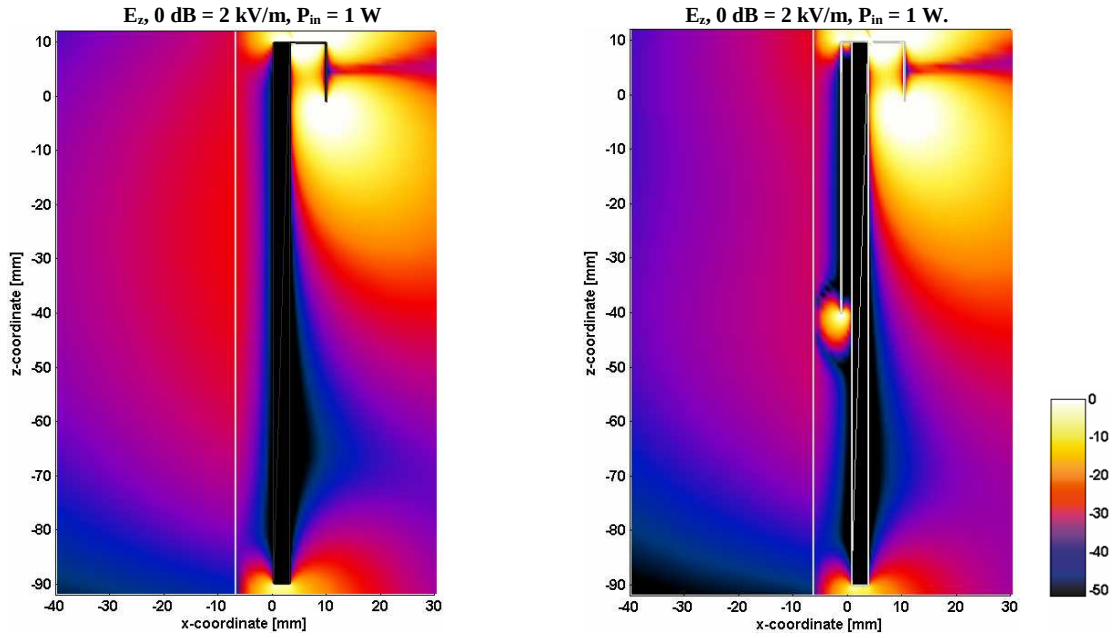

a) b)

Figure 6.12 The z-component of the E-field at 900 MHz. a) Antenna without a parasitic b) antenna having a 50 mm long parasitic plate attached to the chassis. The distance between the chassis and the dielectric block is 7 mm.

From Figure 6.11 it can be seen that the x-component of the electric field around locations where z = -40…10 mm and x = -20…0 mm is very much stronger when the 50 mm long plate is present. So, the x-component of the electric field gets stronger also inside the material. However, since the parallel components of the electric field dominate inside the dielectric material whose ε_r' is high, this increase is not significant in the overall field strength. On the other hand, from Figure 6.12 it can be seen that the z-component of the electric field inside the material decreases substantially when the plate is present. This decrease causes significant reduction also in the overall field strength inside the material (seen in Figure 6.10) and thus the significant reduction in the *SAR* value.

As discussed, in the case when the distance between the antenna and the dielectric block was d = 7 mm, the best performance was obtained with the plate length of l = 50 mm. However, when the antenna was brought closer to the block (d = 3 mm), it was noticed that the behavior of *SAR* and radiation efficiency completely changed. For example, with the smaller distance d = 3 mm, a maximum in *SAR* and a minimum in radiation efficiency were found around plate lengths of 50 mm. In order to come up with an explanation to these rather controversial results, the near field plots are repeated for the case d = 3 mm in Figures 6.13 - 6.15. The order is the same as in Figures 6.10 - 6. 12, i.e. at first the overall (*RMS*) field is plotted in Figure 8.13 and then the x- and z-components respectively in Figures 6.14 and 6.15.

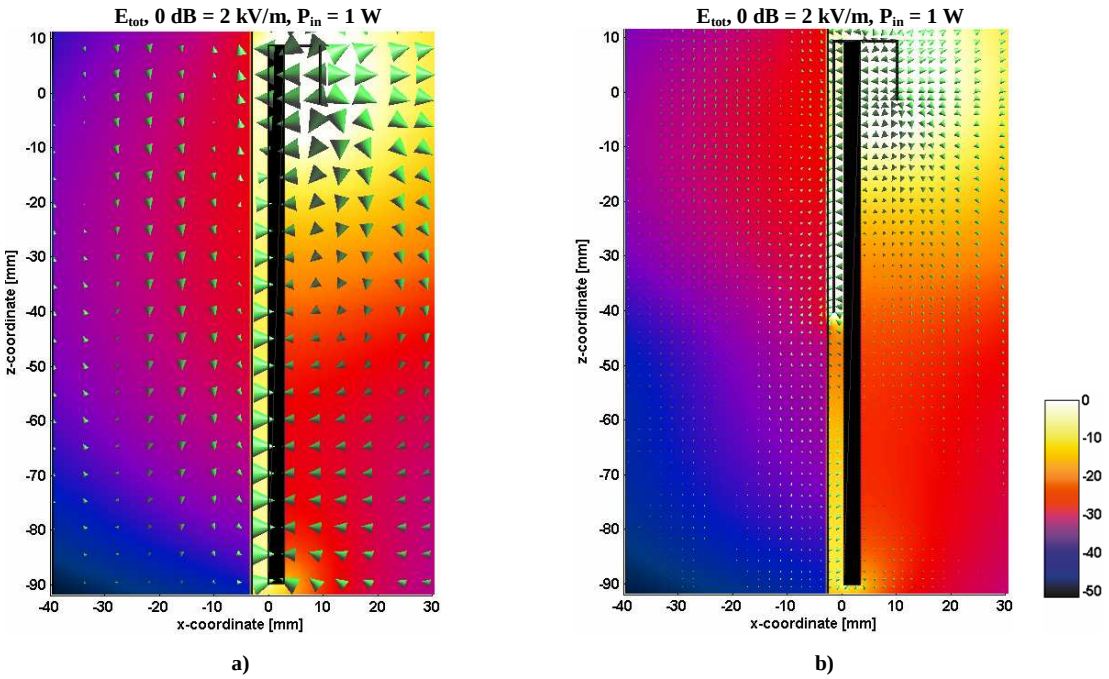

Figure 6.13 Total (RMS) E-field at 900 MHz. a) Antenna without a parasitic b) antenna having a 50 mm long parasitic plate attached to the chassis. The distance between the chassis and the dielectric block is 3 mm.

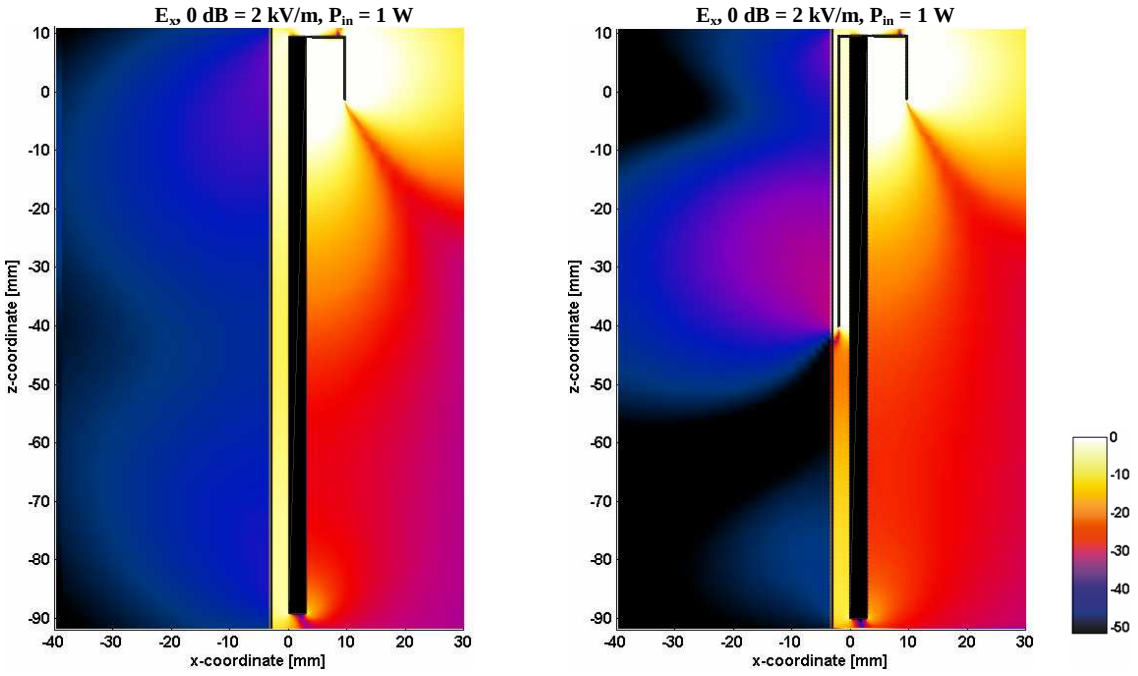

a) **b)**

Figure 6.14 The x-component of the E-field at 900 MHz. a) Antenna without a parasitic b) antenna having a 50 mm long parasitic plate attached to the chassis. The distance between the chassis and the dielectric block is 3 mm.

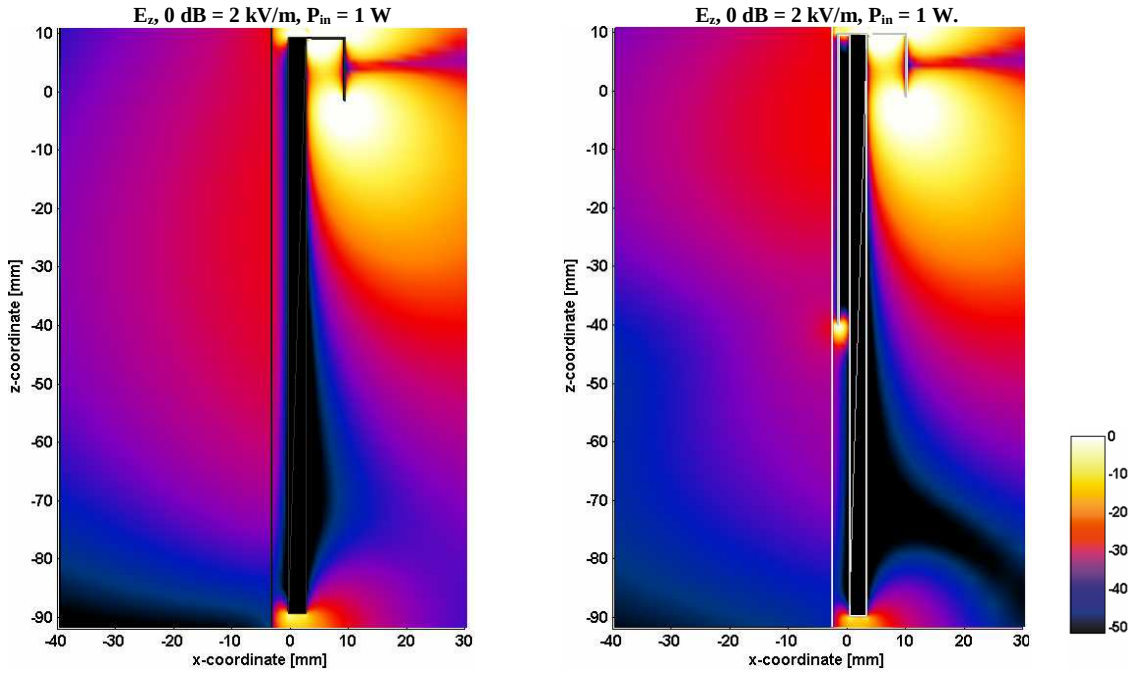

a) **b)**

Figure 6.15 The z-component of the E-field at 900 MHz. a) Antenna without a parasitic b) antenna having a 50 mm long parasitic plate attached to the chassis. The distance between the chassis and the dielectric block is 3 mm.

The overall E-field with d = 3 mm in the case when no parasitic plate is added to the antenna (Figure 6.13a)) is quite similar to that of the case when d = 7 mm. This can be seen by comparing Figures 6.10a) and 6.13a). However, as soon as the 50 mm plate is introduced, significant differences between the overall E-fields can be observed. With d = 3 mm, the electric field is much stronger around the plate (Figure 6.13b)) than in the case d = 7 mm (Figure 6.10b)). In addition, the direction of the electric field between the chassis and the parasitic plate has changed to the opposite. This is not clearly seen due to the fact that the green arrows that show the directions of the fields are very small in size in Figure 6.13b).

By comparing Figures 6.11b) and 6.14b) it can be seen that the x-component of the electric field not only gets stronger inside the dielectric material but also changes pretty much in shape when the distance between the antenna and the dielectric block is reduced from 7 mm to 3 mm. Rather than having only one maximum close to the center point of the parasitic plate around z = -10 mm in Figure 6.11b), the x-component has two maxima close to both edges of the plate in Figure 6.14b). From Figure 6.15b) it can be seen how the strength of the z-component of the electric field is increased compared to the case d = 7 mm when the antenna is brought closer to the dielectric block. This further causes the significant increase in the *SAR* values.

6.5 Simulations with the head model

In Section 6.4, the user was modeled with the simple block model filled with material having the same dielectric parameters as the brain tissue. The results showed that significant improvement in the performance according to *SAR* and radiation efficiency can be achieved by adding a parasitic plate of certain length to the chassis of the antenna. In order to see how the introduced method works in a more realistic situation, the method is in this section tested by replacing the block model with the SAM phantom head model. In the simulations with the head model, the distance between the head and the chassis of the antenna is fixed to d = 3 mm. It should be noted that the distances that were used in the previous section (6.4) in the case of the block model (d = 3 mm and d = 7 mm) are not straightforwardly comparable with the distance that is used in this section. At first, the surface of the head is not completely flat, which means that the distance between the head and the antenna changes slightly depending on the location. The second difference between the two models is that in the block model the high-permittivity brain tissue starts immediately at the surface, while in the head model the brain tissue simulating liquid starts after a few millimeter-thick low-permittivity shell.

6.5.1 SAR

*SAR*s as a function of the length of the parasitic plate were simulated again by increasing the length of the plate in 5 mm steps. Two frequencies (900 MHz and 1800 MHz) were analyzed. The results are presented in Figure 6.16.

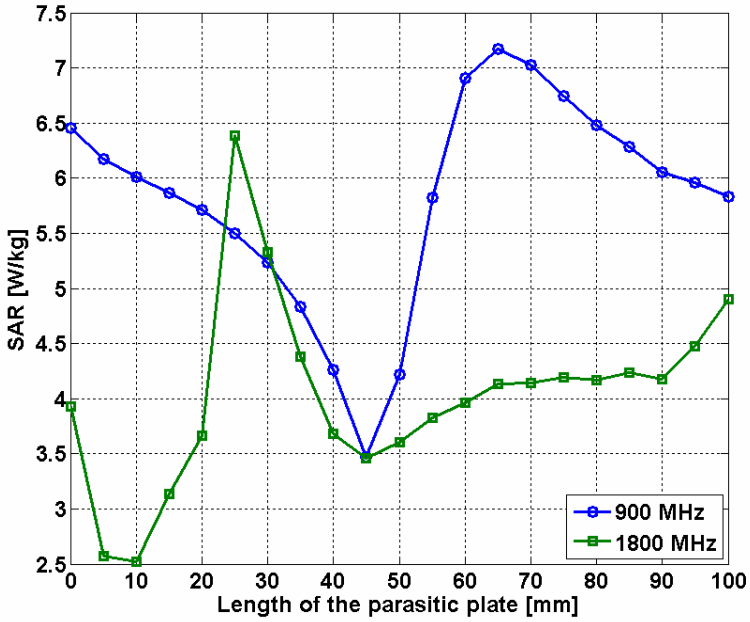

Figure 6.16 SAR in head model with different lengths of parasitic plate (10 g avg SAR [W/kg], P_{in} = 1 W).

It can be seen that the general trends in the results accurately follow the results that were obtained with the block model in the case d = 7 mm. At 900 MHz, the minimum *SAR* is obtained when the length of the parasitic plate is 45 mm. With this length, the value of *SAR* decreases from about 6.5 W/kg (antenna without the plate) to 3.5 W/kg, i.e. approximately 46 %. At 1800 MHz, the minimum *SAR* is again reached already with a 10 mm long plate. The highest *SAR* at 1800 MHz occurs at l = 25 mm. With the 45 mm plate which gives the best performance at 900 MHz, *SAR* has already decreased below the original. As an interesting coincidence, with the 45 mm long plate, the values of *SAR*s are almost exactly the same at both frequencies.

As was the case in the simulations with the block model, also beside the head the locations of the high *SAR* values move under the plate. The *SAR* distributions on the surface of the head without the plate and with the 45 mm long plate at 900 MHz are presented in Figure 6.17. It can be seen that the high *SAR*s that originally were generated close to the vertical center point of the chassis are significantly attenuated when the plate is added to the chassis. The highest *SAR*s with the antenna having the 45 mm plate are found in the upper parts of the chassis, under the parasitic plate. The

strange lines in the *SAR* distribution plots in Figure 6.17 are caused by the staircasing in the head model. However, this shouldn't have significant effect on the *SAR* values, since they are in this thesis always averaged over 10 g tissue mass.

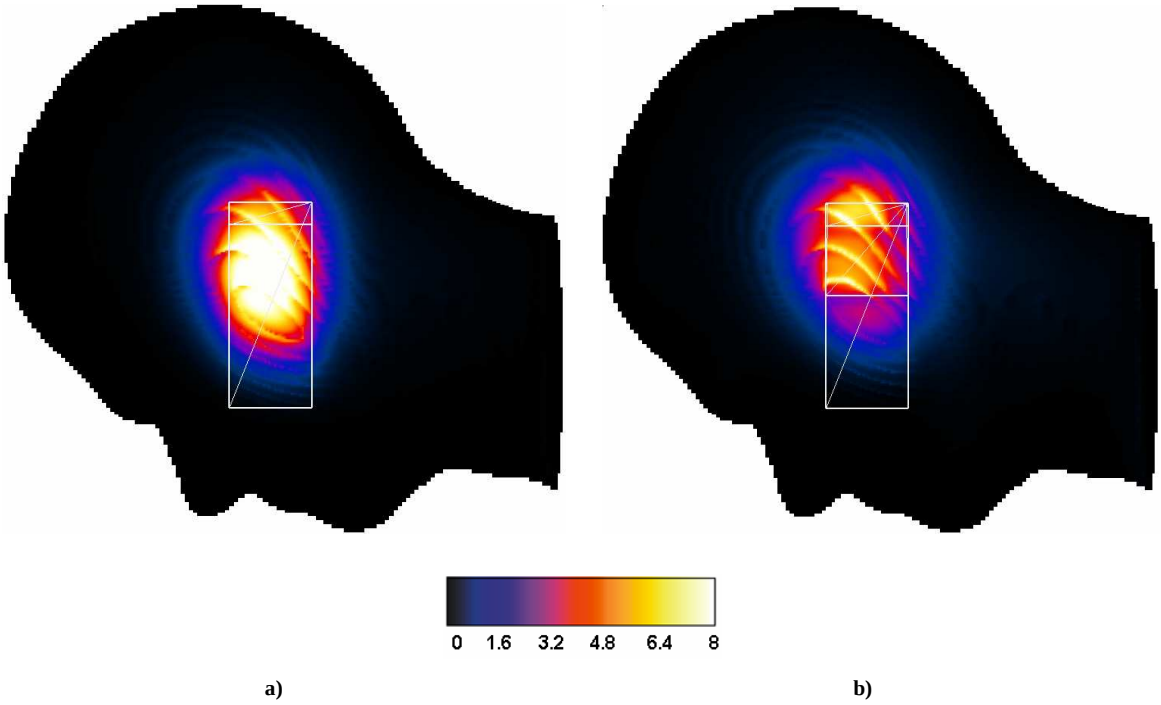

Figure 6.17 SAR distribution [W/kg] (unaveraged) on the surface of the head at 900 MHz. a) Antenna without the parasitic plate, b) antenna with a 45 mm long parasitic plate. The distance between the chassis of the antenna and the head the block is 3 mm. P_{in} *= 1 W.*

6.5.2 Radiation efficiency

Radiation efficiencies at 900 MHz and 1800 MHz when the antenna was placed beside the head model (d = 3 mm) are presented in Figure 6.18. It can be seen that radiation efficiency beside the head model agrees well with the corresponding *SAR*s. As a logical result, with plate lengths that give good performance in terms of *SAR*, the radiation efficiency is also at its maximum. At 900 MHz, with the 50 mm long plate the radiation efficiency increases from about 23 % (without the plate) to approximately 39 %, i.e. 16 %-units. At 1800 MHz, the radiation efficiency is over 50 % except for the few points around l = 25 mm. However, even the lowest value of radiation efficiency at 1800 MHz is still higher than the highest value at 900 MHz, which shows that even if it is interesting to study the trends at both frequency bands, the real significance, as far as radiation efficiency and *SAR* are concerned, stays at the GSM900 band.

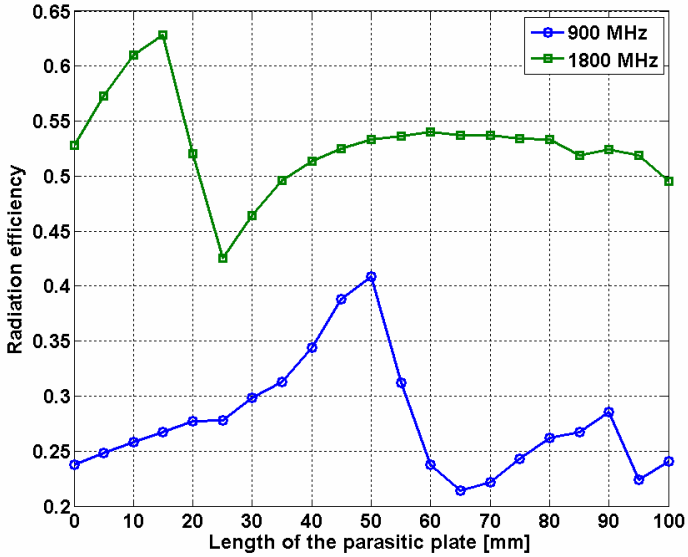

Figure 6.18 Radiation efficiency beside the head at a) 900 MHz and b) 1800 MHz. The distance between the chassis of the antenna and the block is 3 mm and 7 mm.

6.5.3 Bandwidth

In the previous section (6.4) it was shown that in the case when the antenna is placed beside the dielectric block, the achievable bandwidth gets narrower with plate lengths that give the best performance in terms of *SAR* and radiation efficiency. The behavior of *SAR*, radiation efficiency and bandwidth seems to follow this trend also when the antenna is placed beside the head model. The bandwidth potential of the antenna beside the head is plotted in Figure 6.19.

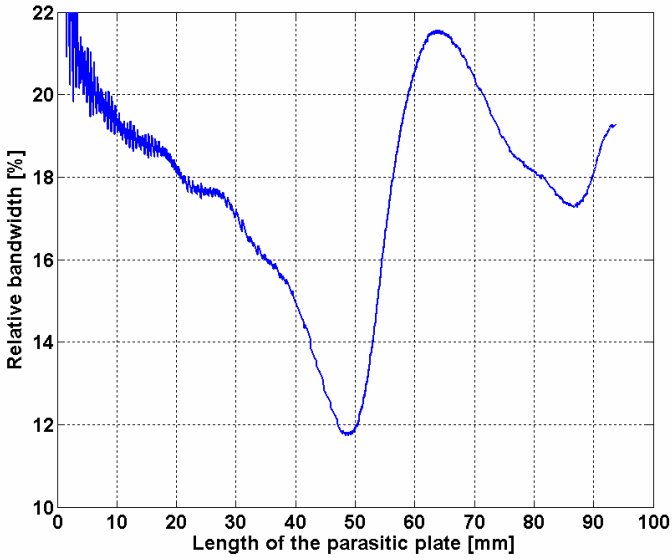

Figure 6.19 Bandwidth potential at 900 MHz.

6.5.4 Near field distributions

In Section 6.4, it was concluded that when the antenna is placed beside the dielectric block model, the z-component of the electric field that radiates towards the material is reduced with a parasitic plate having a certain length, which further results in a significant reduction in *SAR* values. It was shown also that at the same time, an increase in the radiation efficiency occurs.

The same thing happens in the case when the antenna is placed beside the head. It can be seen from Figures 6.20 - 6.22 that the overall electric near field that is generated inside the head (Figure 6.20) is lower when the 45 mm long plate is attached to the antenna even if the x-component of the field around the plate increases compared to the case when no plate is present (Figure 6.21). This can be explained by the significantly reduced z-component of the electric field inside the head, which can be seen by comparing Figures 6.22a) and 6.22b).

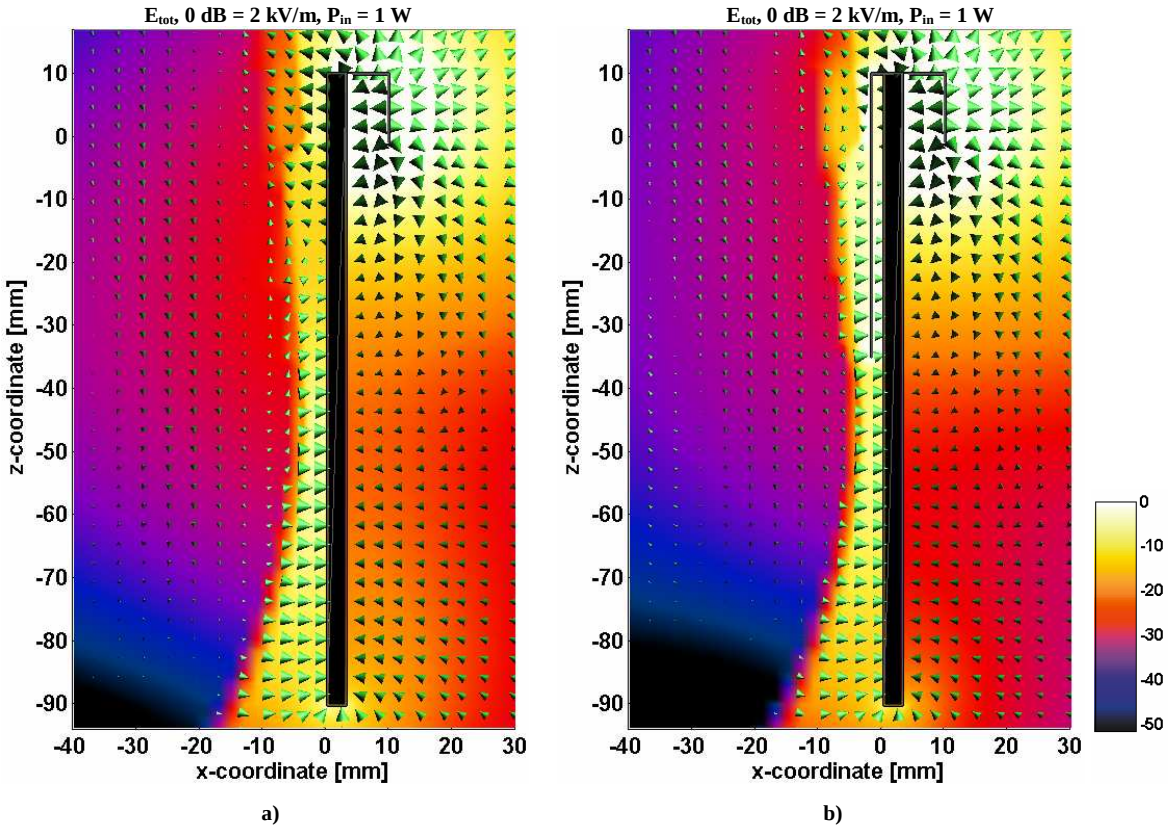

Figure 6.20 Total (RMS) E-field at 900 MHz. a) Antenna without a parasitic b) antenna having a 45 mm long parasitic plate attached to the chassis. The distance between the chassis and the head is 3 mm.

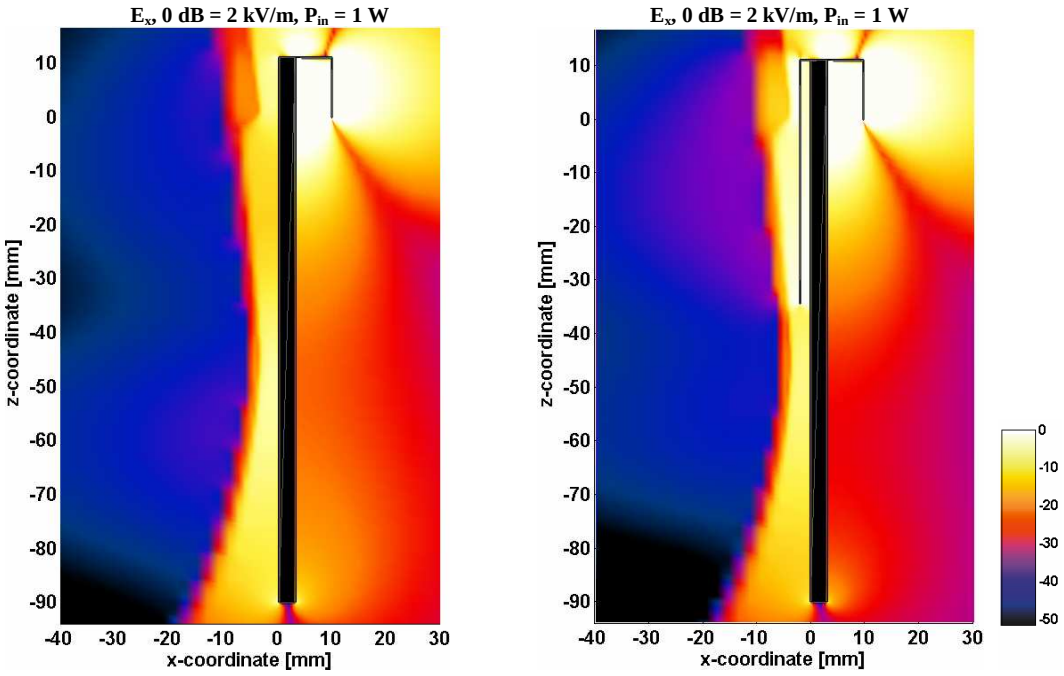

Figure 6.21 The x-component of the E-field at 900 MHz. a) Antenna without a parasitic b) antenna having a 45 mm long parasitic plate attached to the chassis. The distance between the chassis and the head is 3 mm.

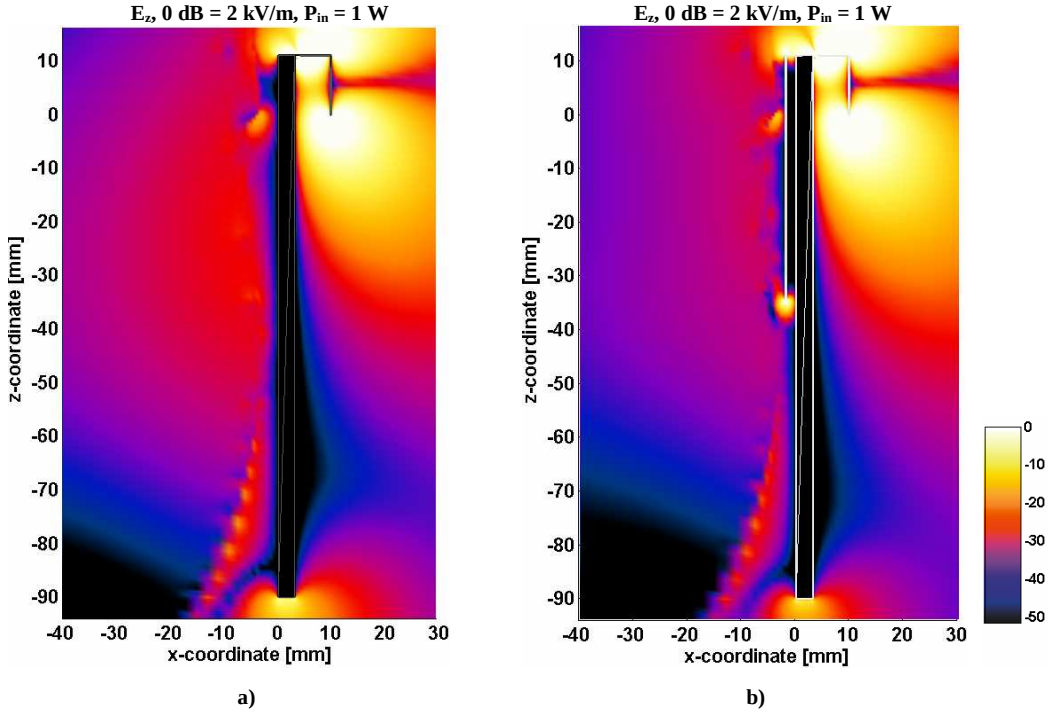

Figure 6.22 The z-component of the E-field at 900 MHz a) Antenna without a parasitic b) antenna having a 45 mm long parasitic plate attached to the chassis. The distance between the chassis and the head is 3 mm.

6.6 Summary of the studied SAR control method

A method to decrease the *SAR*s and to simultaneously increase the radiation efficiency of the antenna was studied in this chapter. The studied arrangement (presented, and analyzed with a dual-band PIFA in [34]) comprised a metallic plate attached to the chassis of the same coupling element based antenna that had been used already in the earlier parts of this thesis.

At first, the near fields of the antenna were analyzed in free space. It was shown that even if the total electric field that would radiate towards the head gets stronger when a 45 mm long parasitic plate is added to the chassis of the antenna, the z-component of the electric field is significantly lowered especially around the (vertical) center point of the chassis. This was anticipated to have a positive influence on both *SAR* values and on radiation efficiency.

The *SAR*s, radiation efficiencies, bandwidth potentials and near field distributions were then analyzed by modeling the user with a simple block. It was shown that compared to the case when no plate is added to the antenna, up to 42 % reduction in the maximum *SAR* value (averaged over 10 g tissue mass) and an 11 %-unit increase in radiation efficiency can be simultaneously obtained (at 900 MHz) with a 50 mm long plate. This was shown to be a result of the reduced coupling of z-directed electric field components inside the dielectric material. However, it was additionally shown that with the plate lengths that give the best performance in terms of the *SAR*s and radiation efficiency, the bandwidth potential of the antenna decreases. In the case of the head model, the reduction in the relative bandwidth at 900 MHz was from about 20 % (no plate) to 12 %.

The results followed a similar trend when the proposed *SAR* control method was finally tested with the SAM phantom as the head model. At 900 MHz, compared to the reference case (antenna without the plate), a 46 % reduction in the *SAR* value and a 16 %-unit increase in the radiation efficiency were obtained with a 45 mm long plate. However, the bandwidth potential had again a minimum at that plate length.

The results of this chapter show that the parasitic plate attached to the chassis of the coupling element antenna works well in order to decrease *SAR* and to increase the radiation efficiency. However, the studied method seems to be very sensitive even to small changes in the system. In addition, the simulations have been carried out only at a single frequency point. To get a better picture, the method should be studied at least in the whole GSM900 band (824 - 960 MHz).

7 CONCLUSIONS

The studies of this master's thesis aimed at improving understanding on how mobile terminal antennas behave in the vicinity of a user. As a motivation for the work, it was considered especially interesting to find out whether it would be possible to predict the behavior of bandwidth, efficiency, *SAR* and other parameters of the antenna beside the user based on the performance of the antenna in free space.

The work was started by introducing the general theory behind mobile terminal antennas. It was found that the continuous desire to reduce the size of the terminal sets very fundamental limitations to the antenna performance. It was shown that designing a small antenna is always a trade-off between size, impedance bandwidth and radiation efficiency. The fundamentals of the interaction between a mobile terminal antenna and the user were also discussed.

After introducing the general theory behind mobile terminal antennas, the thesis continued by taking a look at some of the recently suggested solutions for internal mobile terminal antennas. The concepts of PIFA (Planar Inverted-F Antenna), DRA (Dielectric Resonator Antenna), chip antenna and coupling element based antenna were briefly explained. This part was, however, started by studying the effect of the mobile phone chassis on the antenna performance. Based on the earlier studies related to the issue, it was concluded that regardless of the antenna structure in question, the chassis has a strong role in the behavior of parameters such as impedance bandwidth, *SAR* and radiation efficiency. Also the radiation properties of an antenna were said to be very much dependent on the chassis.

The theory of how radiowaves propagate in dielectric materials was studied next. It was found that losses inside dielectric material can be divided into ionic losses that are caused by the current

generated inside the material by the Ohm's law, and into dielectric losses that result from the response of the polar molecules to the oscillating electric field. Especially when dealing with human body tissues, both ionic and dielectric losses were said to be commonly included in the so-called effective conductivity which, in turn, would be included in the imaginary part of the permittivity of the tissue. A table that included values for the dielectric parameters of human tissues in a wide frequency range was also presented. After this, a review of the earlier studies on the basic energy absorption mechanisms in human tissue was given. It was concluded that the research results presented in these studies are rather controversial and that obviously additional research would be needed in this field.

The simulation studies on the interaction between a mobile terminal antenna and the user were started by analyzing the near fields of a coupling element based antenna inside and nearby dielectric material. In the first phase, the user was modeled with a simple block model filled with material having different dielectric parameters. It was concluded that the electric field components that are normal to the surface of the dielectric material do not easily penetrate inside a high-permittivity material and thus do not generate high electric field inside the material. The attenuation of field components that are parallel with respect to the surface of the dielectric material, in turn, were shown to be significantly lower at the boundary of the material thus causing high electric field also inside the material. In the case of the used coupling element based antenna, the strong areas of electric field inside the high-permittivity material followed the current distribution on the surface of the chassis of the antenna. As a quite expected result, it was further concluded that in the case of low-permittivity material, in turn, the electric field inside the material is strong close to locations where also the total (*RMS*) electric field in the free space was strong. A logical consequence from these observations was that as the permittivity of the material increases, the electric field inside the material is forced to direct more and more parallel to the surface of the material. All these results were fully supported by the presented boundary conditions derived from Maxwell's equations. The effect of the conductivity of the material on the near field distributions was also studied. It was found that increasing the conductivity of the material only results in a faster attenuation of the field inside the material; the directions of the fields were not affected.

Next, the performance of the coupling element based antenna beside a user was studied in terms of the resonance frequency, bandwidth, radiation efficiency and *SAR*. The simulations were made at a frequency range of 0.6 GHz - 6 GHz. In the first phase, the user was still modeled with the simple block model. The results were presented for two tissues, muscle (high-permittivity case) and fat (low-permittivity case). In the simulations, it was found that the resonance frequency of an antenna/chassis combination can increase when dielectric material is brought beside the antenna. This was explained by the decrease in the electrical length of the chassis due to the nearby

dielectric material. The bandwidth, *SAR* and radiation efficiency in many respects behaved as could be expected based on the earlier studies; at the low-order resonances of the chassis, a local maximum in both bandwidth and *SAR* were reached, but at the same time a minimum in radiation efficiency occurred. At higher frequencies, the wavemodes of the chassis were not anymore the main contributor because of the increased radiation of the coupling element. However, it was found that especially with the high-permittivity material, even if the resonance frequency changed when the material was brought closer to the antenna, neither the high values of *SAR* nor the maxima in bandwidth shifted accordingly. The inspection of the peak *SAR* locations showed that in high-permittivity material, the locations of the high *SAR* values accurately follow the current distribution of the chassis. However, this trend was not evident in the low-permittivity case. The results that were obtained from simulations when the antenna was placed beside the head model were of similar kind to the results that were obtained with the high-permittivity (muscle) block model. This was considered to be quite expected, since the dielectric parameters of the brain tissue are rather close to those of the muscle tissue. However, small differences in the results were noticed and concluded to be caused by the non-flat shape of the head model.

A method to bring help in terms of *SAR* and efficiency to the problematic GSM900 band was studied in the last part of the thesis. The studied arrangement comprised a metallic plate attached to the chassis of the coupling element antenna. The *SAR*s, radiation efficiencies, bandwidth potentials and near field distributions were analyzed with a block model and with a head model. In the case of the block model, a 42 % reduction in *SAR* value and an 11 %-unit increase in the radiation efficiency were simultaneously achieved with a 50 mm long metallic plate. With the head model, the best performance (46 % reduced *SAR* and 16 %-unit higher radiation efficiency) was obtained with a 45 mm long plate. The good performance was concluded to be caused by the fact that the electric field components that are parallel with respect to the surface of the dielectric material decrease substantially when the plate is added to the antenna. As the major drawback of the proposed method, it was shown that the achievable bandwidth of the antenna somewhat decreases due to the plate.

The initial goal of this thesis was to find out whether it is possible to predict how the nearby user changes the performance of the mobile terminal antenna and on the other hand to find out whether it would be possible to predict the behavior of bandwidth, efficiency and *SAR*, based on the performance of the antenna in free space. Even if the prediction based on free space performance seems to be a difficult task, the results of this thesis show that with simple simulation models, the trends in the performance of the antenna can be seen. Many of the observed trends led to conclusions that can be utilized in designing mobile terminal antennas that operate optimally in all possible using environments.

REFERENCES

[1] A. Räisänen and A. Lehto, *Radiotekniikan perusteet (Foundations of Radio Engineering, in Finnish)*, 11th edition. Helsinki: Otatieto, 2003, 292 p.

[2] O. Kivekäs, *Design of High-Efficiency Antennas for Mobile Communication Devices*, Thesis for the degree of Doctor of Science in Technology, Helsinki University of Technology. Espoo: Otamedia, 2005, 50 p.

[3] I. Lindell and K. Nikoskinen, *Antenniteoria (Antenna Theory, in Finnish)*, 3rd edition. Helsinki: Otatieto, 1995, 345 p.

[4] Web page of Ficora, *Radiotaajuuksien käyttöön liittyvät Viestintäviraston määräykset*, available online <URL:http://www.ficora.fi/attachments/suomi_R_Y/5lf6Jmnxl/Files/CurrentFile/TJT_suomi12122006.pdf>, [Cited May 28, 2007]

[5] H.F. Pues and A.R. van de Capelle, "An impedance-matching technique for increasing the bandwidth of microstrip antennas", *IEEE Transactions on Antennas and Propagation*, vol. 37, no. 11, November 1989, pp 1345-1354.

[6] J. Villanen, *Compact Antenna Structure for Mobile Handset*, Master's thesis, Helsinki University of Technology. Espoo: 2003, 83 p.

[7] K. Siwiak, *Radiowave Propagation and Antennas for Personal Communications*, second edition. Norwood: Artech House, 1998, 418 p.

[8] A. Lehto and A. Räisänen, *RF- ja mikroaaltotekniika (RF and Microwave Engineering, in Finnish)*, 7th edition. Helsinki: Otatieto, 2002, 267 p.

[9] IEEE, *IEEE Standard Definitions of Terms for Antennas*, IEEE STD-145, 1993, 30 p.

[10] J. Holopainen, *Antenna for Handheld DVB Terminal*, Master's thesis, Helsinki University of Technology. Espoo: 2005, 91 p.

[11] K. Jokela, D. Leszczynski, W. Paile, S. Salomaa, L. Puranen and P. Hyysalo, *Radiation safety of mobile phones and base stations*, Radiation and Nuclear Safety Authority, Report A161, Helsinki, 1999, 76 p.

[12] ANSI / IEEE Std C95.1, 1999 Edition, *IEEE Standard for Safety Levels with Respect to Human Exposure to Radio Frequency Electromagnetic Fields, 3 kHz to 300 GHz*, April 1999, 73 p.

[13] International Commission on Non-Ionizing Radiation Protection (ICNIRP), "Guidelines for limiting exposure to time-varying electric, magnetic, and electromagnetic fields (up to 300 GHz)", *Health Physics*, vol. 74, no. 4, April 1998, pp. 494-522.

[14] O. Kivekäs, J. Ollikainen, T. Lehtiniemi and P. Vainikainen, "Bandwidth, SAR, and efficiency of internal mobile phone antennas", *IEEE Transactions on Electromagnetic Compatibility*, vol. 46, no. 1, February 2004, pp. 71-86.

[15] P. Vainikainen, J. Ollikainen, O. Kivekäs and I. Kelander, "Resonator-based analysis of the combination of mobile handset antenna and chassis", *IEEE Transactions on Antennas and Propagation*, vol. 50, no. 10, October 2002, pp. 1433-1444.

[16] J. Villanen, J. Poutanen, C. Icheln and P. Vainikainen, "A wideband study of the bandwidth, SAR and radiation efficiency of mobile terminal antenna structures", *Proceedings of International Workshop on Antenna Technology 2007 (IWAT07),* Cambridge, UK, 2007, pp. 49-52.

[17] A. Petosa, A. Ittipiboon, Y.M.M Antar, D. Roscoe and M. Cuhaci, "Resent advances in dielectric-resonator antenna technology", *IEEE Transactions on Antennas and Propagation*, vol. 40, no. 3, June 1998, pp 35-48.

[18] O. Kivekäs, J. Ollikainen and P. Vainikainen, "Wideband dielectric resonator antenna for mobile phones", *Microwave and Optical Technology Letters*, vol. 36, no. 1, January 2003, pp. 25-26.

[19] P. Rezaei, M. Hakkak, K. Forooraghi, "Dielectric resonator antenna for wireless LAN applications", *IEEE Antennas and Propagation Society International Symposium 2006*, July 2006, pp. 1005-1008.

[20] K. Wong, *Planar Antennas for Wireless Communications.* New Jersey: John Wiley & Sons, 2003, 301 p.

[21] O. Lehmus, *Miniaturization Methods of Handset Antennas.* Master's thesis, Helsinki University of Technology. Espoo: 1999, 98 p.

[22] J. Ollikainen, O. Kivekäs, A. Toropainen and P. Vainikainen, "Internal dual-band patch antenna for mobile phones", *Proceedings of the AP2000 Millennium Conference on Antennas and Propagation*, Davos, Switzerland, April 2000, CD-ROM SP-444, paper p1112.pdf.

[23] K. Wong, Y. Chen, S. Su and Y. Kuo, "Diversity dual-band planar inverted-F antenna for WLAN operation", *Microwave and Optical Technology Letters*, vol. 38, no. 3, August 2003, pp. 223-225.

[24] C-L Ta, "2.4/5.2 GHz Dual-Band Chip Antenna for WLAN Applications", *Antennas and Propagation Society International Symposium*, vol. 1, July 2005, pp 455-458.

[25] D. Manteuffel, A. Bahr and P. Waldow, "Numerical analysis of absorption mechanisms for mobile phones with integrated multiband antennas", *Proceedings of Antennas and Propagation Symposium*, Boston, 2001, pp. 82-85.

[26] J. Villanen, J. Ollikainen, O. Kivekäs and P. Vainikainen, "Coupling element based mobile terminal antenna structures", *IEEE Transactions on Antennas and Propagation*, vol. 54, no. 7, July 2006, pp 2142-2153.

[27] A. Sihvola and I. Lindell, *Sähkömagneettinen kenttäteoria. 2: Dynaamiset kentät (Electromagnetic Field Theory. 2: Dynamic Fields, in Finnish),* 4th edition. Helsinki: Hakapaino, 2004, 200 p.

[28] S. Gabriel, R. W. Lau and C. Gabriel, “The dielectric properties of biological tissues: III. Parametric models for the dielectric spectrum of tissues”, *Physics in Medicine and Biology* vol. 41, 1996, pp. 2271-2293.

[29] O. Kivekäs, T. Lehtiniemi and P. Vainikainen, “On the general energy-absorption mechanism in the human tissue”, *Microwave and Optical Technology Letters*, vol. 43, no. 3, November 2004, pp. 195-201.

[30] R. F. Harrington, *Time-Harmonic Electromagnetic Fields*. New York: McGraw-Hill, 1961, 480 p.

[31] N. Kuster and Q. Balzano, “Energy absorption mechanism by biological bodies in the near field of dipole antennas above 300 MHz”, *IEEE Transactions on Vehicular Technology*, vol. 41, no. 1, February 1992, pp. 17-23.

[32] H. R. Chuang, “Numerical computation of fat layer effects on microwave near-field radiation to the abdomen of a full-scale human body model”, *IEEE Transactions on Microwave Theory and Techniques*, vol. 45, no.1, January 1997, pp. 118-125.

[33] Web page of SEMCAD, Schmid & Partner Engineering AG, <URL: http://www.semcad.com>, [Cited May 28, 2007]

[34] M. Sager, M. Forcucci and T. Kristensen, “A novel technique to increase the realized efficiency of a mobile phone antenna placed beside a head-phantom”, *IEEE Antennas and Propagation Symposium*, vol. 2, June 2003, pp 1013- 1016.